ENCLOSURE 8

TENNESSEE VALLEY AUTHORITY
BROWNS FERRY NUCLEAR PLANT (BFN)
UNITS 1, 2, AND 3

TECHNICAL SPECIFICATIONS (TS) CHANGES TS-431 AND TS-418 - EXTENDED POWER UPRATE (EPU) - STEAM DRYER EVALUATIONS

CDI REPORT NO. 07-06NP, "FINITE ELEMENT MODEL FOR STRESS ASSESSMENT OF BROWNS FERRY NUCLEAR UNIT 2 AND 3 STEAM DRYERS TO 250 HZ"

(NON-PROPRIETARY VERSION)

Attached is the **Non-Proprietary Version** of CDI Report No. 07-06, "Finite Element Model for Stress Assessment of Browns Ferry Nuclear Unit 2 and 3 Steam Dryers to 250 Hz."

This Document Does Not Contain Continuum Dynamics, Inc. Proprietary Information

CDI Report No. 07-06NP

Finite Element Model for Stress Assessment of Browns Ferry Nuclear Unit 2 and 3 Steam Dryers to 250 Hz

Revision 0

Prepared by

Continuum Dynamics, Inc.
34 Lexington Avenue
Ewing, NJ 08618

Prepared under Purchase Order No. 00053157 for

TVA / Browns Ferry Nuclear Plant
Nuclear Plant Road, P. O. Box 2000 PAB-2M
Decatur, AL 35609

Approved by

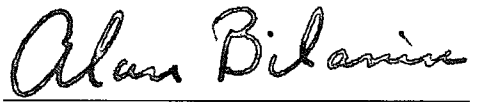

Alan J. Bilanin

Reviewed by

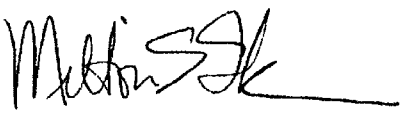

Milton E. Teske

July 2007

This report complies with Continuum Dynamics, Inc. Nuclear Quality Assurance Program currently in effect.

Executive Summary

The finite element model and analysis methodology used to assess stresses induced by the flow of steam through the steam dryer at Brown Ferry Nuclear Unit 2/3 (BFN2/3), are described and applied to obtain stresses at CLTP conditions. The analysis is carried out in the frequency domain, which confers a number of useful computational advantages over a time accurate transient analysis including the ability to assess the effects of frequency scalings in the loads without the need for additional finite element calculations. [[

(3)]]

The analysis begins by developing a series of unit stress solutions corresponding to the application of a unit pressure at a MSL at specified frequency, f. Each unit solution is obtained by first calculating the associated acoustic pressure field using a separate analysis that solves the damped Helmholtz equation within the steam dryer [1]. This pressure field is then applied to a finite element structural model of the steam dryer and the harmonic stress response at frequency, f, calculated using the commercial ANSYS 10.0 finite element analysis software. This stress response, constitutes the unit solution and is stored as a file for subsequent processing. Once all unit solutions have been computed, the stress response for any combination of MSL pressure spectrums (obtained by fast Fourier transform of the pressure histories in the MSLs) is determined by a simple matrix multiplication of these spectrums with the unit solutions.

This report provides details of the ANSYS 10.0 finite element structural model of the BFN2/3 steam dryer and reviews pertinent modeling considerations. It also summarizes the framework underlying the development and application of unit solutions in the frequency domain and shows how these solutions are used to develop stress histories for general load conditions. Next, it reviews the assessment of these stresses for compliance with the ASME B&PV Code, Section III, subsection NG, for the load combination corresponding to normal operation (the Level A Service Condition). [[

(3)]]

Results obtained from application of the methodology to the BFN2/3 steam dryer show that at nominal CLTP operation the minimum stress ratio (SR) anywhere on the steam dryer is SR=1.06. The loads used to obtain this value account for all the end-to-end biases and uncertainties in the loads model [2]. In order to account for uncertainties in the finite element model the stresses are also computed for loads that are shifted in the frequency domain by ±2.5%, ±5%, ±7.5% and ±10%. The minimum stress ratio encountered at any frequency shift is found to be SR=0.49 occurring at the -10% shift. Further inspection of the stresses shows that virtually all of the response results from a strong 218 Hz signal in the loading and stresses which is identified with dead head safety valve standpipes in the system. This signal can be removed by plugging these unused standpipes. In that case the minimum stress ratio associated with alternating stresses at any frequency shift more than triples to SR=1.77. Given that the biases and uncertainties in loads are already accounted for, this stress ratio is expected to qualify the dryer with considerable margin at EPU. The stress ratio due to maximum stresses is dominated by static loads and is SR=0.93 (with the 218 Hz signal included) and SR=1.32 (218 Hz signal removed).

Table of Contents

1. Introduction and Purpose

Plans to qualify the Browns Ferry nuclear plant for operation at Extended Power Uprate (EPU) operating condition require an assessment of the steam dryer stresses experienced under the increased loads. The steam dryer loads due to pressure fluctuations in the main steam lines (MSLs) are potentially damaging and the cyclic stresses from these loads can produce fatigue cracking if loads are sufficiently high. The industry has addressed this problem with physical modifications to the dryers, as well as a program to define steam dryer loads and their resulting stresses.

The purpose of the stress analysis discussed here is to calculate the maximum and alternating stresses generated during Current Licensed Thermal Power (CLTP) and determine the margins that exist when compared to stresses that comply with the ASME Code (ASME B&PV Code, Section III, subsection NG). This step establishes whether the modifications done prior to commercial operations are adequate for sustaining structural integrity and preventing future weld cracking under planned EPU operating conditions. The load combination considered here corresponds to normal operation (the Level A Service Condition) and includes fluctuating pressure loads developed from Browns Ferry Unit 2 (BFN2) main steam line data, and weight. The fluctuating pressure loads, induced by the flowing steam, are predicted using a separate acoustic circuit analysis of the steam dome and main steam lines [3]. Level B service conditions, which include seismic loads, are not included in this evaluation.

[[

[3]]] This approach also affords a number of additional computational advantages over transient simulations including: [[

[3]]] This last advantage is realized through the use of "unit" solutions representing the stress distribution resulting from the application of a unit fluctuating pressure at one of the MSLs at a particular frequency. [[

[3]]]

This report describes the overall methodology used to obtain the unit solutions in the frequency domain and how to assemble them into a stress response for a given combination of pressure signals in the MSLs. This is followed by details of the BFN2/3 steam dryer finite

element model including the elements used and overall resolution, treatment of connections between elements, the hydrodynamic model, the implementation of structural damping and key idealizations/assumptions inherent to the model. Post-processing procedures are also reviewed including the computation of maximum and alternating stress intensities, identification of high stress locations, adjustments to stress intensities at welds and evaluation of stress ratios used to establish compliance with the ASME Code. The results in terms of stress intensity distributions and stress ratios are presented next together with PSDs of the dominant stress components. The latter show that the load and structural response are dominated by a strong 218 Hz component that is due to dead head safety valve standpipes and is responsible for all of the lowest stress ratios. Results are also presented with the 218 Hz signal removed. In this case the lowest alternating stress ratio due to acoustic loads is 1.77.

2. Methodology

2.1 Overview

Based on previous analysis undertaken at Quad Cities Units 1 and 2, the steam dryer can experience strong acoustic loads due to the fluctuating pressures in the MSLs connected to the steam dome containing the dryer. CDI has developed an acoustic circuit model (ACM) that, given a collection of strain gauge measurements [4] of the fluctuating pressures in the MSLs, predicts the acoustic pressure field anywhere inside the steam dome and on the steam dryer [1-3]. The ACM is formulated in frequency space and contains two major components that are directly relevant to the ensuing stress analysis of concern here. [[

[3]]]

[[

[3]]]

[[

[3]]]

2.2 [[

[3]]]

[[

[3]]]

2.3 Computational Considerations

Focusing on the structural computational aspects of the overall approach, there are a number of numerical and computational considerations requiring attention. The first concerns the transfer of the acoustic forces onto the structure, particularly the spatial and frequency resolutions. The ANSYS finite element program inputs general distributed pressure differences using the table format. This consists of regular 3D rectangular (i.e., block) $n_x \times n_y \times n_z$ mesh where n_α is the number of mesh points in the i-th Cartesian direction and the pressure difference is provided at each mesh point (see Section 3.10). These tables are generated separately using a program that reads the loads provided from the ACM software, distributes these loads onto the finite element mesh using a combination of interpolation procedures on the surface and simple diffusion schemes off the surface (off surface loads are required by ANSYS to ensure proper interpolation of forces), and written to ASCII files for input to ANSYS. A separate load file is written at each frequency for the real and imaginary component of the complex force.

The acoustic field is stored at 5 Hz intervals from 0 to 250 Hz. While a 5 Hz resolution is sufficient to capture frequency dependence of the acoustic field (i.e., the pressure at a point varies gradually with frequency), it is too coarse for representing the structural response especially at low frequencies. For 1% critical structural damping, one can show that the frequency spacing needed to resolve a damped resonant peak at natural frequency, f_n, to within 5% accuracy is $\Delta f = 0.0064 \times f_n$. Thus for $f_n = 10$ Hz where the lowest structural response modes occur, a frequency interval of 0.064 Hz or less is required. In our calculations we require that 5% maximum error be maintained over the range from $f_n = 5$ Hz to 250 Hz resulting in a finest frequency interval of 0.0321 Hz at the low frequency end (this adequately resolves all structural modes up to 250 Hz). Since there are no structural modes between 0 to 5 Hz, a 0.5 Hz spacing is used over this range with minimal (less than 5%) error. The unit load, $\hat{\mathbf{f}}_n(\omega, \mathbf{R})$, at any frequency, ω_k, is obtained by linear interpolation of the acoustic solutions at the two nearest frequencies, ω_i and ω_{i+1}, spaced 5 Hz apart. Linear interpolation is sufficient since the pressure load varies slowly over the 5 Hz range (linear interpolation of the structural response would not be acceptable over this range since it varies much more rapidly over the same interval).

Solution Management

[[

[3]]]

Upon completion of each frequency calculation, ANSYS is instructed to export the stresses which are stored in text files. There is one file per MSL per frequency per real/imaginary

component and each file contains the complete stress state over all nodes on the dryer. This format is convenient from a solution point of view. However, it makes it difficult to extract the stress response at a node since, in order to do so, thousands of files must be opened and searched through thousands of nodes until the node of interest is reached. [[

$^{(3)}$]]

Structural Damping

In harmonic analysis one has a broader selection of damping models than in transient simulations. A damping factor, z, of 1% critical damping is used in the structural analysis. In transient simulations, this damping can only be enforced exactly at two frequencies (where the damping model is "pinned"). Between these two frequencies the damping factor can by considerably smaller, for example 0.5% or less depending on the pinning frequencies. Outside the pinning frequencies, damping is higher. With harmonic analysis it is straightforward to enforce very close to 1% damping over the entire frequency range. In this damping model, the damping matrix, **D**, is set to

$$\mathbf{D} = \frac{2z}{\omega}\mathbf{K} \tag{7}$$

where **K** is the stiffness matrix and ω the forcing frequency. One can show that with this model the damping factor varies between 0.995% and 1.005% which is a much smaller variation than using the pinned model required in transient simulation.

Load Frequency Rescaling

One way to evaluate the sensitivity of the stress results to approximations in the structural modeling and applied loads is to rescale the frequency content of the applied loads. In this procedure the nominal frequencies, ω_k, are shifted to $(1+\lambda)\omega_k$, where the frequency shift, λ, ranges between $\pm 10\%$, and the response recomputed for the shifted loads. The objective of the frequency shifting can be explained by way of example. Suppose that in the actual dryer a strong structural-acoustic coupling exists at a particular frequency, ω^*. This means that the following conditions hold simultaneously: (i) the acoustic signal contains a significant signal at ω^*; (ii) the structural model contains a resonant mode of natural frequency, ω_n, that is near ω^* and (iii) the associated structural mode shape is strongly coupled to the acoustic load (i.e., integrating the product of the mode shape and the surface pressure over the steam dryer surface produces a significant modal force). Suppose now that because of discretization errors and modeling idealizations that the predicted resonance frequency differs from ω^* by a small amount (e.g., 1.5%). Then condition (ii) will be violated and the response amplitude therefore significantly diminished. By shifting the load frequencies one re-establishes condition (ii) when $(1+\lambda)\omega^*$ is near ω_n. The other two requirements also hold and a strong structural acoustic interaction is restored.

[[

[3]]]

Evaluation of Maximum and Alternating Stress Intensities

Once the unit solutions have been obtained, the computationally most intensive steps in the generation of stress intensities are: (i) the FFTs to evaluate stress time histories from (5) and (ii) the calculation of alternating stress intensities. [[

[3]]]

The high computational penalty incurred in calculating the alternating stress intensities is due to the fact that this calculation involves comparing the stress tensors at every pair of points in the stress history. This comparison is necessary since in general the principal stress directions can vary during the response, thus for N samples in the stress history, there will be (N-1)N/2 such pairs or, for N=64K (the number required to accurately resolve the spectrum up to 250 Hz in 0.01 Hz intervals), 2.1×10^9 calculations per node each requiring the determination of the roots to a cubic polynomial. [[

[3]]]

3. Finite Element Model Description

A description of the ANSYS model of the Browns Ferry Unit 2 and 3 steam dryer follows.

3.1 Steam Dryer Geometry

A geometric representation of the Browns Ferry Unit 2/3 steam dryer was developed from available drawings (provided by TVA and included in the design record file, DRF-TVA-250B) within the Workbench module of ANSYS. The completed model is shown in Figure 1. This model includes anticipated modifications to the Browns Ferry Unit 2/3 steam dryer. Namely, top tie rods are replaced with the thicker ones currently installed on Unit 1. The gussets on the top of the outer hoods supporting the steam dam plate were also cut away to facilitate installation of the new tie bars and possibly alleviate local stresses.

The modified areas are shown in Figure 2.

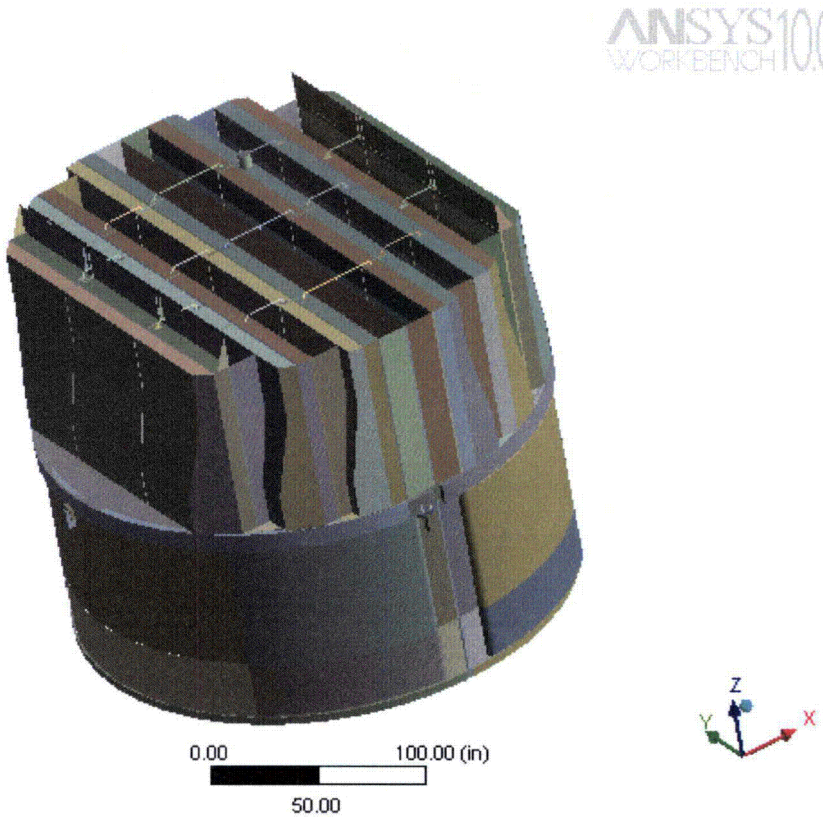

Figure 1. Overall geometry of the Browns Ferry Unit 2/3 steam dryer model.

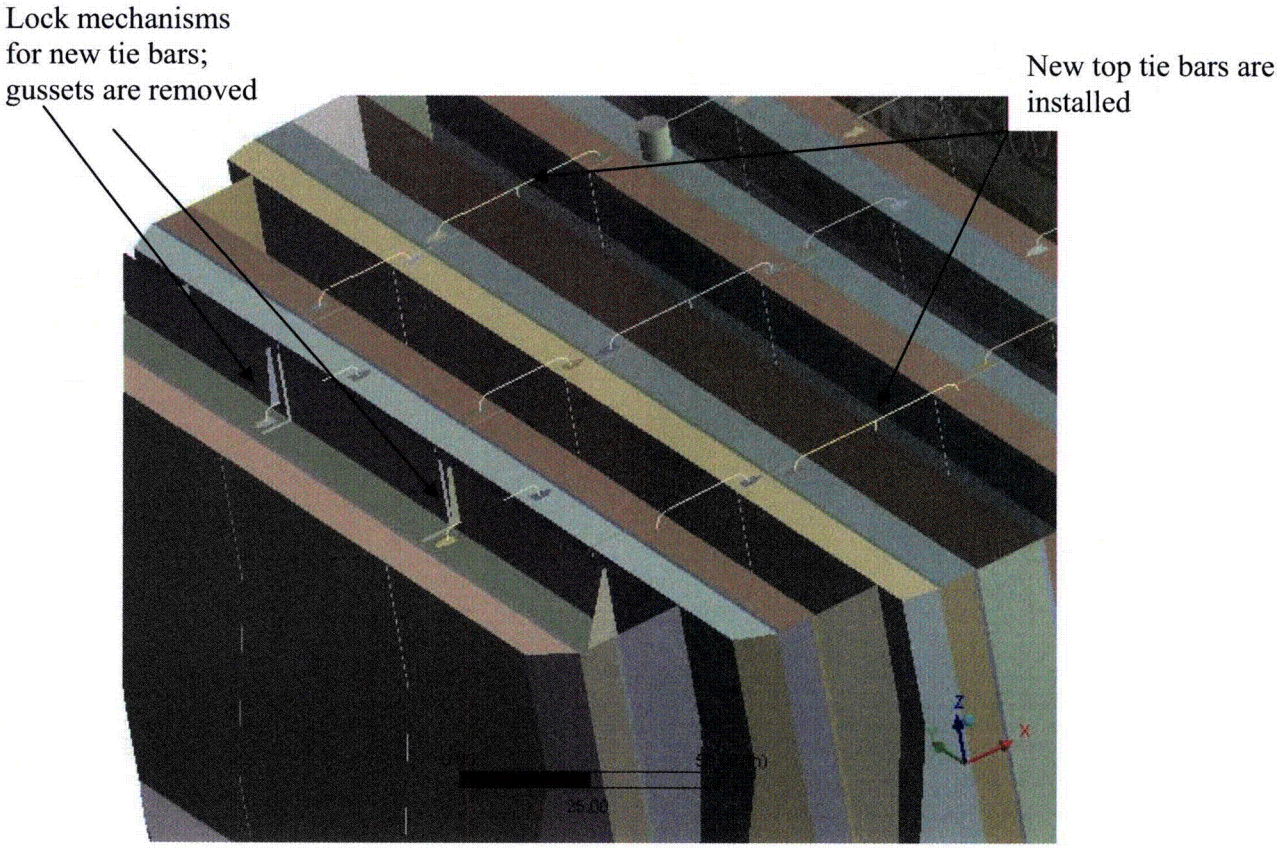

Figure 2. Anticipated modifications accounted for in the model and associated geometrical details.

3.2 Material Properties

The steam dryer is constructed from Type 304 stainless steel and has an operating temperature of 550°F. Properties used in the analysis are summarized below in Table 1.

Table 1. Material properties.

	Young's Modulus (10^6 psi)	Density (lbm/in^3)	Poisson Ratio
structural steel	25.55	0.284	0.3
structural steel with added water inertia	25.55	1.055	0.3

The structural steel modulus is taken from Appendix A of the ASME Code for Type 304 Stainless Steel at an operating temperature 550°F. The effective properties of perforated plates and submerged parts are discussed in Sections 3.4 and 3.6. Note that the increased effective density for submerged components is only used in the harmonic analysis. When calculating the stress distribution due to the static dead weight load, the unmodified density of steel (0.284 lbm/in^3) is used throughout.

3.3 Model Simplifications

The following simplifications were made to achieve reasonable model size while maintaining good modeling fidelity for key structural properties:

- Perforated plates were approximated as continuous plates using modified elastic properties designed to match the static and modal behaviors of the perforated plates. The perforated plate structural modeling is summarized in Section 3.4 and Appendix C.

- The drying vanes were replaced by point masses attached to the corresponding trough bottom plates and vane bank top covers. The bounding perforated plates, vane bank end plates, and vane bank top covers were explicitly modeled (see Section 3.5).

- The added mass properties of the lower part of the skirt below the reactor water level were obtained using a separate hydrodynamic analysis (see Section 3.6).

- [[

  (3)]]

- Four steam dryer support brackets that are located on the reactor vessel and spaced at 90° intervals were explicitly modeled. Fixed constraints (zero displacement) were imposed at the outer side of each bracket where it makes contact with the vessel wall. Nodal constraints (zero relative displacement) were introduced in the areas of contact between steam dryer and support brackets.

- Most welds were replaced by node-to-node connections; interconnected parts share common nodes along the welds. In other locations the constraint equations between nodal degrees of freedom were introduced as described in Section 3.9.

3.4 Perforated Plate Model

The perforated plates were modeled as solid plates with adjusted elastic and dynamic properties. Properties of the perforated plates were assigned according to the type and size of perforation. Based on [7], for an equilateral square pattern with given hole size and spacing, the effective moduli of elasticity were found.

The adjusted properties for the perforated plates are shown in Table 2 as ratios to material properties of structural steel, provided in Table 1. Locations of perforated plates are classified by steam entry / exit vane bank side and vertical position.

Tests were carried out to verify that this representation of perforated plates by continuous ones with modified elastic properties preserves the modal properties of the structure. These tests are summarized in Appendix C and compare the predicted first modal frequency for a cantilevered perforated plate against an experimentally measured value. The prediction was obtained for a 40% open area plate (the maximum open area ratio of the perforated plates at BFN2/3, as seen in Table 2) using the analytical formula for a cantilevered plate and the modified Young's modulus and Poisson's ratio given by O'Donnell [7]. The measured and predicted frequencies are in close agreement, differing by less than 3%.

[[

[3]]]

[[

[3]]]

Figure 3. [[

[3]]]

Table 2. Material properties of perforated plates.

[[

[3]]]

3.5 Vane Bank Model

The vane bank assemblies consist of many vertical angled plates that are computationally expensive to model explicitly, since a prohibitive number of elements would be required. These parts have significant weight which is transmitted through the surrounding structure, so it is important to capture their gross inertial properties. Here the vane banks are modeled as a collection of point masses located at the center of mass for each vane bank section (Figure 4). The following masses were used for the vane bank sections, based on data found on provided drawings:

inner banks, 1575 lbm, 4 sections per bank;

middle banks, 1450 lbm, total 4 sections per bank; and
outer banks, 1515 lbm, 3 sections per bank.

These masses were applied to the base plates and vane top covers using the standard ANSYS point mass modeling option, element MASS21. ANSYS automatically distributes the point mass inertial loads to the nodes of the selected structure. The distribution algorithm minimizes the sum of the squares of the nodal inertial forces, while ensuring that the net forces and moments are conserved. Vane banks are not exposed to main steam lines directly, but rather shielded by the hoods.

The collective stiffness of the vane banks is expected to be small compared to the surrounding support structure and is neglected in the model. In the static case it is reasonable to expect that this constitutes a conservative approach, since neglecting the stiffness of the vane banks implies that the entire weight is transmitted through the adjacent vane bank walls and supports. In the dynamic case the vane banks exhibit only a weak response since (i) they have large inertia so that the characteristic acoustically-induced forces divided by the vane masses and inertias yield small amplitude motions, velocities and accelerations; and (ii) they are shielded from acoustic loads by the hoods, which transfer dynamic loads to the rest of the structure. Thus, compared to the hoods, less motion is anticipated on the vane banks so that approximating their inertial properties with equivalent point masses is justified. Nevertheless, the bounding parts, such as perforated plates, side panels, and top covers, are retained in the model. Errors associated with the point mass representation of the vane banks are compensated for by frequency shifting of the applied loads.

3.6 Water Inertia Effect on Submerged Panels

Water inertia was modeled by an increase in density of the submerged structure to account for the added hydrodynamic mass. This added mass was found by a separate hydrodynamic analysis (included in DRF-TVA-250B supporting this report) to be 0.1928 lbm/in^2 on the submerged skirt area. This is modeled by effectively increasing the material density for the submerged portions of the skirt. Since the skirt is 0.25 inches thick, the added mass is equivalent to a density increase of 0.771 lbm/in^3. This added water mass was included in the ANSYS model by appropriately modifying the density of the submerged structural elements when computing harmonic response. For the static stresses, the unmodified density of steel is used throughout.

3.7 Structural Damping

Structural damping was defined as 1% of critical damping for all frequencies. This damping is consistent with guidance given on pg. 10 of NRC RG-1.20 [11].

3.8 Mesh Details and Element Types

Shell elements were employed to model the skirt, hoods, perforated plates, side and end plates, trough bottom plates, reinforcements, base plates and cover plates. Specifically, the four-node, Shell Element SHELL63, was selected to model these structural components. This element models bending and membrane stresses, but omits transverse shear. The use of shell elements is appropriate for most of the structure where the characteristic thickness is small compared to the other plate dimensions. For thicker structures, such as the upper and lower

support rings, solid brick elements were used to provide the full 3D stress. Tie bars were modeled with BEAM188 beam elements. The elements SURF154 are used to assure proper application of pressure loading to the structure. Mesh details and element types are shown in Table 3 and Table 4, respectively.

The mesh is generated automatically by ANSYS with adaptive refinement near edges. The maximum allowable mesh spacing is specified by the user. Here a 3 inch maximum allowable spacing is specified everywhere except in the following areas: drain pipes (2 inch maximum spacing); base plates (2.75 inches); perforated plates (2 inches); top tie rods (0.75 inches); and the curved portions of the drain channels (1.5 inches). Details of the finite element mesh are shown in Figure 5. Numerical experiments carried out using the ANSYS code applied to simple analytically tractable plate structures with dimensions and mesh spacings similar to the ones used for the steam dryer, confirm that the natural frequencies are accurately recovered (less than 1% errors for the first modes). These errors are compensated for by the use of frequency shifting.

3.9 Connections Between Structural Components

Most connections between parts are modeled as node-to-node connections. This is the correct manner (i.e., within the finite element framework) of joining elements away from discontinuities. At joints between shells, this approach omits the additional stiffness provided by the extra weld material. Also, locally 3D effects are more pronounced. The latter effect is accounted for using weld factors. The deviation in stiffness due to weld material is negligible, since weld dimensions are on the order of the shell thickness. The consequences upon modal frequencies and amplitude are, to first order, proportional to t/L where t is the thickness and L a characteristic shell length. The errors committed by ignoring additional weld stiffness are thus small and readily compensated for by performing frequency shifts.

When joining shell and solid elements, however, the problem arises of properly constraining the rotations, since shell element nodes contain both displacement and rotational degrees of freedom at every node whereas solid elements model only the translations. A node-to-node connection would effectively appear to the shell element as a simply supported, rather than (the correct) cantilevered restraint and significantly alter the dynamic response of the shell structure.

To address this problem, constraint equations are used to properly connect adjacent shell- and solid-element modeled structures. Basically, all such constraints express the deflection (and rotation for shell elements) of a node, $\mathbf{R}_1$, on one structural component in terms of the deflections/rotations of the corresponding point, $\mathbf{P}_2$, on the other connected component. Specifically, the element containing $\mathbf{P}_2$ is identified and the deformations at $\mathbf{P}_2$ determined by interpolation between the element nodes. The following types of shell-solid element connections are used in the steam dryer model including the following:

1. Connections of shell faces to solid faces (Figure 6a). While only displacement degrees of freedom are explicitly constrained, this approach also implicitly constrains the rotational degrees of freedom when multiple shell nodes on a sufficiently dense grid are connected to the same solid face.
2. Connections of shell edges to solids (e.g., connection of the bottom of closure plates with the upper ring). Since solid elements do not have rotational degrees of freedom, the

coupling approach consisted of having the shell penetrate into the solid by one shell thickness and then constraining both the embedded shell element nodes (inside the solid) and the ones located on the surface of the solid structure (see Figure 6b). Numerical tests involving simple structures showed that this approach and penetration depth reproduce both the deflections and stresses of the same structure modeled using only solid elements or ANSYS' bonded contact technology. Continuity of rotations and displacements is achieved.

The use of constraint conditions rather than the bonded contacts advocated by ANSYS for connecting independently meshed structural components confers better accuracy and useful numerical advantages to the structural analysis of the steam dryer including better conditioned and smaller matrices. The smaller size results from the fact that equations and degrees of freedom are eliminated rather than augmented (in Lagrange multiplier-based methods) by additional degrees of freedom. Also, the implementation of contact elements relies on the use of very high stiffness elements (in penalty function-based implementations) or results in indefinite matrices (Lagrange multiplier implementations) with poorer convergence behavior compared to positive definite matrices.

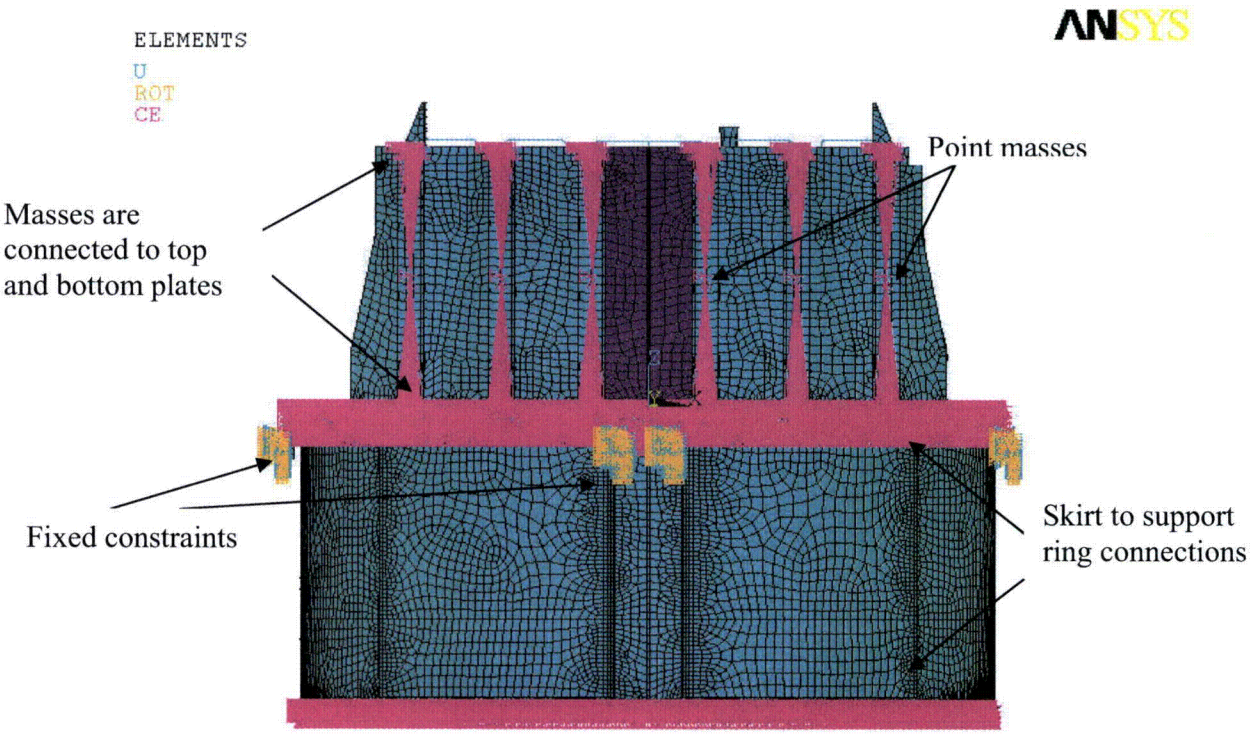

Figure 4. Point masses representing the vanes. The pink shading represents where constraint equations between nodes are applied.

Table 3. FE Model Summary.

Description	Quantity
Total Nodes[1]	94,655
Total Elements	115,645

1. Not including additional damper nodes and elements.

Table 4. Listing of Element Types.

Generic Element Type Name	Element Name	ANSYS Name
20-Node Quadratic Hexahedron	SOLID186	20-Node Hexahedral Structural Solid
10-Node Quadratic Tetrahedron	SOLID187	10-Node Tetrahedral Structural Solid
4-Node Elastic Shell	SHELL63	4-Node Elastic Shell
Mass Element	MASS21	Structural Mass
Pressure Surface Definition	SURF154	3D Structural Surface Effect
Beam element	BEAM188	3-D Finite Strain Beam
Damper element	COMBIN14	Spring-Damper

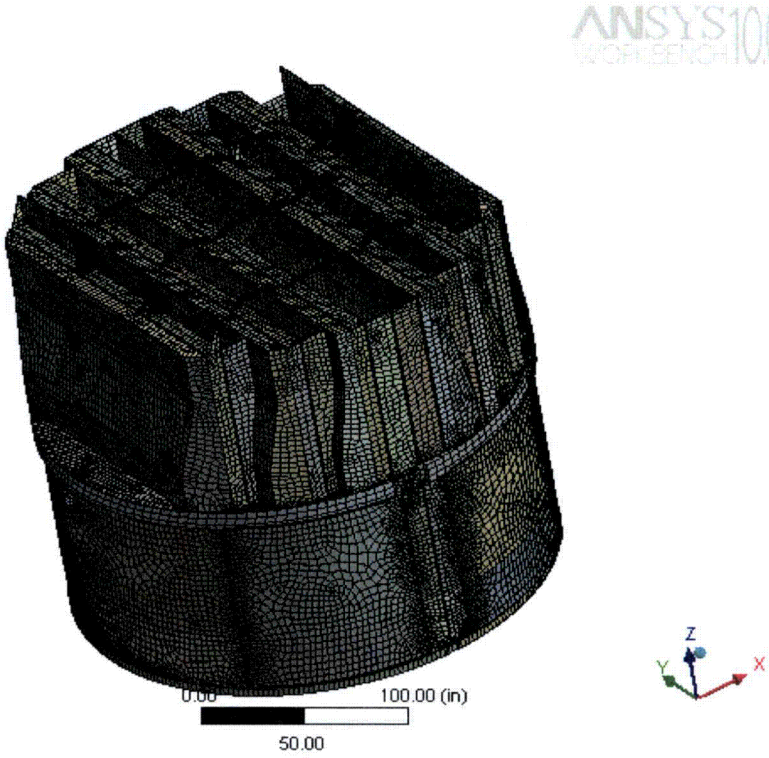

Figure 5a. Mesh overview.

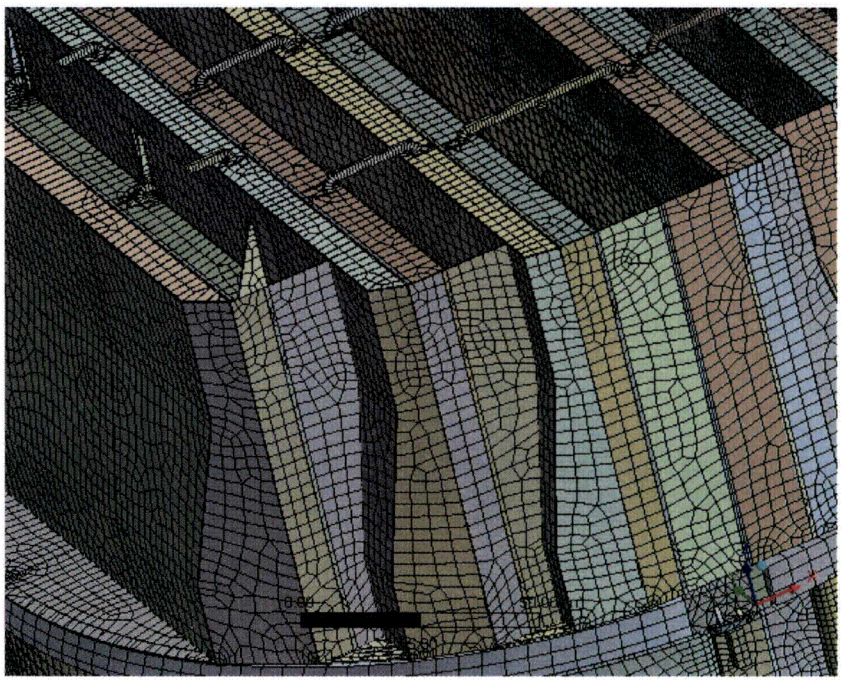

Figure 5b. Close-up of mesh showing modified tie bars.

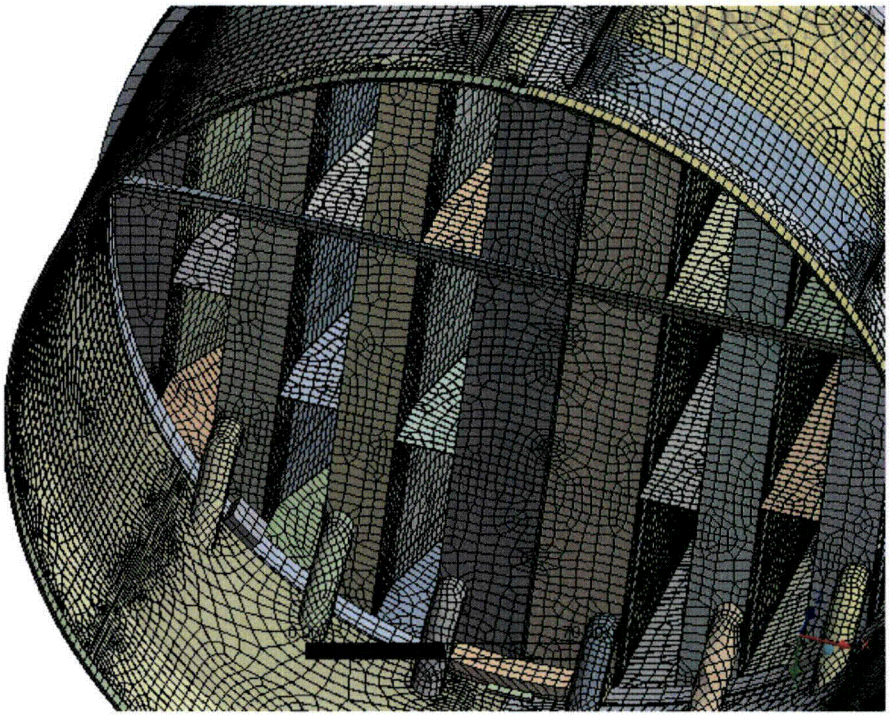

Figure 5c. Close-up of mesh showing drain pipes and hood supports.

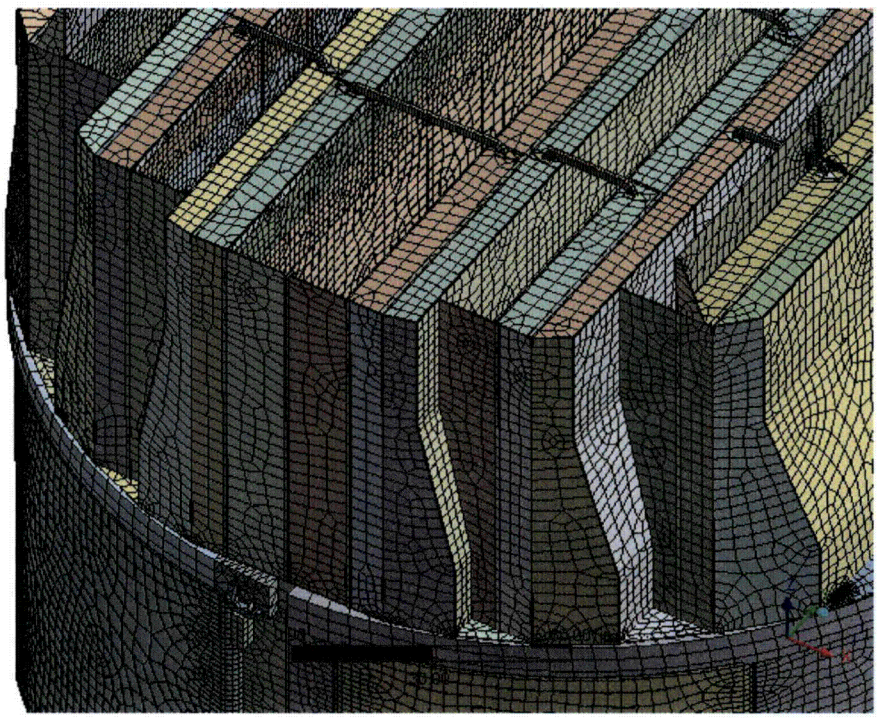

Figure 5d. Close-up of mesh showing node-to-node connections between various plates.

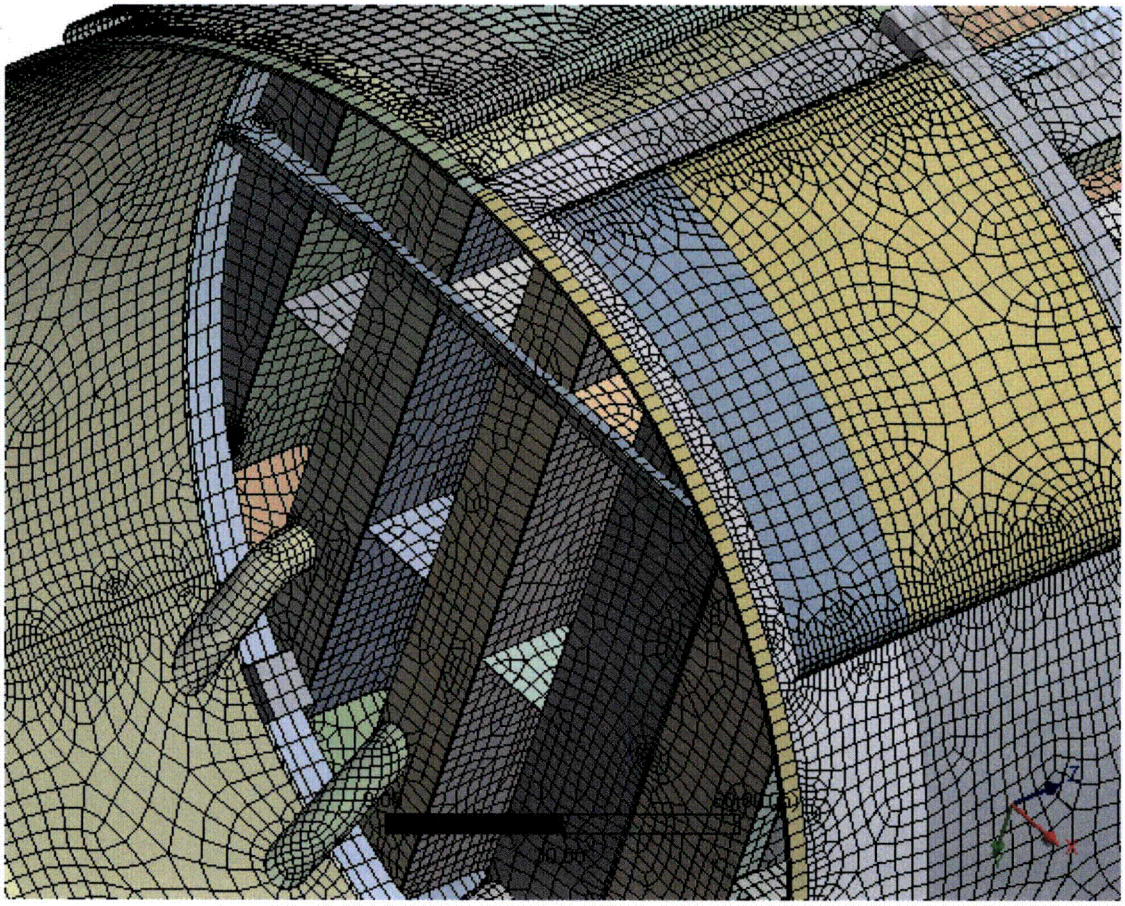

Figure 5e. Close-up of mesh showing node-to-node connections between the skirt and drain channels; supporting beams and base plates; hood supports and hoods.

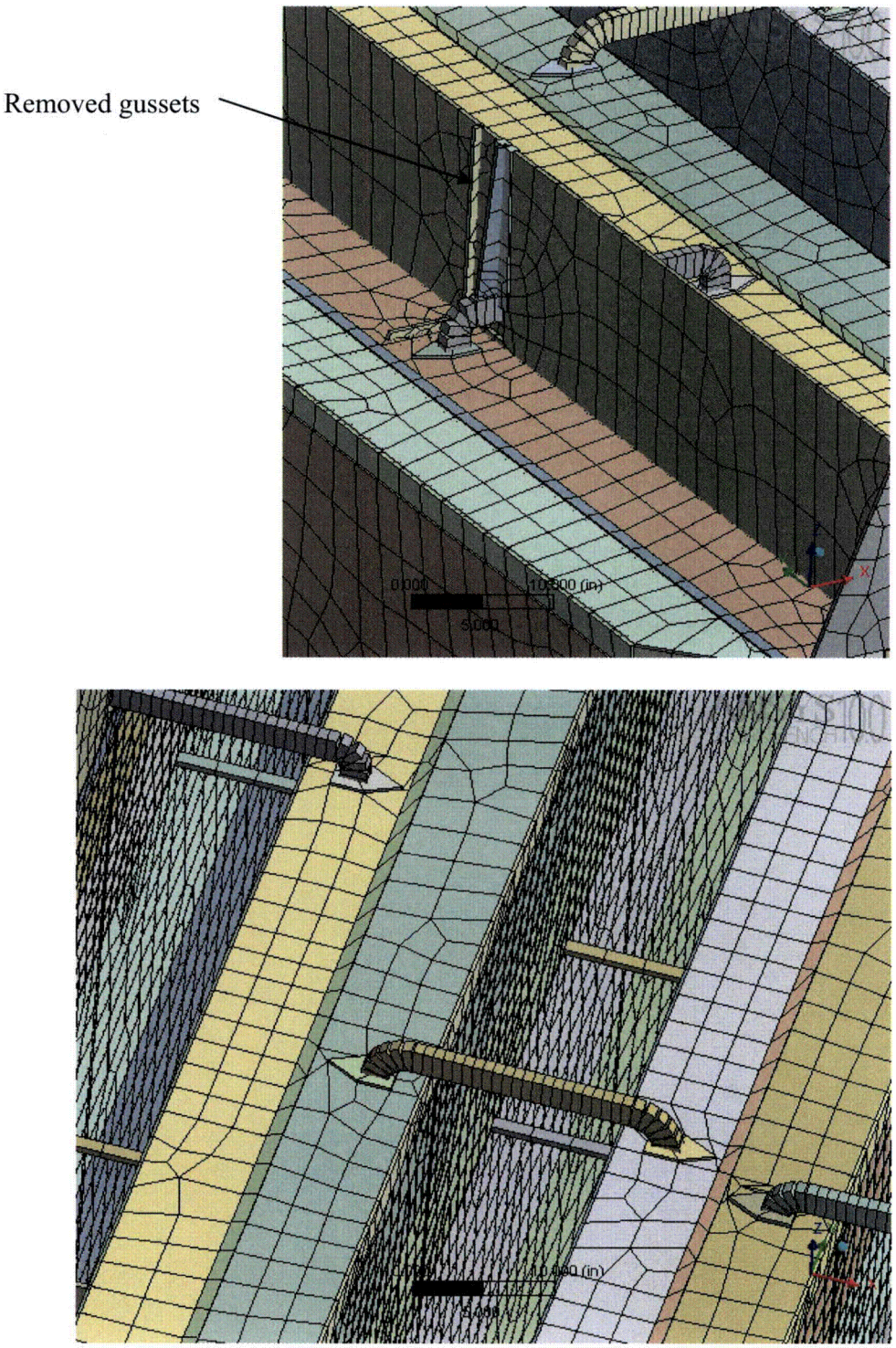

Figure 5f. Close-up view of tie bars connecting vane cover plates and adjacent to the steam dam.

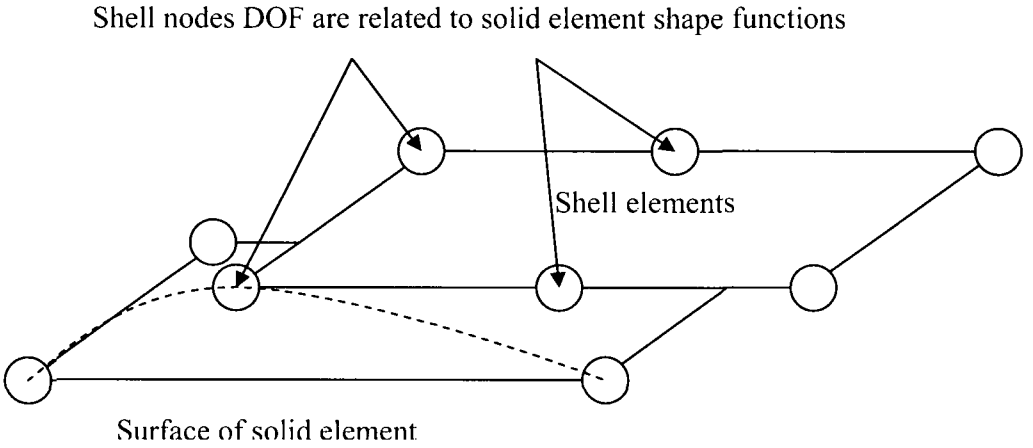

Figure 6a. Face-to-face shell to solid connection.

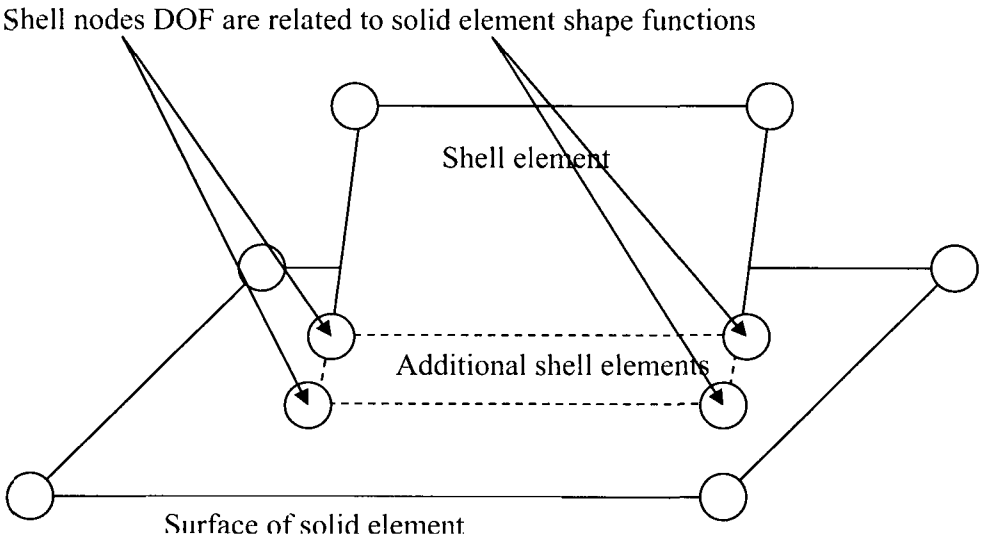

Figure 6b. Shell edge-to-solid face connection.

3.10 Pressure Loading

The harmonic loads are produced by the pressures acting on the exposed surfaces of the steam dryer. At every frequency and for each MSL, the pressure distribution corresponding to a unit pressure at the MSL inlet is represented on a three-inch grid lattice grid (i.e., a mesh whose lines are aligned with the x-, y- and z-directions) that is superimposed over the steam dryer surface. This grid is compatible with the "TableLoads" format used by ANSYS to "paint" general pressure distributions upon structural surfaces. The pressures are obtained from the Helmholtz solver routine in the acoustic analysis [1].

In general, the lattice nodes do not lie on the surface, so that to obtain the pressure differences at the surface it is necessary to interpolate the pressure differences stored at the lattice nodes. This is done using simple linear interpolation between the eight forming nodes of the lattice cell containing the surface point of interest. Inspection of the resulting pressures at selected nodes shows that these pressures vary in a well-behaved manner between the nodes with prescribed pressures. Graphical depictions of the resulting pressures and comparisons between the peak pressures in the original nodal histories and those in the final surface load distributions produced in ANSYS, all confirm that the load data are interpolated accurately and transferred correctly to ANSYS.

The harmonic pressure loads are only applied to surfaces above the water level, as indicated in Figure 7. In addition to the pressure load, the static loading induced by the weight of the steam dryer is analyzed separately. The resulting static and harmonic stresses are linearly combined to obtain total values which are then processed to calculate maximum and alternating stress intensities for assessment in Section 5.

[[

[3]]] This is useful since revisions in the loads model do not necessitate recalculation of the unit stresses.

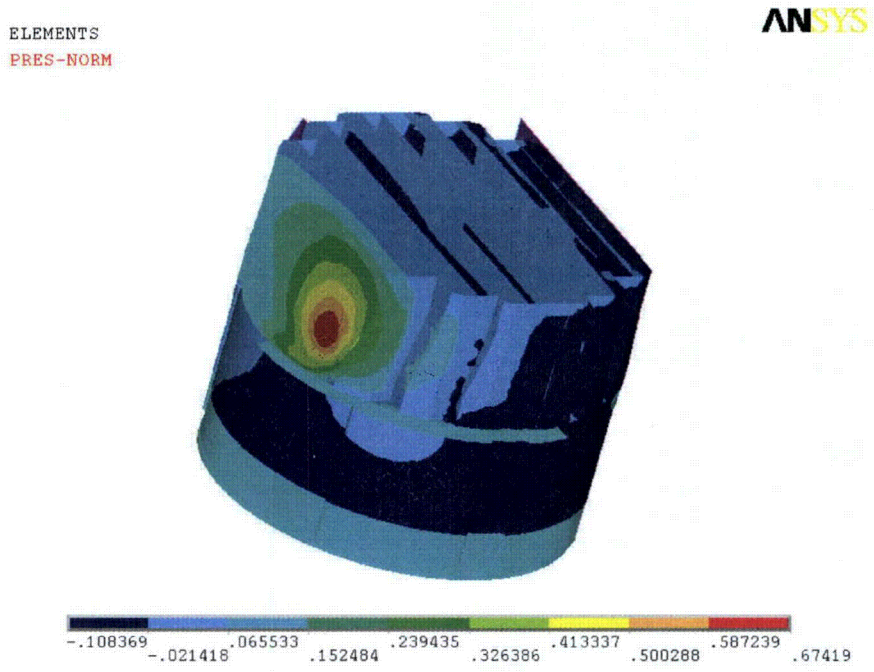

Frequency no. 372: 50.2 Hz

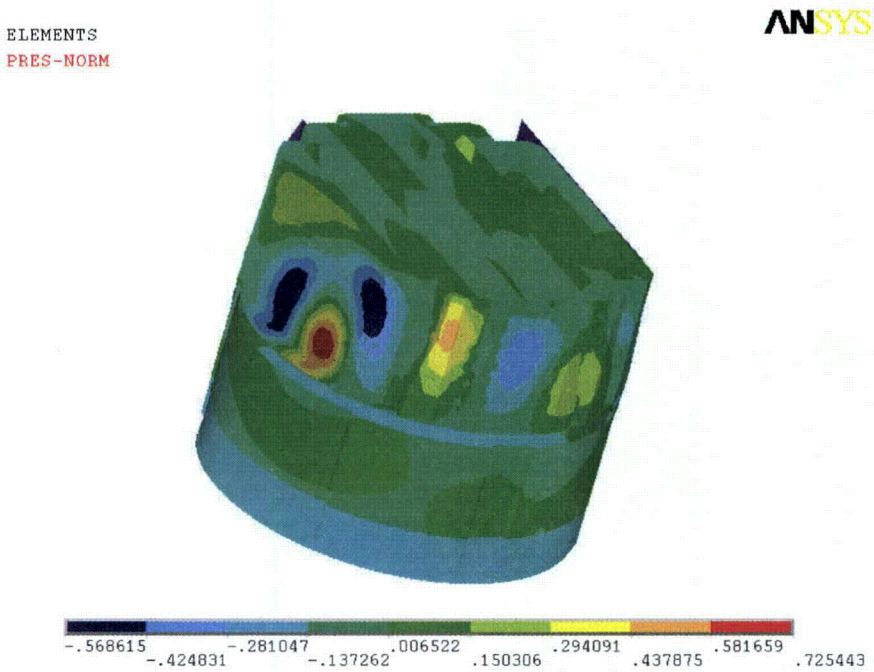

Frequency no. 589: 200.89 Hz

Figure 7. Real part of unit pressure loading MSL C (in psid) on the steam dryer at different frequencies. No loading is applied to the submerged light blue surface, solid support rings and dividing plates above the outer hoods.

4. Structural Analysis

The solution is decomposed into static and harmonic parts, where the static solution produces the stress field induced by the supported structure subjected to its own weight and the harmonic solution accounts for the harmonic stress field due to the unit pressure of given frequency in one of the main steam lines. All solutions are linearly combined, with amplitudes provided by signal measurements in each steam line, to obtain the final displacement and stress time histories. This decomposition facilitates the prescription of the added mass model accounting for hydrodynamic interaction and allows one to compare the stress contributions arising from static and harmonic loads separately. Proper evaluation of the maximum membrane and membrane+bending stresses requires that the static loads due to weight be accounted for. Hence both static and harmonic analyses are carried out.

4.1 Static Analysis

The results of the static analysis are shown in Figure 8. The locations with highest stress include the upper support ring areas near support brackets with stress intensity 6,496 psi; outer hood above upper support ring with stress intensity 5,158 psi; top of closure plates with stress intensity 4,048 psi. Close up views of these locations are shown in Figure 9.

4.2 Harmonic Analysis

The harmonic pressure loads were applied to the structural model at all surface nodes described in Section 3.10. Typical stress intensity distributions over the structure are shown in Figure 10. Stresses were calculated for each frequency, and results from static and harmonic calculations were combined.

To evaluate maximum stresses, the stress harmonics including the static component are transformed into a time history using FFT, and the maximum and alternating stress intensities for the response, evaluated. According to ASME B&PV Code, Section III, Subsection NG-3216.2 the following procedure was established to calculate alternating stresses. For every node, the stress difference tensors, $\boldsymbol{\sigma}'_{nm} = \boldsymbol{\sigma}_n - \boldsymbol{\sigma}_m$, are considered for all possible pairs of the stresses σ_n and σ_m at different time levels, t_n and t_m. Note that all possible pairs require consideration since there are no "obvious" extrema in the stress responses. However, in order to contain computational cost, extensive screening of the pairs takes place (see Section 2.3) so that pairs known to produce alternating stress intensities less than 1500 psi are rejected. For each remaining stress difference tensor, the principal stresses S_1, S_2, S_3 are computed and the maximum absolute value among principal stress differences, $S_{nm} = \max\{|S_1 - S_2|, |S_1 - S_3|, |S_2 - S_3|\}$, obtained. The alternating stress at the node is then one-half the maximum value of S_{nm} taken over all combinations (n,m), i.e., $S_{alt} = \frac{1}{2}\max_{n,m}\{S_{nm}\}$. This alternating stress is compared against allowable values, depending on the node location with respect to welds.

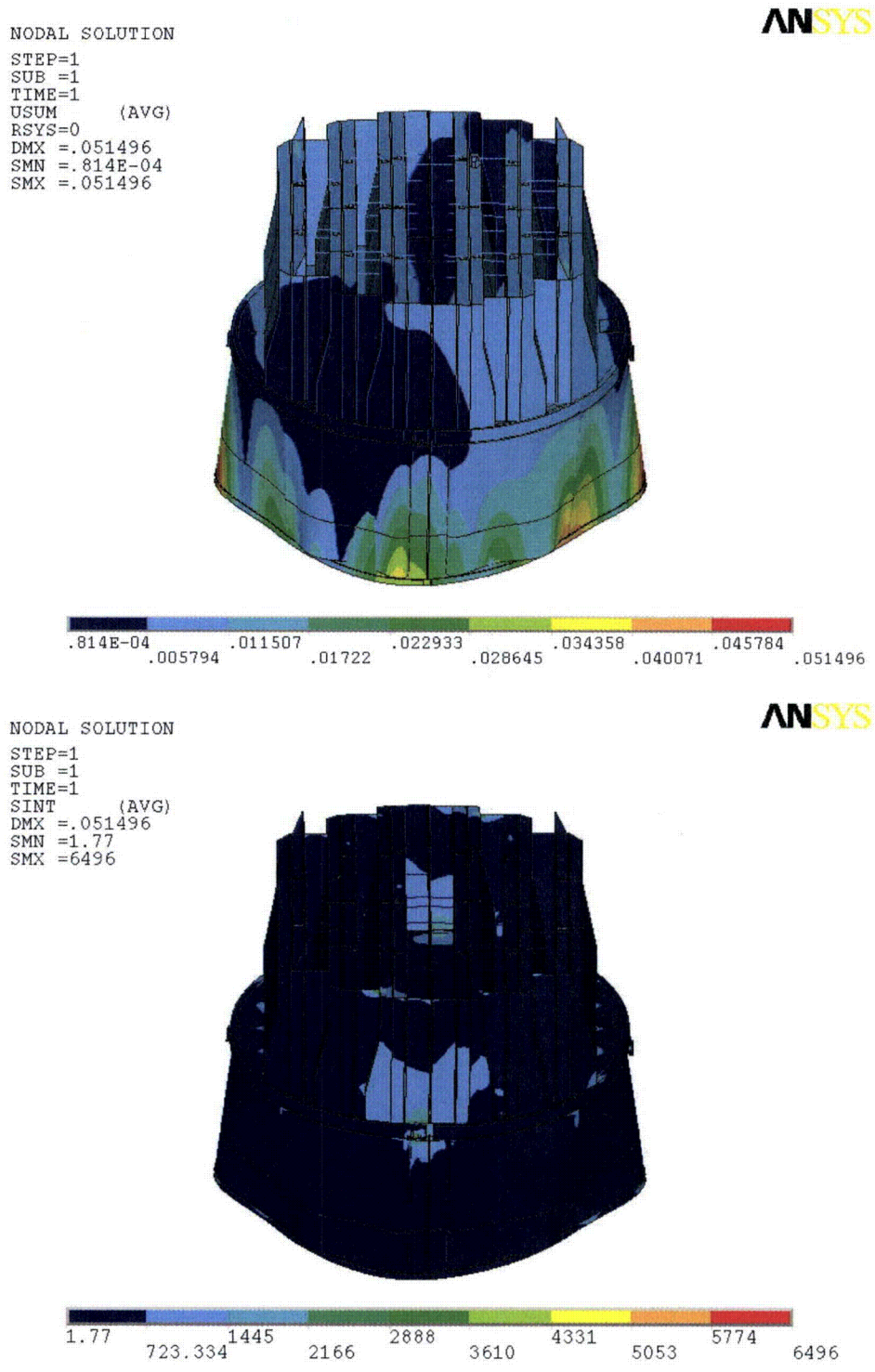

Figure 8. Overview of static calculations showing displacements (top, in inches) and stress intensities (bottom, in psi). Maximum displacement (DMX) is 0.05 inches; maximum stress intensity (SMX) is 6,496 psi. Note that displacements are amplified for visualization.

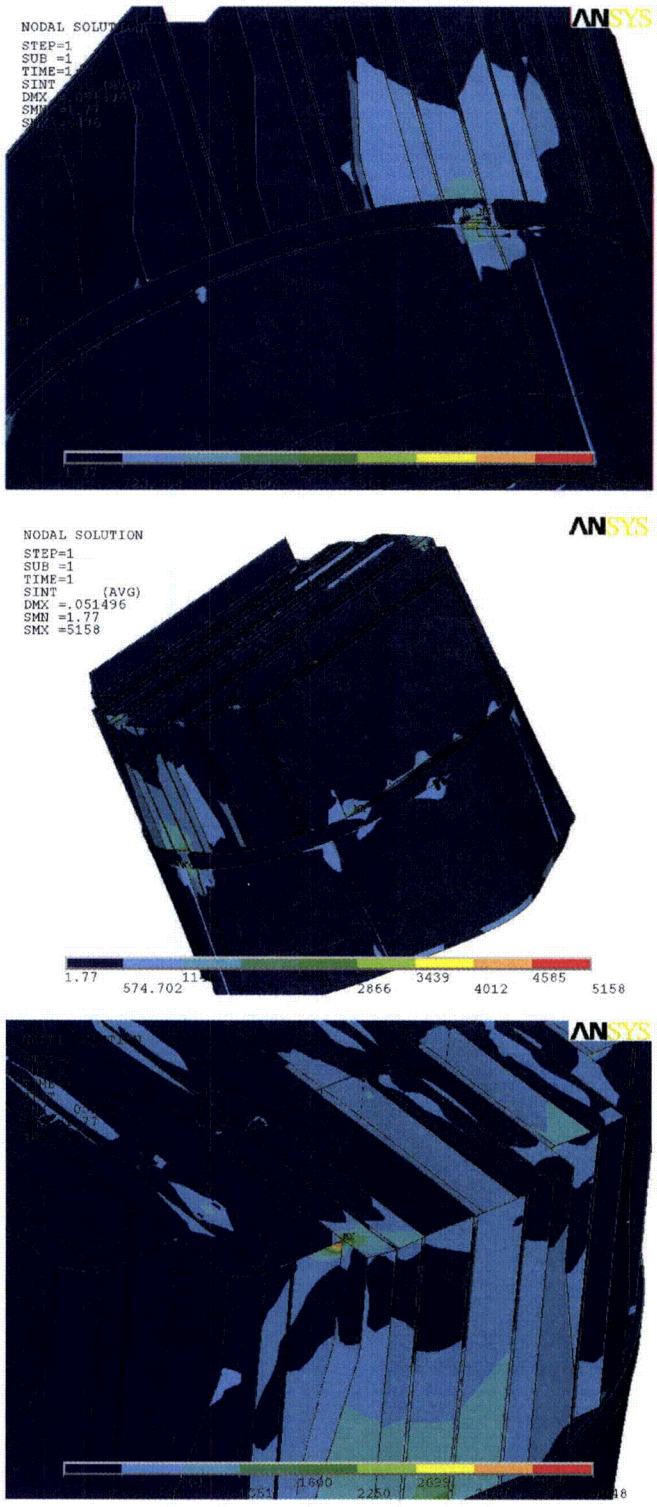

Figure 9. Close-up of high static stress intensity (in psi) locations near support brackets, at outer hood, and at closure plates.

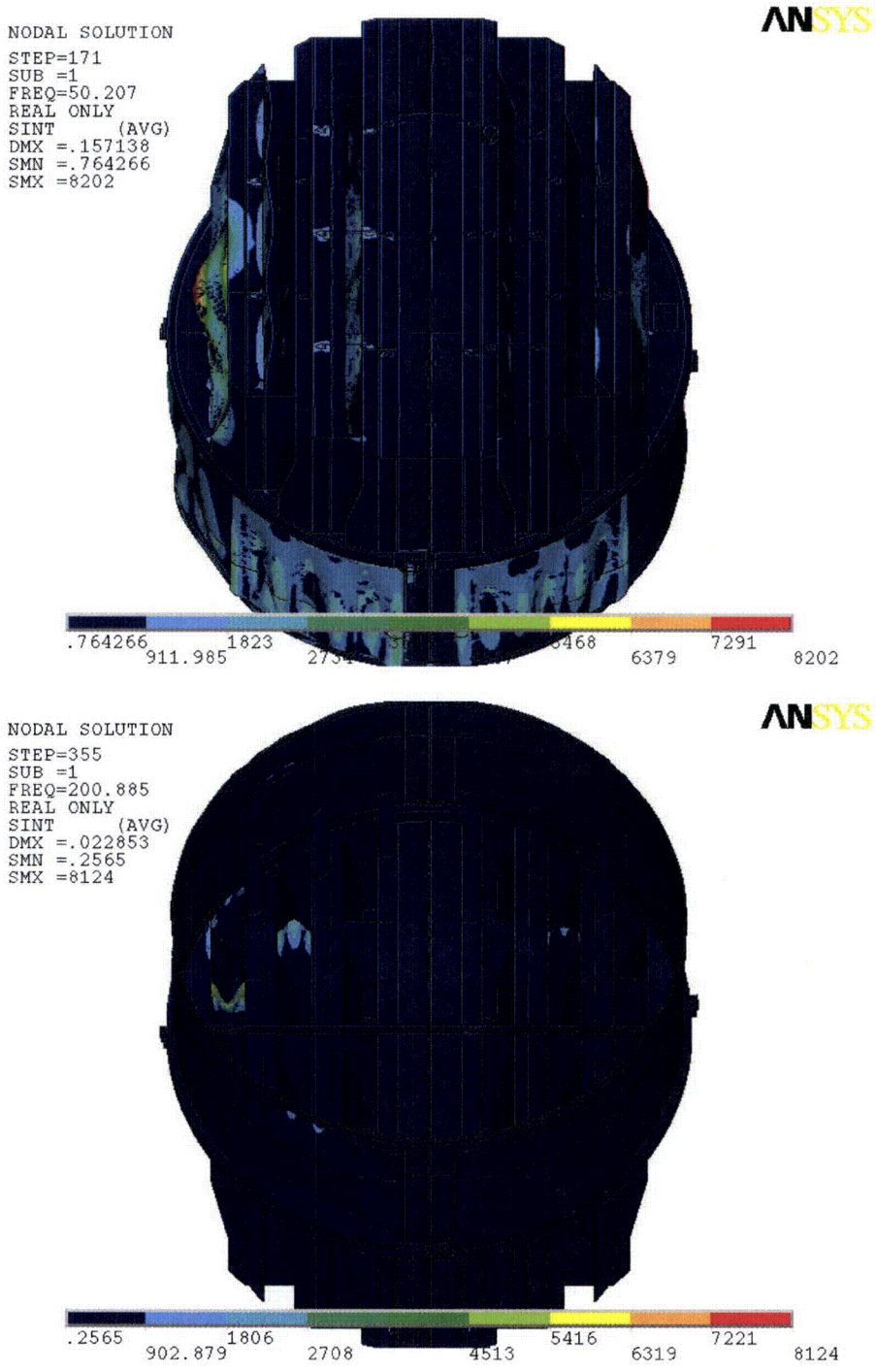

Figure 10. Overview of harmonic calculations showing real part of stress intensities (in psi) along with displacements. Unit loading MSL C for frequencies 50.2 Hz (top) and 200.9 Hz (bottom, oriented to show high stress locations).

4.3 Post-Processing

The static and transient stresses computed at every node with ANSYS were exported into files for subsequent post-processing. These files were then read into separate customized software to compute the maximum and alternating stresses at every node. The maximum stress was defined for each node as the largest stress intensity occurring during the time history. Alternating stresses were calculated according to the ASME standard described above. For shell elements the maximum stresses were calculated separately at the mid-plane, where only membrane stress is present, and at top/bottom of the shell, where bending stresses are also present.

For nodes that are shared between several structural components or lie on junctions, the maximum and alternating stress intensities are calculated as follows. First the nodal stress tensor is computed separately for each individual component by averaging over all finite elements meeting at the node and belonging to the same structural component. The time histories of these stress tensors are then processed to deduce the maximum and alternating stress intensities for each structural component. Finally for nodes shared across multiple components the highest of the component-wise maximum and alternating stresses is recorded as the "nodal" stress. This approach prevents averaging of stresses across components and thus yields conservative estimates for nodal stresses at the weld locations where several components are joined together.

The maximum stresses are compared against allowable values which depend upon the stress type (membrane, membrane+bending, alternating – Pm, Pm+Pb, S_{alt}) and location (at a weld or away from welds). These allowables are specified in the following section. For solid elements the most conservative allowable for membrane stress, Pm, is used, although bending stresses are nearly always present also. The structure is then assessed in terms of stress ratios formed by dividing allowables by the computed stresses at every node. Stress ratios less than unity imply that the associated maximum and/or alternating stress intensities exceed the allowable levels. Post-processing tools calculate the stress ratios, identifying the nodes with low stress ratios and generating files formatted for input to the 3D graphics program, TecPlot, which provides more general and sophisticated plotting options than currently available in ANSYS.

4.4 Computation of Stress Ratios for Structural Assessment

The ASME B&PV Code, Section III, subsection NG provides different allowable stresses for different load combinations and plant conditions. The stress levels of interest in this analysis are for the normal operating condition, which is the Level A service condition. The load combination for this condition is:

Normal Operating Load Combination = Weight + Pressure + Thermal

The weight and fluctuating pressure contributions have been calculated in this analysis and are included in the stress results. The static pressure differences and thermal expansion stresses are small, since the entire steam dryer is suspended inside the reactor vessel and all surfaces are exposed to the same conditions. Seismic loads only occur in Level B and C cases, and are not considered in this analysis.

Allowable Stress Intensities

The ASME B&PV Code, Section III, subsection NG shows the following (Table 5) for the maximum allowable stress intensity (Sm) and alternating stress intensity (Sa) for the Level A service condition. The allowable stress intensity values for type 304 stainless steel at operating temperature 550°F are taken from Table I-1.2 and Fig. I-9.2.2 of Appendix I of Section III, in the ASME B&PV Code. The calculation for different stress categories is performed in accordance with Fig. NG-3221-1 of Division I, Section III, subsection NG.

Table 5. Maximum Allowable Stress Intensity and Alternating Stress Intensity for all areas other than welds. The notation Pm represents membrane stress; Pb represents stress due to bending; Q represents secondary stresses (from thermal effects and gross structural discontinuities, for example); and F represents additional stress increments (due to local structural discontinuities, for example).

Type	Notation	Service Limit	Allowable Value (psi)
Maximum Stress Allowables:			
General Membrane	Pm	Sm	18,300
Membrane + Bending	Pm + Pb	1.5 Sm	27,450
Primary + Secondary	Pm + Pb + Q	3.0 Sm	54,900
Alternating Stress Allowable:			
Peak = Primary + Secondary + F	S_{alt}	Sa	13,600

When evaluating welds, either the calculated or allowable stress was adjusted, to account for stress concentration factor and weld quality. Specifically:

- For maximum allowable stress intensity, the allowable value is decreased by multiplying its value in Table 5 by 0.55.

- For alternating stress intensity, the calculated weld stress intensity is multiplied by a weld stress intensity (fatigue) factor of 1.8, before comparison to the Sa value given above.

The weld factors of 0.55 and 1.8 were selected based on the observable quality of the shop welds and liquid penetrant NDE testing of all welds (excluding tack and intermittent welds, which were subject to 5X visual inspection) during fabrication. These factors are consistent with fatigue strength reduction factors recommended by the Welding Research Council, [12], and stress concentration factors at welds, provided in [13] and [14]. In addition, critical welds are subject to periodical visual inspections in accordance with the requirements of GE SIL 644 SIL and BWR VIP-139 [15]. Therefore, for weld stress intensities, the allowable values are shown in Table 6.

These factors (0.55 and 1.8) also conservatively presume that the structure is joined using fillet welds unless specified otherwise. Since fillet welds correspond to larger stress concentration factors than other types of welds, this assumption is a conservative one.

Table 6. Weld Stress Intensities.

Type	Notation	Service Limit	Allowable Value (psi)
Maximum Stress Allowables:			
General Membrane	Pm	0.55 Sm	10,065
Membrane + Bending	Pm + Pb	0.825 Sm	15,098
Primary + Secondary	Pm + Pb + Q	1.65 Sm	30,195
Alternating Stress Allowables:			
Peak = Primary + Secondary + F	S_{alt}	Sa	13,600

Comparison of Calculated and Allowable Stress Intensities

The classification of stresses into general membrane or membrane + bending types was made according to the exact location, where the stress intensity was calculated; namely, general membrane, Pm, for middle surface of shell element, and membrane + bending, Pm + Pb, for other locations. For solid elements the most conservative, general membrane, Pm, allowable is used.

The structural assessment is carried out by computing stress ratios between the computed maximum and alternating stress intensities, and the allowable levels. Locations where any of the stresses exceed allowable levels will have stress ratios less than unity. Since computation of stress ratios and related quantities within ANSYS is time-consuming and awkward, a separate FORTRAN code was developed to compute the necessary maximum and alternating stress intensities, Pm, Pm+Pb, and S_{alt}, and then compare it to allowables. Specifically, the following quantities were computed at every node:

1. The maximum membrane stress intensity, Pm (evaluated at the mid-thickness location for shells),
2. The maximum membrane+bending stress intensity, Pm+Pb, (taken as the largest of the maximum stress intensity values at the bottom, top, and mid thickness locations, for shells),
3. The alternating stress, S_{alt}, (the maximum value over the three thickness locations is taken).
4. The stress ratio due to a maximum stress intensity assuming the node lies at a non-weld location (note that this is the minimum ratio obtained considering both membrane stresses and membrane+bending stresses):
   SR-P(nw) = min{ Sm/Pm, 1.5 * Sm/(Pm+Pb) }.
5. The alternating stress ratio assuming the node lies at a non-weld location,
   SR-a(nw) = Sa / (1.1 * S_{alt}),
6. The same as 4, but assuming the node lies on a weld,
   SR-P(w)=SR-P(nw) * f_{sw} * 0.55
7. The same as 5, but assuming the node lies on a weld,
   SR-a(w)=SR-a(nw) * f_{sw} / 1.8.

where f_{sw}=1 at all welds (when justified, f_{sw} can be adjusted to reflect different weld types). Note that in steps 4 and 6, the minimum of the stress ratios based on Pm and Pm+Pb, is taken. The allowables listed in Table 5, Sm=18,300 psi and Sa=13,600 psi. The factors, 0.55 and 1.8, are the weld factors discussed above. The factor of 1.1 accounts for the differences in Young's moduli for the steel used in the steam dryer and the values assumed in alternating stress allowable. According to NG-3222.4 in subsection NG of Section III of the ASME Code, the effect of elastic modulus upon alternating stresses is taken into account by multiplying alternating stress S_{alt} at all locations by the ratio, E/E_{model}=1.1, where:

$E = 28.3\ 10^6$ psi, as shown on Fig. I-9.2.2. ASME BP&V Code
$E_{model} = 25.55\ 10^6$ psi (Table 1)

The nodes with stress ratios lower than 4 are plotted in TecPlot (a 3D graphics plotting program widely used in engineering communities [16]) to establish whether they lie on a weld or not. The appropriate maximum and alternating stress ratios, SR-P and SR-a, are thus determined and a final listing of nodes having the smallest stress ratios is generated. These nodes are tabulated and depicted in the Results Sections.

5. Results

5.1 General Stress Distribution and High Stress Locations

The maximum stress intensities obtained by post-processing the ANSYS stress histories for CLTP at nominal frequency and with frequency shift operating conditions are listed in Table 7. Contour plots of the stress intensities over the steam dryer structure are shown on Figure 11 (nominal frequency), Figure 12 (maximum stress over all nine frequency shifts including nominal), Figure 13 (-10% frequency shift), and Figure 14 (+10% frequency shift). The figures are oriented to emphasize the high stress regions. Note that these stress intensities *do not* account for weld factors. Further, it should be noted that since the allowable stresses vary with location, stress intensities do not necessarily correspond to regions of primary structural concern. Instead, structural evaluation is more accurately made in terms of the stress ratios which compare the computed stresses to allowable levels with due account made for stress type and weld factors. Comparisons on the basis of stress ratios are made in Section 5.2.

The tabulated stresses are obtained by computing the relevant stress intensities at every node and then sorting the nodes according to stress levels. The highest stress node is noted and all neighboring nodes within 10 inches of the highest stress node and its symmetric images (i.e., reflections across the x=0 and y=0 planes) are "blanked" (i.e., excluded from the search for subsequent high stress locations). Of the remaining nodes, the next highest stress node is identified and its neighbors (closer than 10 inches) blanked. The third highest stress node is similarly located and the search continued in this fashion until all nodes are either blanked or have stresses less than half the highest value on the structure or stress ratios lower than 4. The blanking of neighboring nodes is intended to prevent extracting peak stress nodes from essentially the same location on the structure.

The maximum stress intensities in most areas are low (less than 500 psi). For the membrane stresses (Pm) the high stress regions tend to occur at: (i) the restraint locations for the upper support ring; (ii) the upper edges of the closure plates and (iii) junctions connecting the bottoms of the hood supports. The first location experiences high stresses since the entire weight of the structure is transmitted through relatively small pads to the external structure. The stress is dominated by the static component since the stress intensities at this location do not vary significantly with frequency shift and alternating stress intensities remain below 1500 psi at all shifts (see first row in Table 7b). The closure plates experience high stresses since they restrain any motion of the adjacent vane banks. The associated stresses also contain a larger contribution from acoustic loading as is evident in the last column in Table 7 recording the alternating stress intensities. The junctions where the hoods, hood supports and base or cover plates meet also experience high stresses. While membrane stresses at these junctions do not change significantly with frequency shift (variations in stress intensity are approximately 1000 psi), the bending and alternating stresses exhibit much stronger frequency dependence as discussed next.

The membrane + bending stress (Pm+Pb) distributions evidence a strong modal response in all cases, especially at the -10% frequency shift. The strongest response (and highest stress intensity) at any frequency shift occurs on the bottoms of the outer hood supports where they connect to the outer hoods and cover plates as seen in Figure 12b and c. The portion of the outer hood between the supports also shows a strong response. The response at this location is also

strongly dependent on frequency shift. At nominal loading (no frequency shift) and +10% frequency shift the stress intensity is approximately one half the value at the -10% shift. Structural acoustic responses are also observed on the skirt and drain channels where high wave number modes occur in both the circumferential and vertical directions (e.g., on the drain channels and skirts respectively in Figure 11b) and the middle closure plates Stress concentrations are observed at several locations coinciding with welds including: (i) junctions between hood supports and other components (hood, vane bank, base plate or cover plate); (ii) where the closure plates connect to the hoods or vane bank end plates; and (iii) along the skirt/drain channel welds.

The alternating stress, S_{alt}, distributions are qualitatively similar to those for Pm+Pb, but are much more localized. This is true for all frequency shifts and is due to the presence of a single 218 Hz dominant frequency in the load spectrum (see discussion in Section 5.3). The alternating stress intensity contour plots essentially record the modes excited by this signal, which here are seen to be confined to: (i) the bottoms of the outer and middle hood supports, especially at -10% to 0% frequency shifts; (ii) the outer hoods (all frequency shifts); (iii) inner closure plates and vane bank end plates (for 0% to +10% frequency shifts) and (iv) the skirt and drain channels (most pronounced at nominal frequency). Interestingly, at -10% frequency shift the hood supports are the only components that are strongly excited with the remaining structure relatively quiescent (see Figure 13c and d). The strong response of these components is not surprising since they essentially comprise plates that are thin (and therefore easily excited) and of large dimension so that they support a significant number of response modes over the applied load frequency range. Since the submerged skirt and hood supports are not subjected to pressure loads the responses are due to modal excitation and transmission from elsewhere in the structure.

Examining Table 7b shows that highest bending+membrane and alternating stress intensities occur at the -10% frequency shift. Due to a dominant 218 Hz signal in the load, the effect of frequency shifting is to simply excite a different collection of modes at each shift. Thus at the -10% shift, the modes at 196 Hz are most strongly excited which, from Figure 13c and d are seen to occur on the hood supports. The +10% shift excites modes near 240 Hz which now occur on the outer hoods. In the nominal case the skirt and drain channels pick up a stronger response, and inner closure plates. For the +10% shift the hood supports show only a weak response.

Three important practical observations can also be made. First, at nominal operation the dryer stresses are below allowables (see Table 8a). This is consistent with the fact that the dryer has been successfully operating for a long time (albeit with different, smaller top tie bars). It also shows that both the load predictions and structural modeling concur with actual experience. Applying frequency shifts is necessary for conservatism in the FE model, but is probably overly conservative here given that the lowest SRs obtained at the -10% shift exceed allowables, yet the actual dryer has continued operation. Secondly, the strong response of the outer and middle hood supports at negative frequency shifts is consistent with modifications made to the Browns Ferry Unit 1 dryer where the outer hood supports were removed and replaced with a combination of thicker outer hoods and external reinforcement channels welded to the outer hoods. Finally, the structural response is dominated by a strong 218 Hz signal indicating that instead of reinforcing the structure in various ways, stresses can alternatively be reduced by addressing and eliminating the sources of this component. This is discussed further in Section 5.3.

Table 7a. Locations with highest predicted stress intensities for CLTP conditions with no frequency shift.

Stress Category	Location		Location (in)				Stress Intensities (psi)		
		Weld	x	y	z	node	Pm	Pm+Pb	S_{alt}
Pm	upper support ring/support	Yes	5.8	122.4	-6.5	7532	7643	7643	<1500
"	outer hood/hood support/cover plate	"	102.0	-28.7	0.0	90804	6665	8023	4601
"	inner hood/middle closure plate/top cover plate	"	31.5	108.4	88.9	84319	5363	5779	1925
"	inner hood/hood support/base plate	"	39.8	-59.8	0.0	90626	4675	5467	2857
"	middle hood/top cover plate/outer closure plate	"	62.5	-85.0	88.9	84199	4358	5544	3406
Pm+Pb	outer hood/cover plate	Yes	102.0	-61.0	0.0	90780	4343	8340	3385
"	outer hood/hood support/base plate	"	-102.0	28.7	0.0	90383	6276	8335	4680
"	submerged drain channel/skirt	"	-91.0	76.7	-100.5	86525	1962	8284	5274
"	upper support ring/support	"	5.8	122.4	-6.5	7532	7643	7643	<1500
"	middle hood/hood support/outer base plate	"	70.8	54.6	0.0	85038	3745	7375	6451
S_{alt}	middle hood/hood support/outer base plate	Yes	70.8	54.6	0.0	85038	3745	7375	6451
"	outer hood/hood support/cover plate	"	102.0	28.7	0.0	83543	4996	8119	5381
"	middle base plate/hood support/vane bank	"	55.0	54.6	0.0	83942	1126	5613	5295
"	submerged drain channel/skirt	"	-91.0	76.7	-100.5	86525	1962	8284	5274
"	submerged drain channel/skirt	"	11.5	118.4	-100.5	81700	1903	5556	4731

Node numbers are retained for further reference.
Spatial coordinates are in a reference frame whose origin is located at the intersection of the steam dryer centerline and the plane containing the base and cover plates (this plane also contains the top of the upper support ring and the bottom edges of the hoods). The y-axis is parallel to the hoods, the x-axis is normal to the hoods pointing from MSL C/D to MSL A/B, and the z-axis is vertical, positive up.

Table 7b. Locations with highest predicted stress intensities taken over all frequency shifts CLTP conditions.

Stress Category	Location	Weld	% Freq. Shift	Location (in)				Stress Intensities (psi)		
				x	y	z	node	Pm	Pm+Pb	S_{alt}
Pm	upper support ring/support	Yes	+7.5	-5.8	-122.4	-6.5	7705	7932	7932	<1500
"	outer hood/hood support/cover plate	"	+7.5	102.0	-28.7	0.0	90804	7048	14558	11151
"	inner hood/middle closure plate/top cover plate	"	+7.5	31.5	108.4	88.9	84319	6010	6936	3172
"	inner hood/hood support/base plate	"	+10	39.8	-59.8	0.0	90626	5204	6959	4637
"	outer hood/cover plate	"	-10	102.0	-61.0	0.0	90780	4888	9838	5004
Pm+Pb	outer hood/hood support/cover plate	Yes	-10	-102.0	-28.7	0.0	81525	5441	16262	13902
"	outer base plate/hood support/vane bank	"	-10	-86.0	-28.7	0.0	82135	1898	13406	12751
"	middle hood/hood support/outer base plate	"	-10	70.8	54.6	0.0	85038	3745	10796	9853
"	outer hood/cover plate	"	-10	102.0	-61.0	0.0	90780	4888	9838	5004
"	submerged drain channel/skirt	"	-5	-91.0	-76.7	-100.5	79884	2904	9542	6649
S_{alt}	outer hood/hood support/cover plate	Yes	-10	-102.0	-28.7	0.0	81525	5441	16262	13902
"	outer base plate/hood support/vane bank	"	-10	-86.0	-28.7	0.0	82135	1898	13406	12751
"	middle hood/hood support/outer base plate	"	-10	70.8	54.6	0.0	85038	3745	10796	9853
"	middle base plate/hood support/vane bank	"	-10	55.0	54.6	0.0	83942	1126	9455	9232
"	outer hood/hood support	"	-10	-102.0	-28.7	11.5	81517	794	8701	8678

See Table 7a for coordinates description.

Table 7c. Locations with highest predicted stress intensities for CLTP conditions with -10% frequency shift.

Stress Category	Location		Location (in)				Stress Intensities (psi)		
		Weld	x	y	z	node	Pm	Pm+Pb	S_{alt}
Pm	upper support ring/support	Yes	-5.8	-122.4	-6.5	7705	7710	7710	<1500
"	outer hood/hood support/cover plate	"	-102.0	28.7	0.0	90383	5959	8846	5176
"	inner hood/middle closure plate/top cover plate	"	31.5	108.4	88.9	84319	5526	5802	1744
"	outer hood/cover plate	"	102.0	-61.0	0.0	90780	4888	9838	5004
"	inner hood/hood support/base plate	"	-39.8	59.8	0.0	90589	4721	5944	3500
Pm+Pb	outer hood/hood support/cover plate	Yes	-102.0	-28.7	0.0	81525	5036	16262	13902
"	outer base plate/hood support/vane bank	"	-86.0	-28.7	0.0	82135	1107	13406	12751
"	middle hood/hood support/outer base plate	"	70.8	54.6	0.0	85038	2490	10796	9853
"	outer hood/cover plate	"	102.0	-61.0	0.0	90780	4888	9838	5004
"	middle base plate/hood support/vane bank	"	55.0	54.6	0.0	83942	795	9455	9232
S_{alt}	outer hood/hood support/cover plate	Yes	-102.0	-28.7	0.0	81525	5036	16262	13902
"	outer base plate/hood support/vane bank	"	-86.0	-28.7	0.0	82135	1107	13406	12751
"	middle hood/hood support/outer base plate	"	70.8	54.6	0.0	85038	2490	10796	9853
"	middle base plate/hood support/vane bank	"	55.0	54.6	0.0	83942	795	9455	9232
"	outer hood/hood support	"	-102.0	-28.7	11.5	81517	486	8701	8678

See Table 7a for coordinates description.

Table 7d. Locations with highest predicted stress intensities for CLTP conditions with +10% frequency shift.

Stress Category	Location		Location (in)				Stress Intensities (psi)		
		Weld	x	y	z	node	Pm	Pm+Pb	S_{alt}
Pm	upper support ring/support	Yes	-5.8	-122.4	-6.5	7705	7729	7729	<1500
"	outer hood/hood support/cover plate	"	102.0	-28.7	0.0	90804	5954	8457	4727
"	inner hood/middle closure plate/top cover plate	"	31.5	108.4	88.9	84319	5708	6506	2704
"	inner hood/hood support/base plate	"	39.8	-59.8	0.0	90626	5204	5461	2933
"	outer hood/cover plate	"	102.0	-61.0	0.0	90780	4217	7815	3220
Pm+Pb	outer hood/hood support/cover plate	Yes	102.0	28.7	0.0	83543	5250	8580	5957
"	outer hood/cover plate	"	102.0	-61.0	0.0	90780	4217	7815	3220
"	upper support ring/support	"	-5.8	-122.4	-6.5	7705	7729	7729	<1500
"	inner hood/middle closure plate/top cover plate	"	-31.5	-108.4	88.9	86029	5441	6680	2890
"	inner side panel/top cover plate/inner closure plate	"	-15.0	-118.9	88.9	83324	1881	6605	4467
S_{alt}	outer hood/hood support/cover plate	Yes	102.0	28.7	0.0	83543	5250	8580	5957
"	outer base plate/hood support/vane bank	"	86.0	28.7	0.0	85129	1310	5574	5093
"	inner side panel/top cover plate/inner closure plate	"	-15.0	-118.9	88.9	83324	1881	6605	4467
"	outer hood/outer end wall	"	99.3	-70.8	31.9	81237	519	4404	4221
"	outer hood	No	96.5	51.1	45.2	47491	407	4130	4116

See Table 7a for coordinates description.

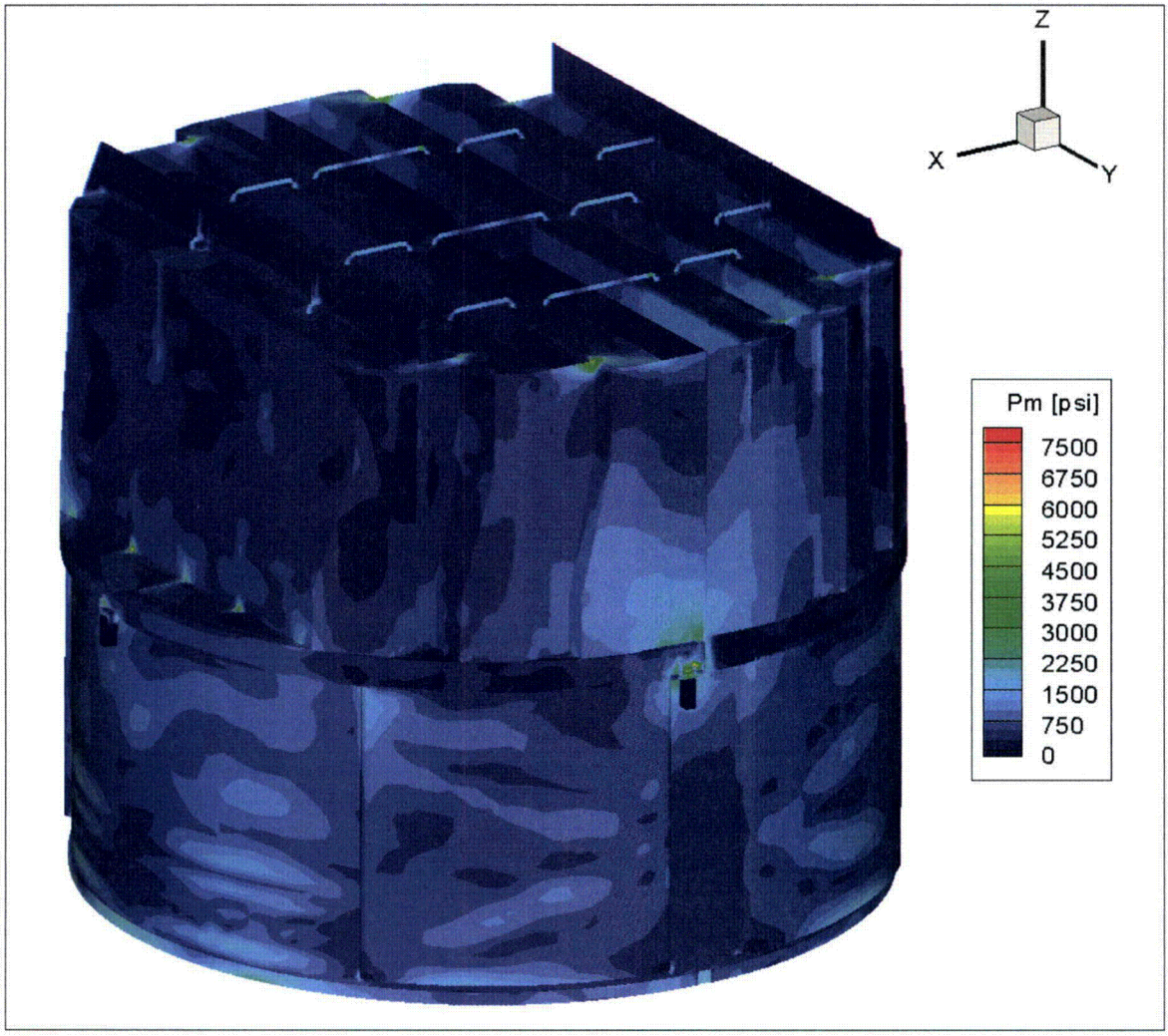

Figure 11a. Contour plot of maximum membrane stress intensity, Pm, for CLTP load. The maximum stress intensity is 7,643 psi.

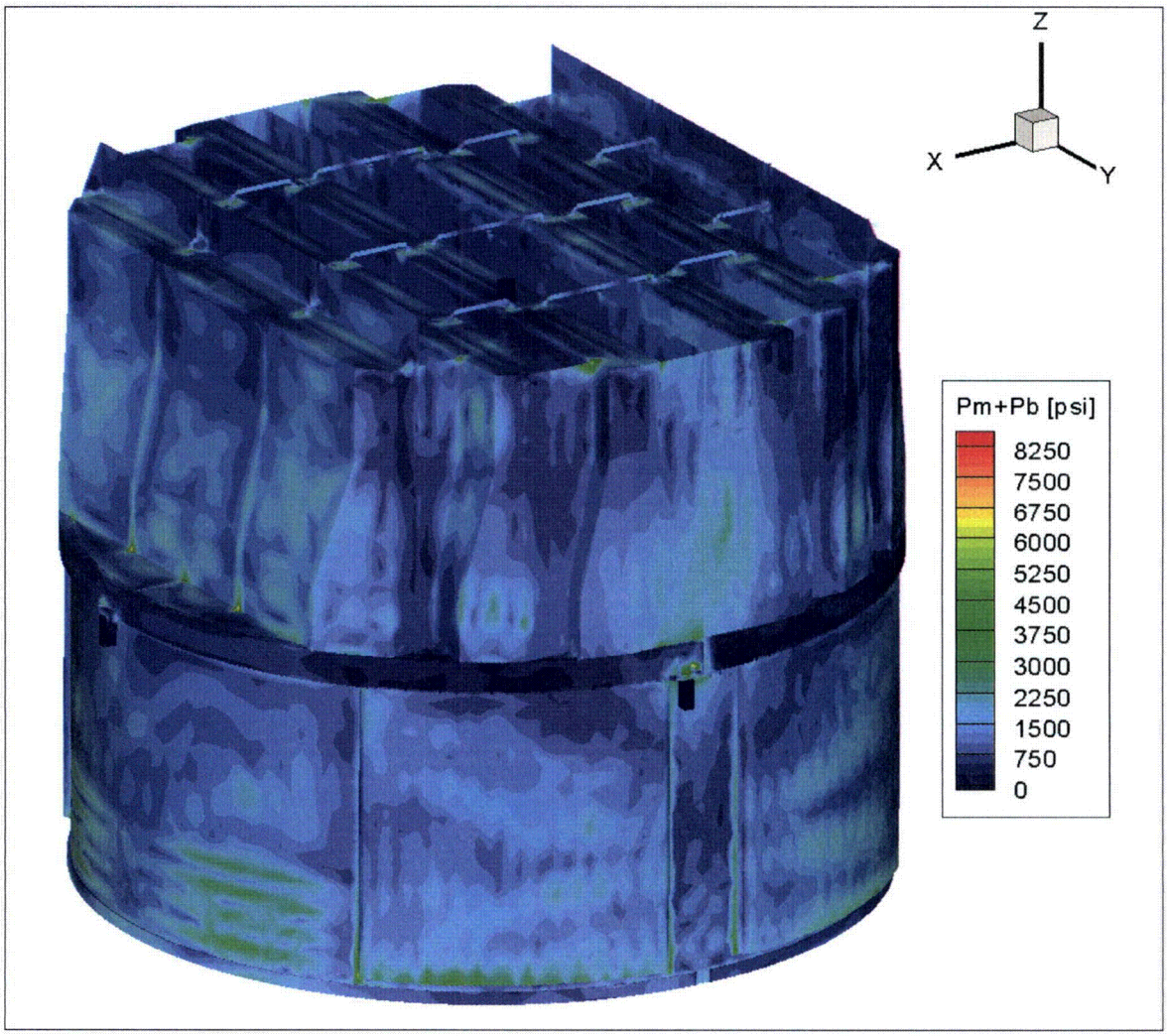

Figure 11b. Contour plot of maximum membrane+bending stress intensity, Pm+Pb, for CLTP load. The maximum stress intensity is 8,340 psi. First view.

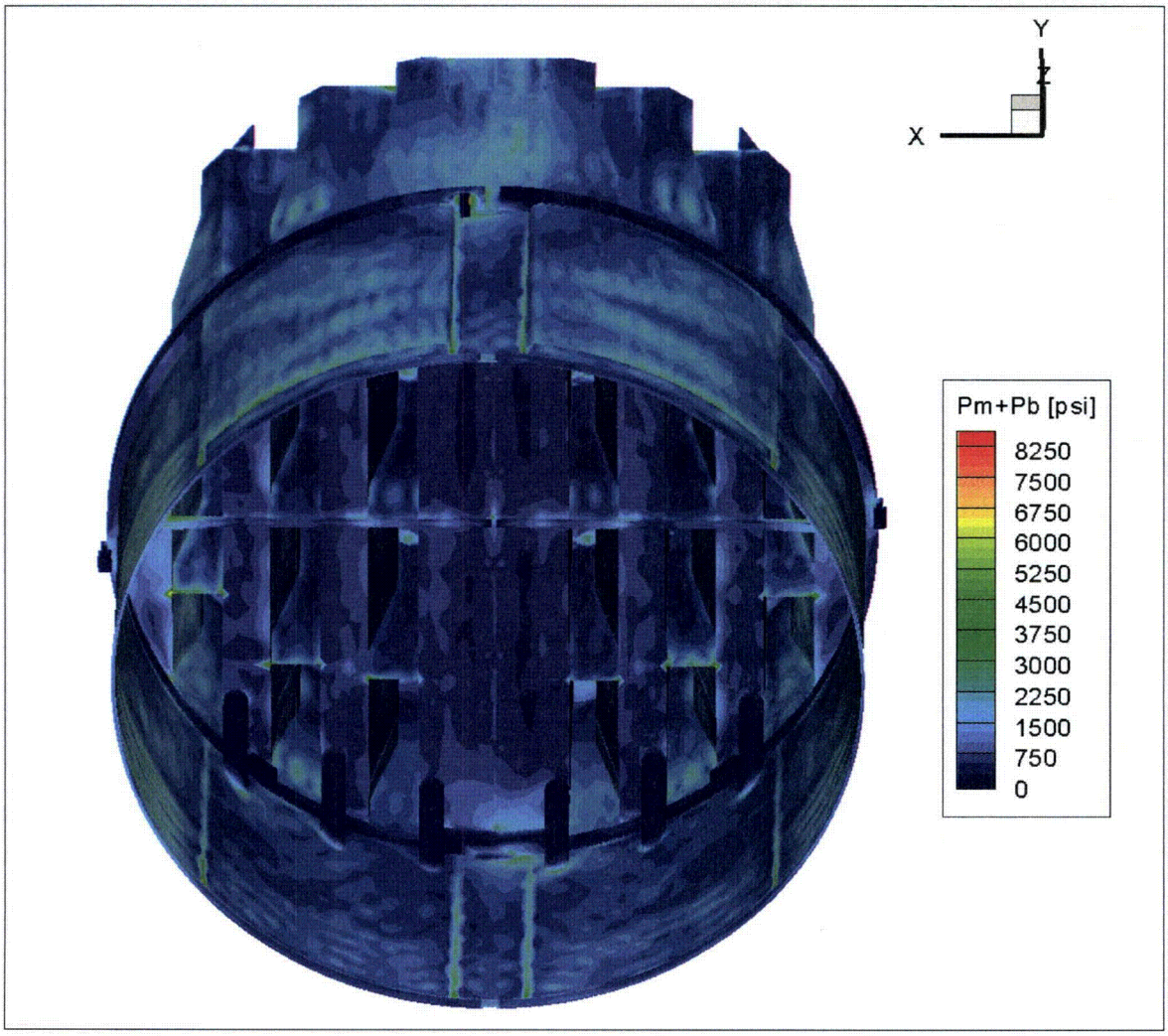

Figure 11c. Contour plot of maximum membrane+bending stress intensity, Pm+Pb, for CLTP load. This second view from below shows the high stress intensities at the bottom of the outer and middle hood supports.

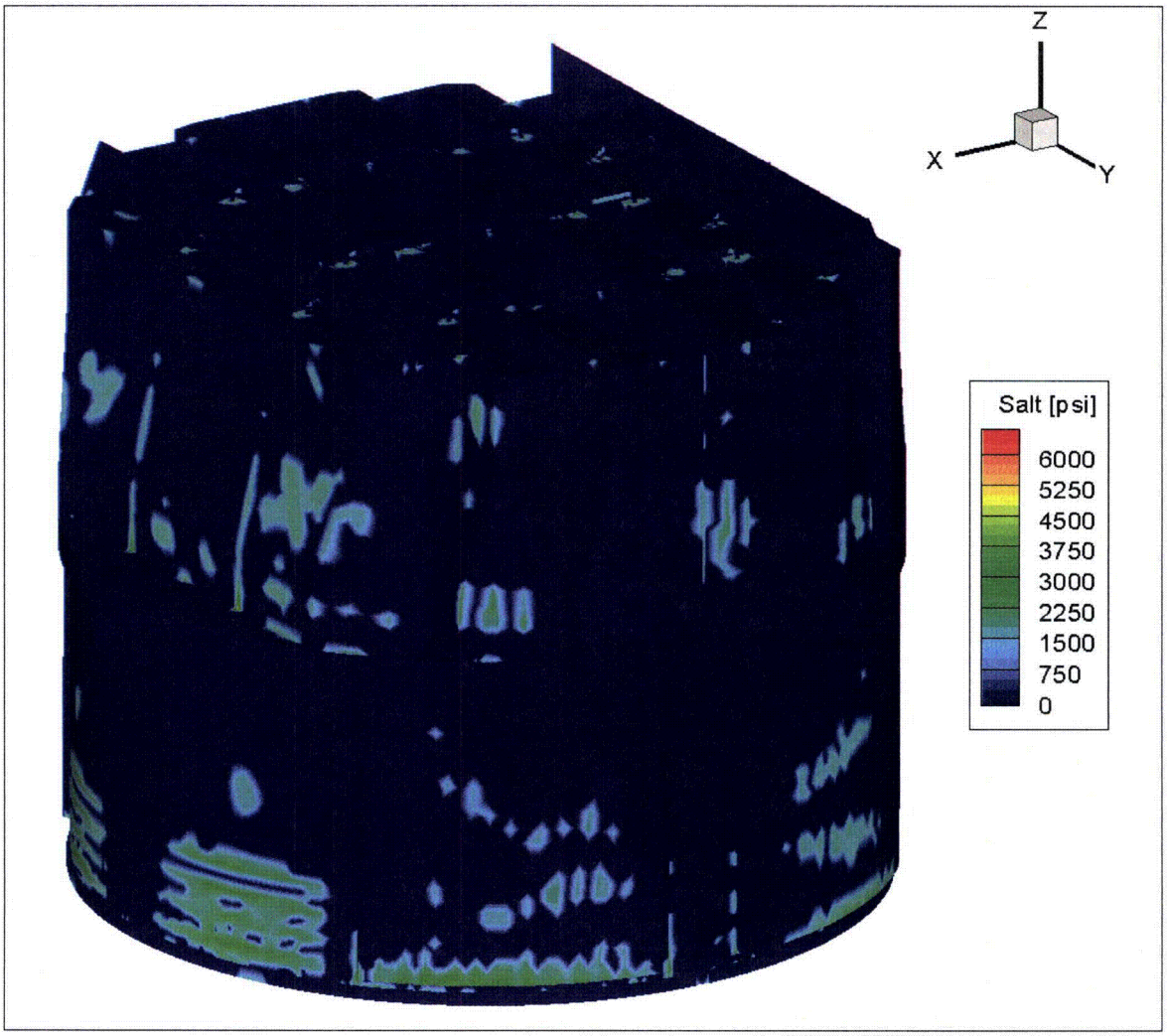

Figure 11d. Contour plot of alternating stress intensity, S_{alt}, for CLTP load. The maximum alternating stress intensity is 6,451 psi. First view.

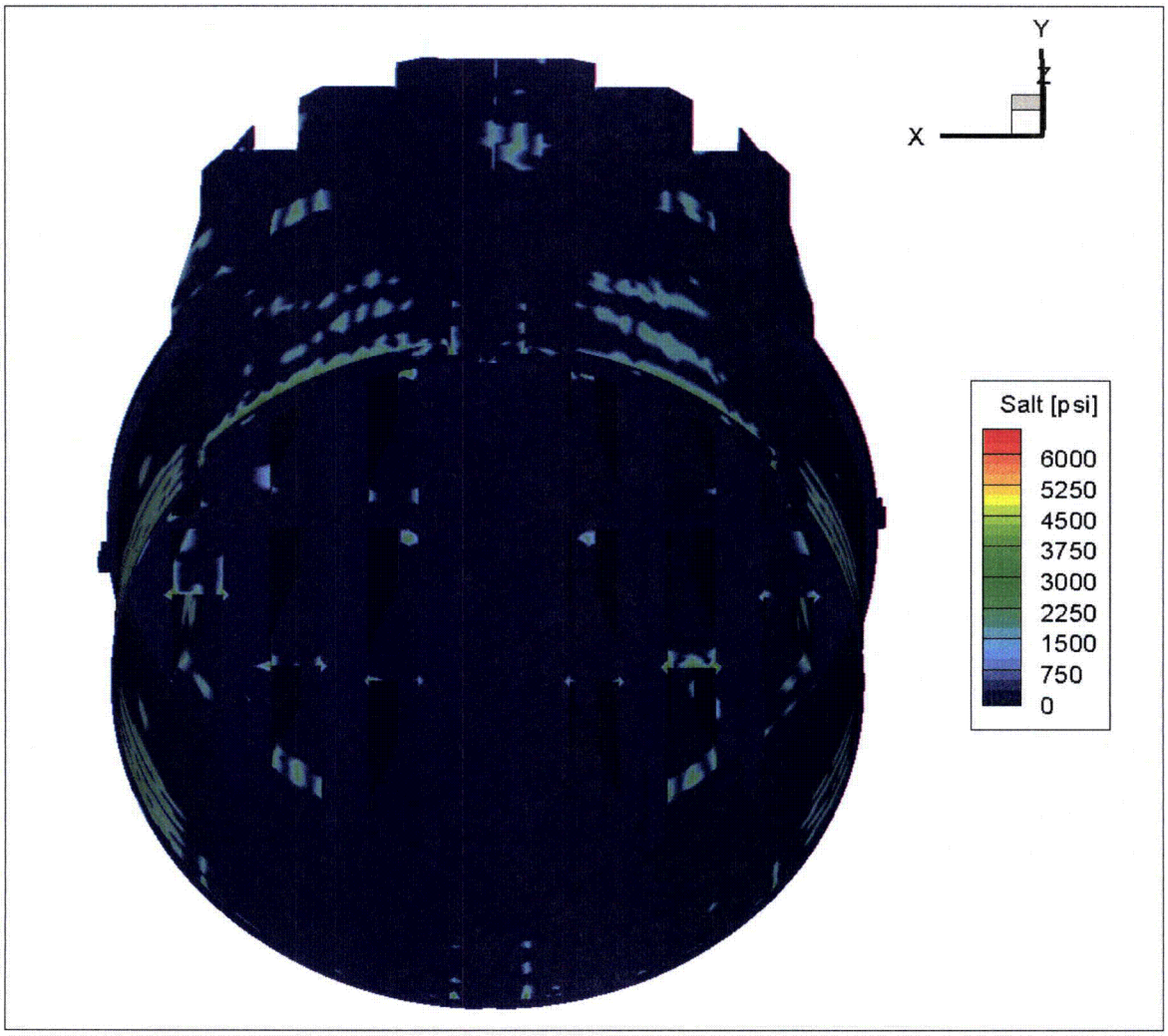

Figure 11e. Contour plot of alternating stress intensity, S_{alt}, for CLTP load. This second view from below shows the high alternating stress intensity at junctions of the outer and middle hood supports with the base and cover plates and hoods.

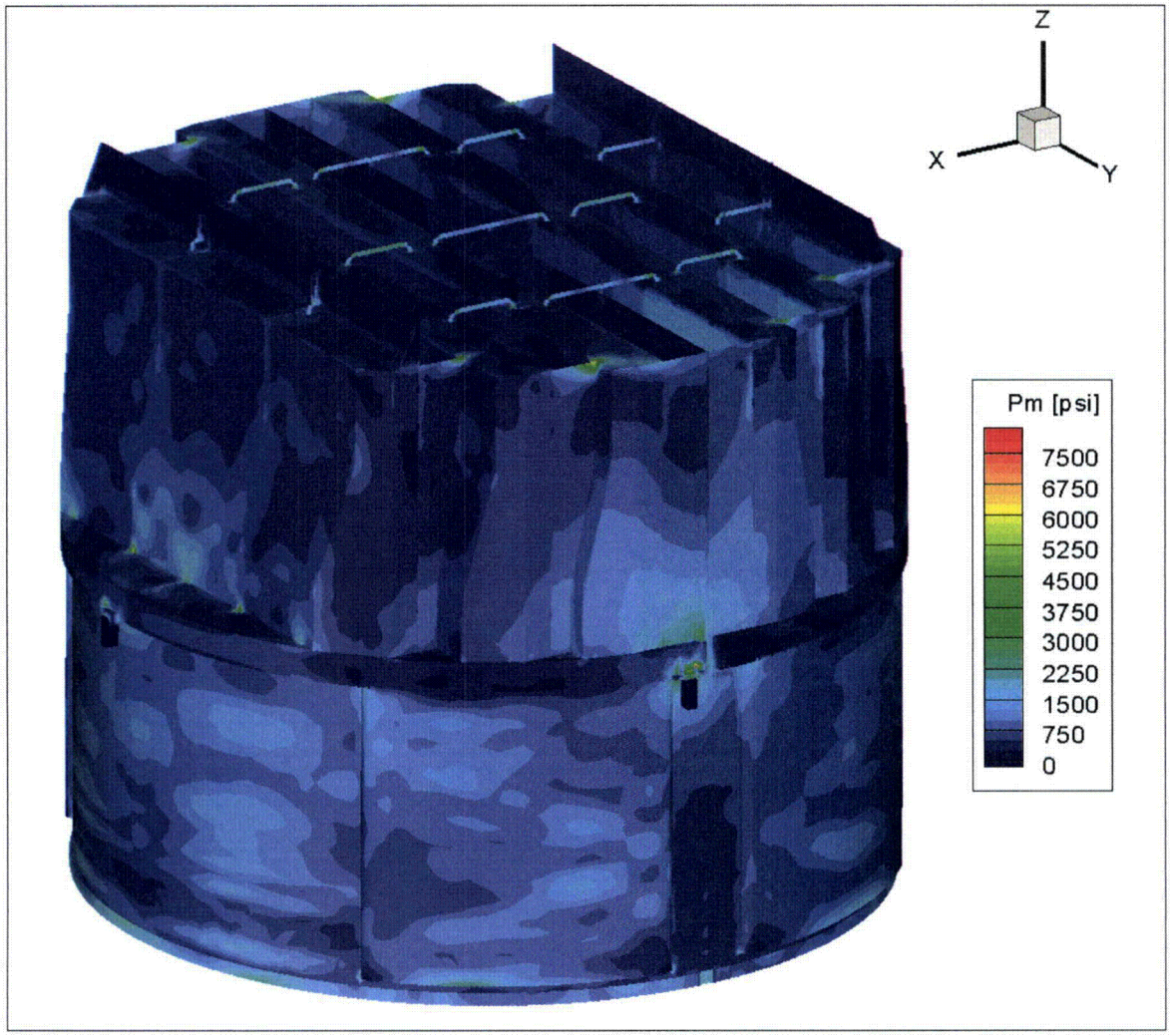

Figure 12a. Contour plot of maximum membrane stress intensity, Pm, for CLTP operation with frequency shifts. The recorded stress at a node is the maximum value taken over all frequency shifts. The maximum stress intensity is 7,932 psi.

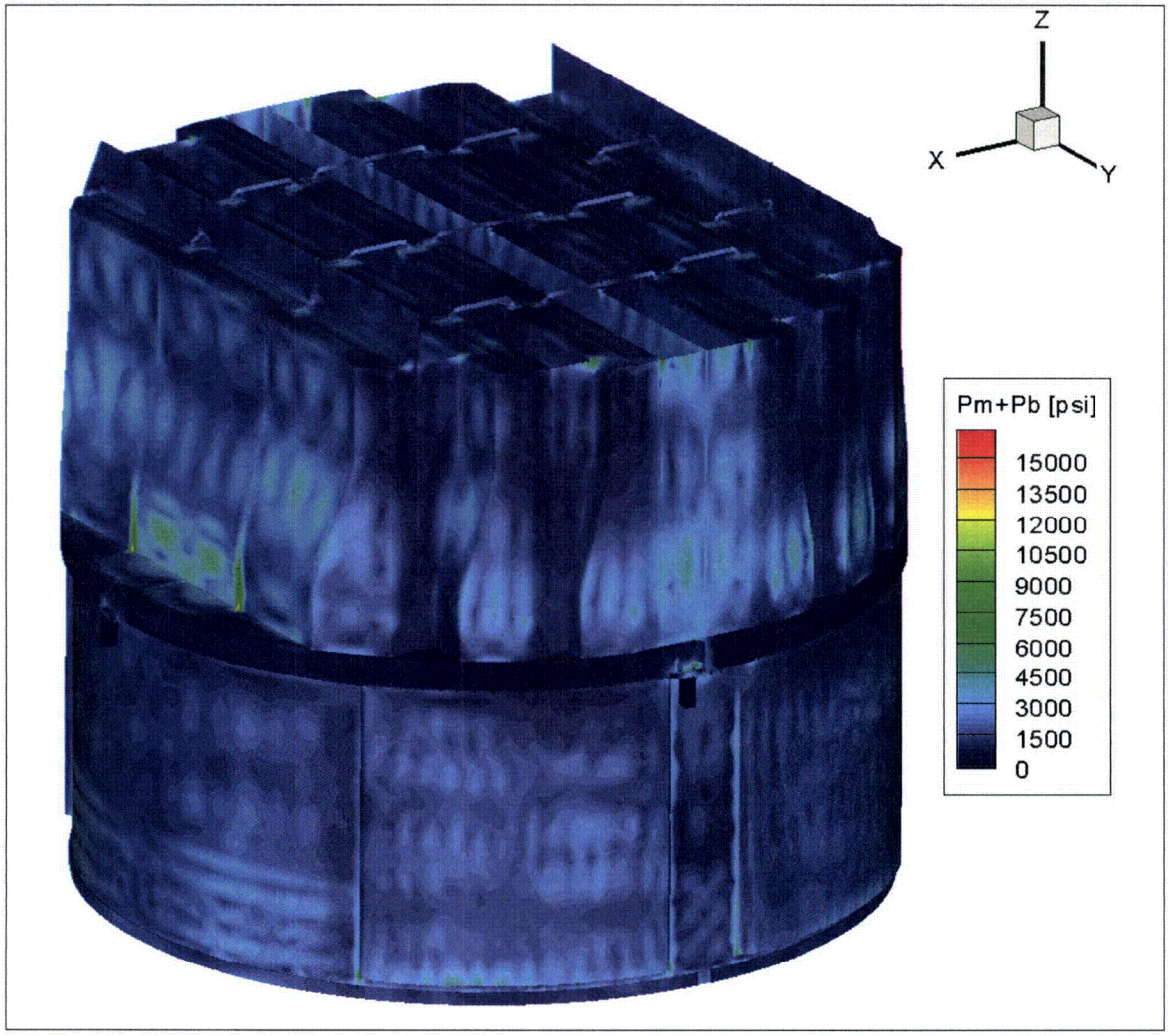

Figure 12b. Contour plot of maximum membrane+bending stress intensity, Pm+Pb, for CLTP operation with frequency shifts. The recorded stress at a node is the maximum value taken over all frequency shifts. The maximum stress intensity is 16,262 psi. First view.

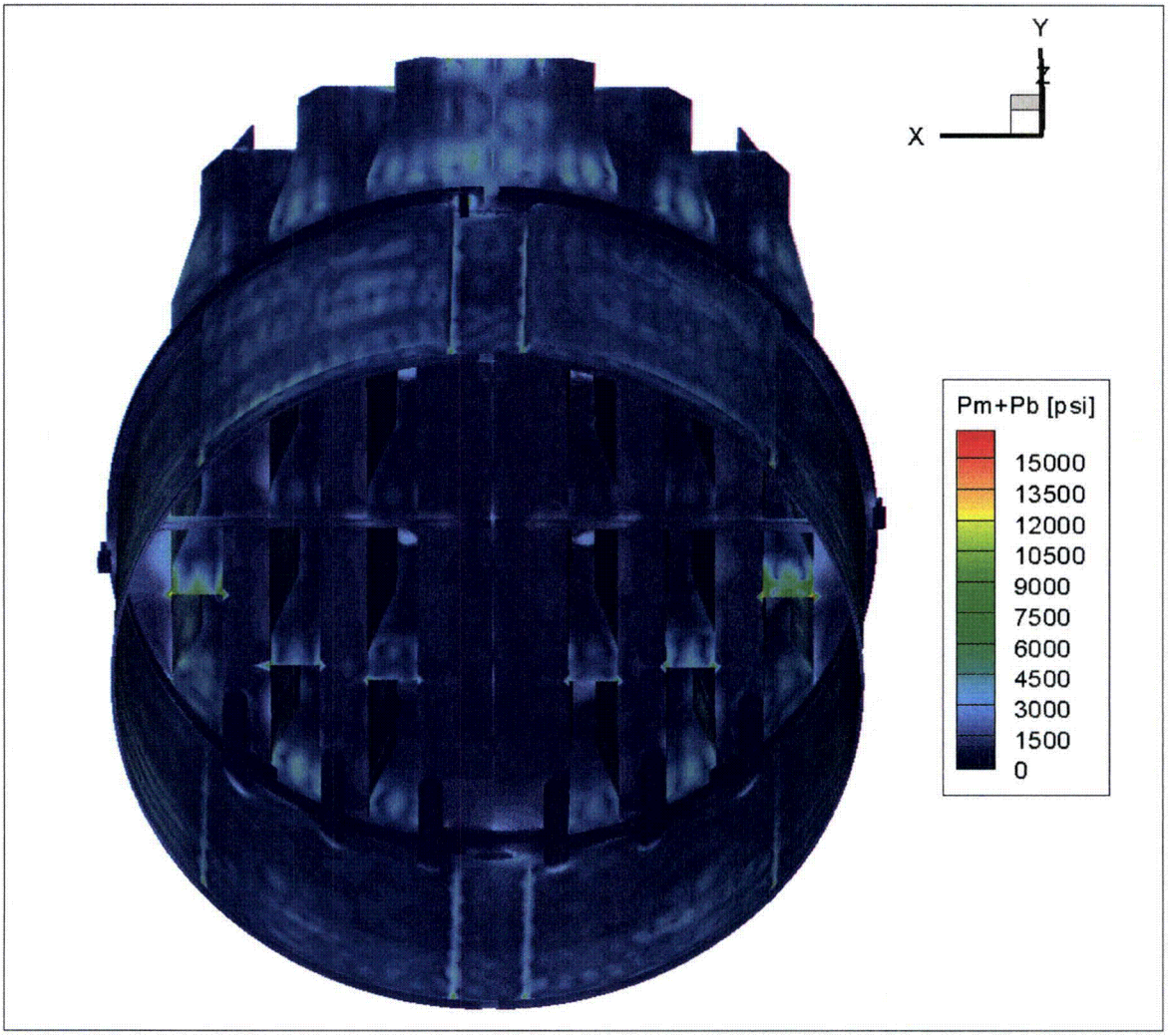

Figure 12c. Contour plot of maximum membrane+bending stress intensity, Pm+Pb, for CLTP operation with frequency shifts. This second view from beneath reveals high stress and modal response of the outer hood supports.

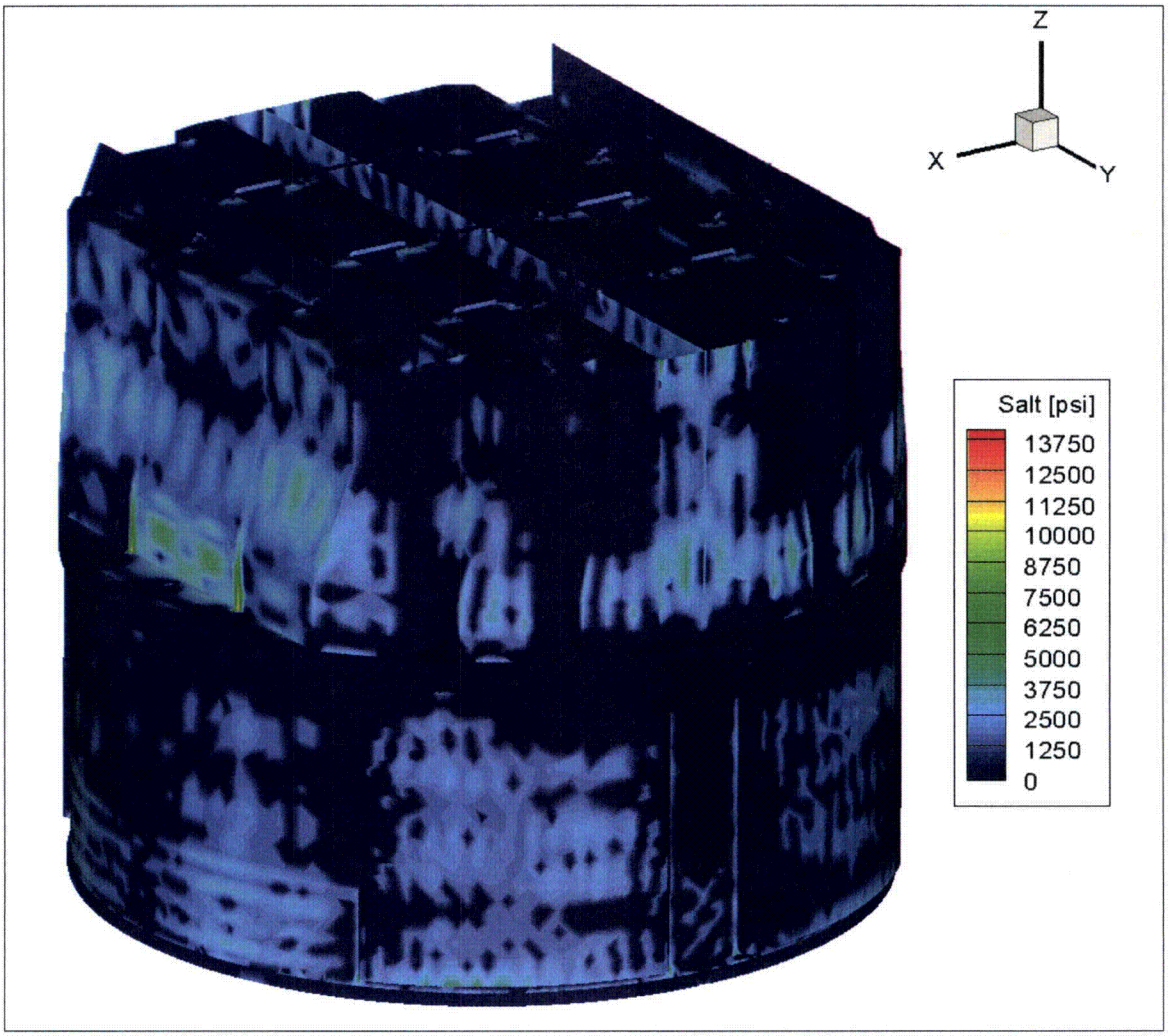

Figure 12d. Contour plot of alternating stress intensity, S_{alt}, for CLTP operation with frequency shifts. The recorded stress at a node is the maximum value taken over all frequency shifts. The maximum alternating stress intensity is 13,902 psi. First view.

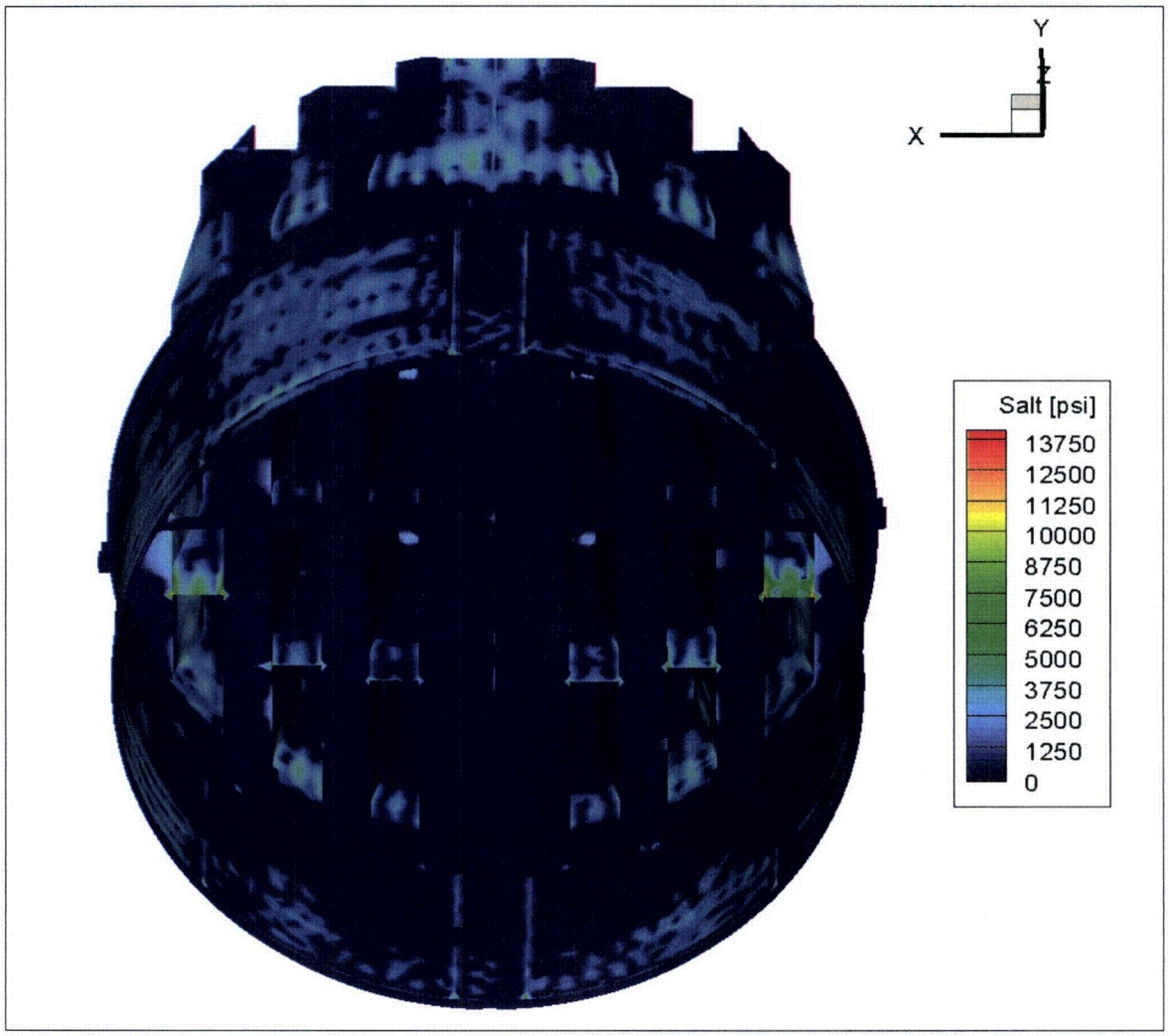

Figure 12e. Contour plot of alternating stress intensity, S_{alt}, for CLTP operation with frequency shifts. This second view from beneath reveals more of the high stress regions on the outer hood supports.

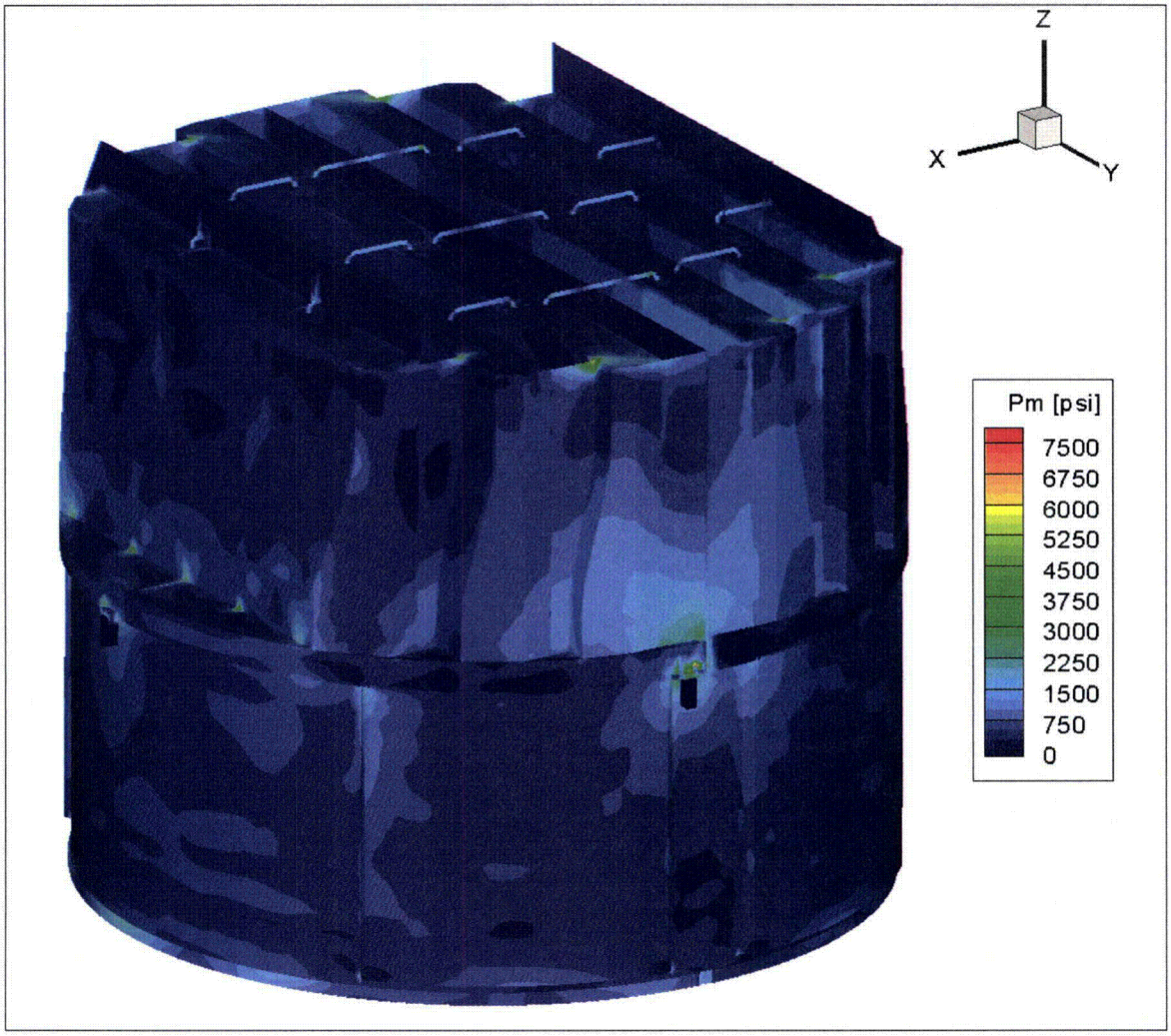

Figure 13a. Contour plot of maximum membrane stress intensity, Pm, for CLTP load with -10% frequency shift. The maximum stress intensity is 7,710 psi.

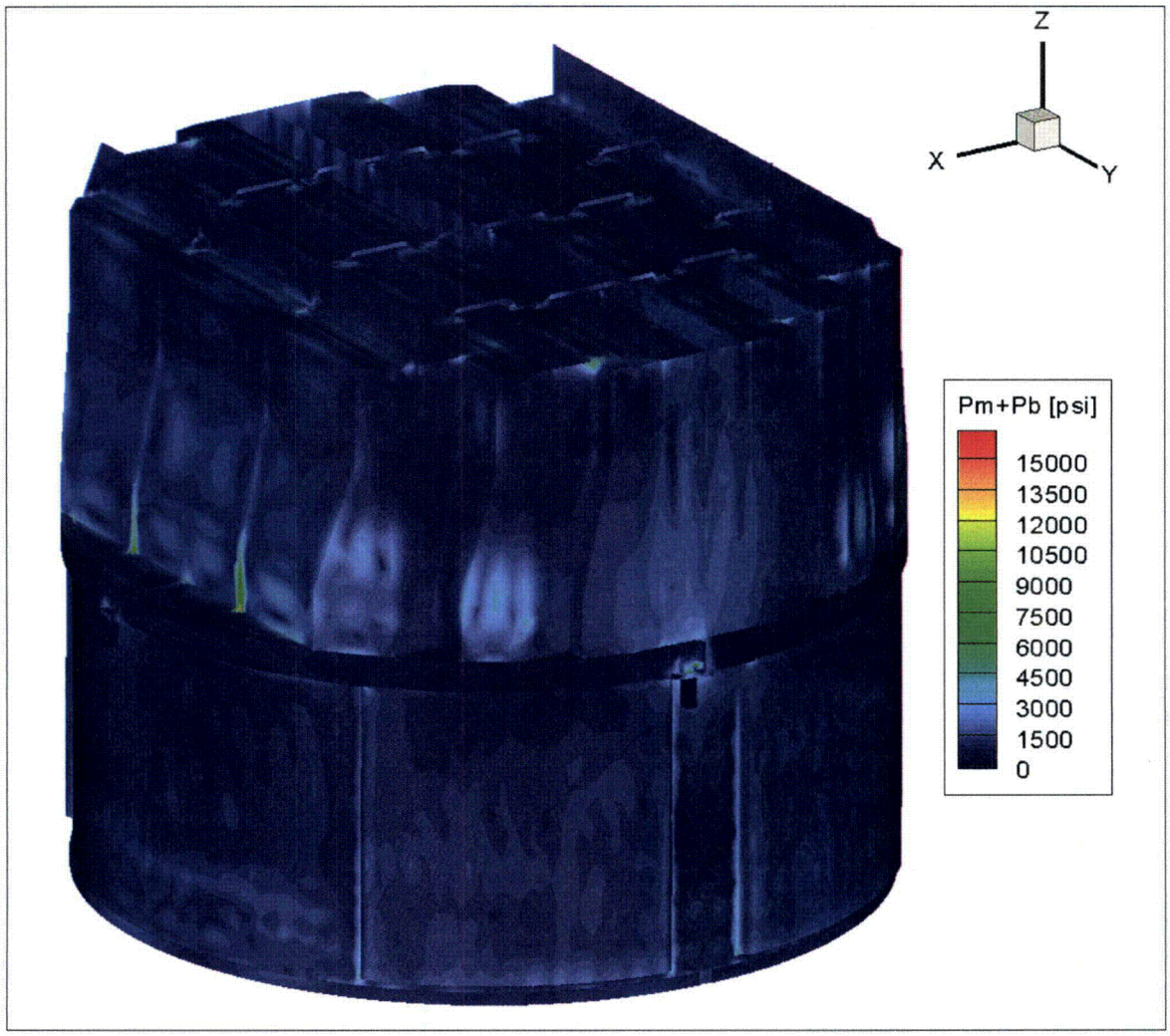

Figure 13b. Contour plot of maximum membrane+bending stress intensity, Pm+Pb, for CLTP load with -10% frequency shift. The maximum stress intensity is 16,262 psi.

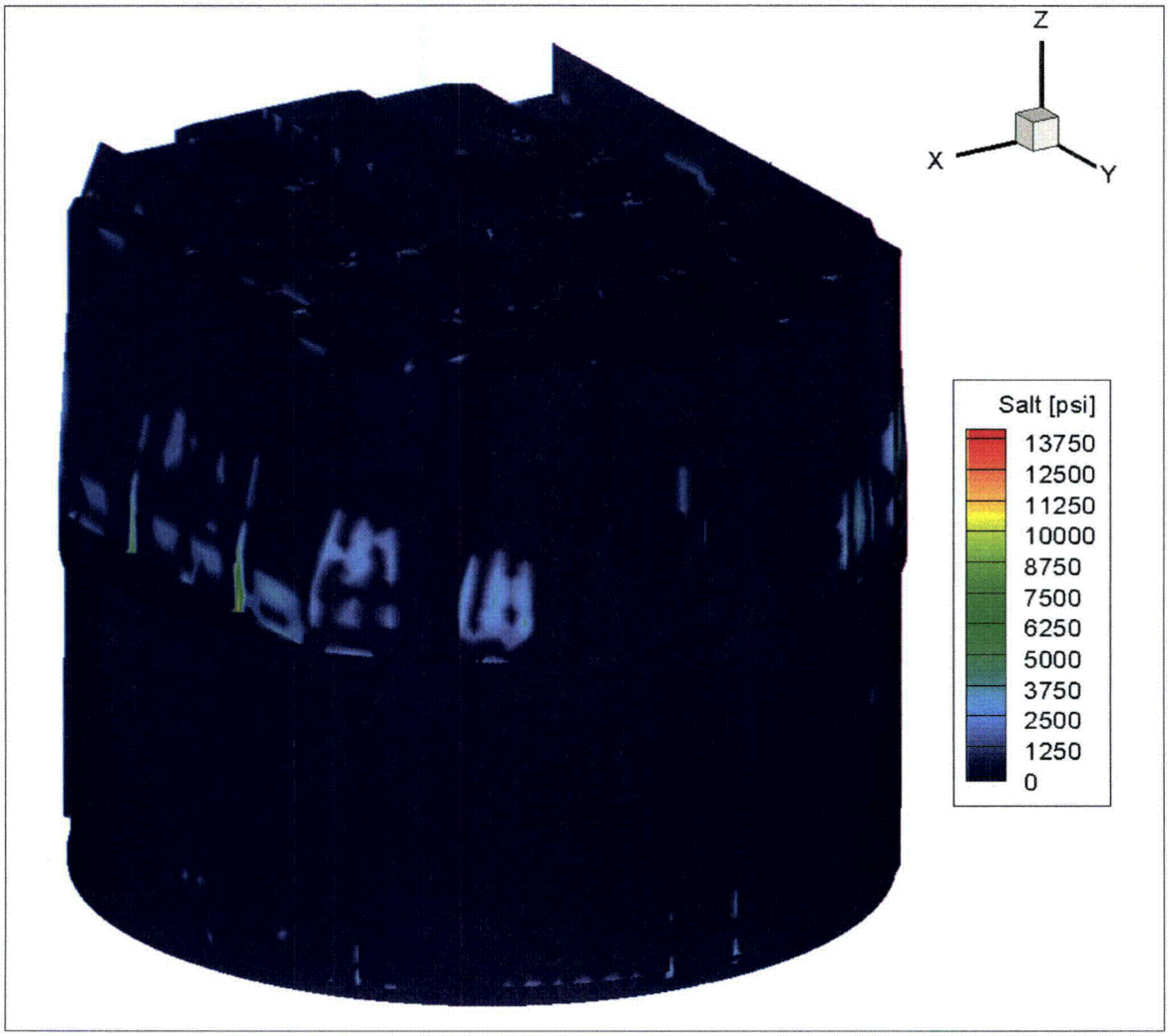

Figure 13c. Contour plot of alternating stress intensity, S_{alt}, for CLTP load with -10% frequency shift. The maximum alternating stress intensity is 13,902 psi. First view.

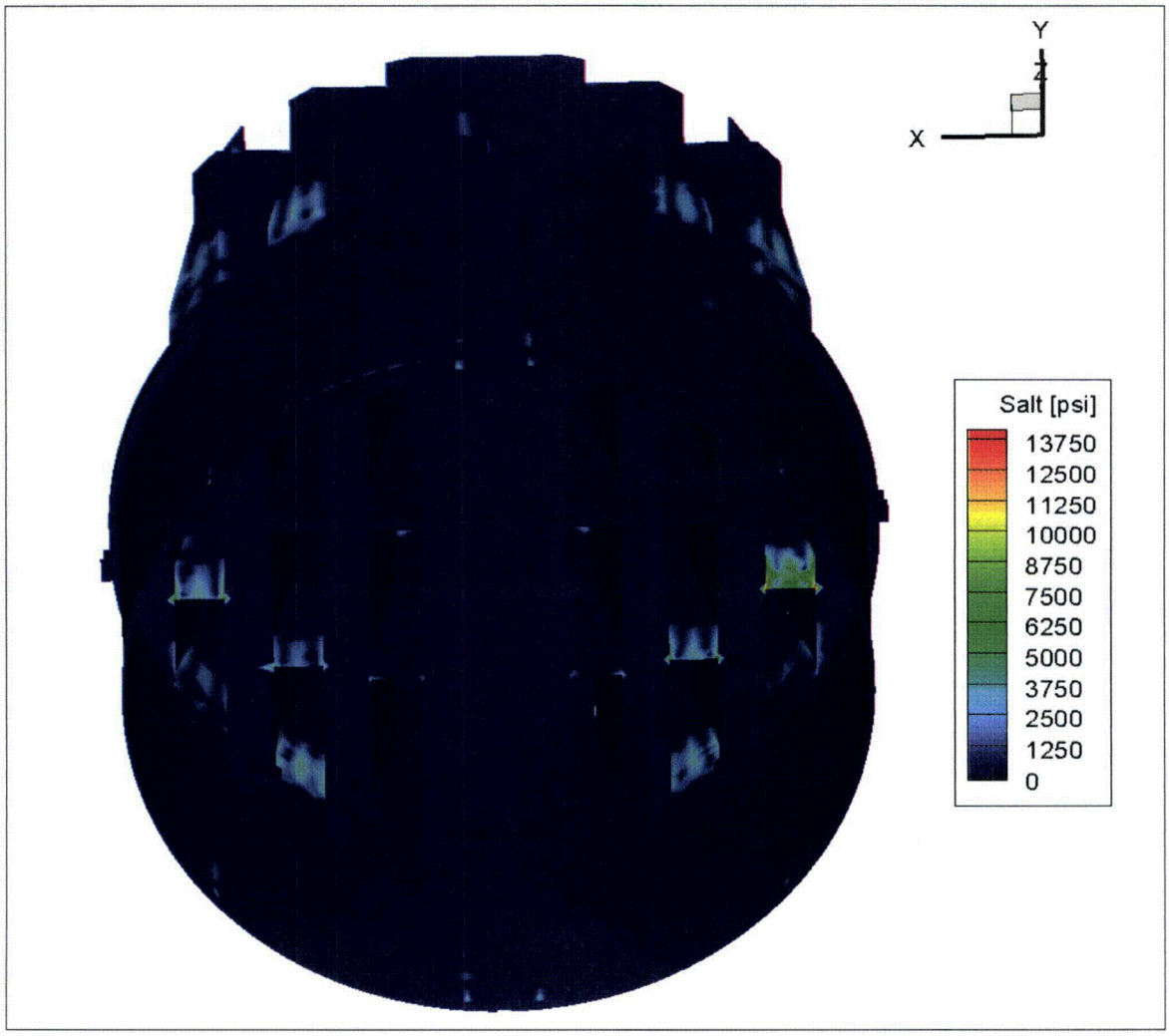

Figure 13d. Contour plot of alternating stress intensity, S_{alt}, for CLTP load with -10% frequency shift. Second view showing high stress locations on outer hood supports.

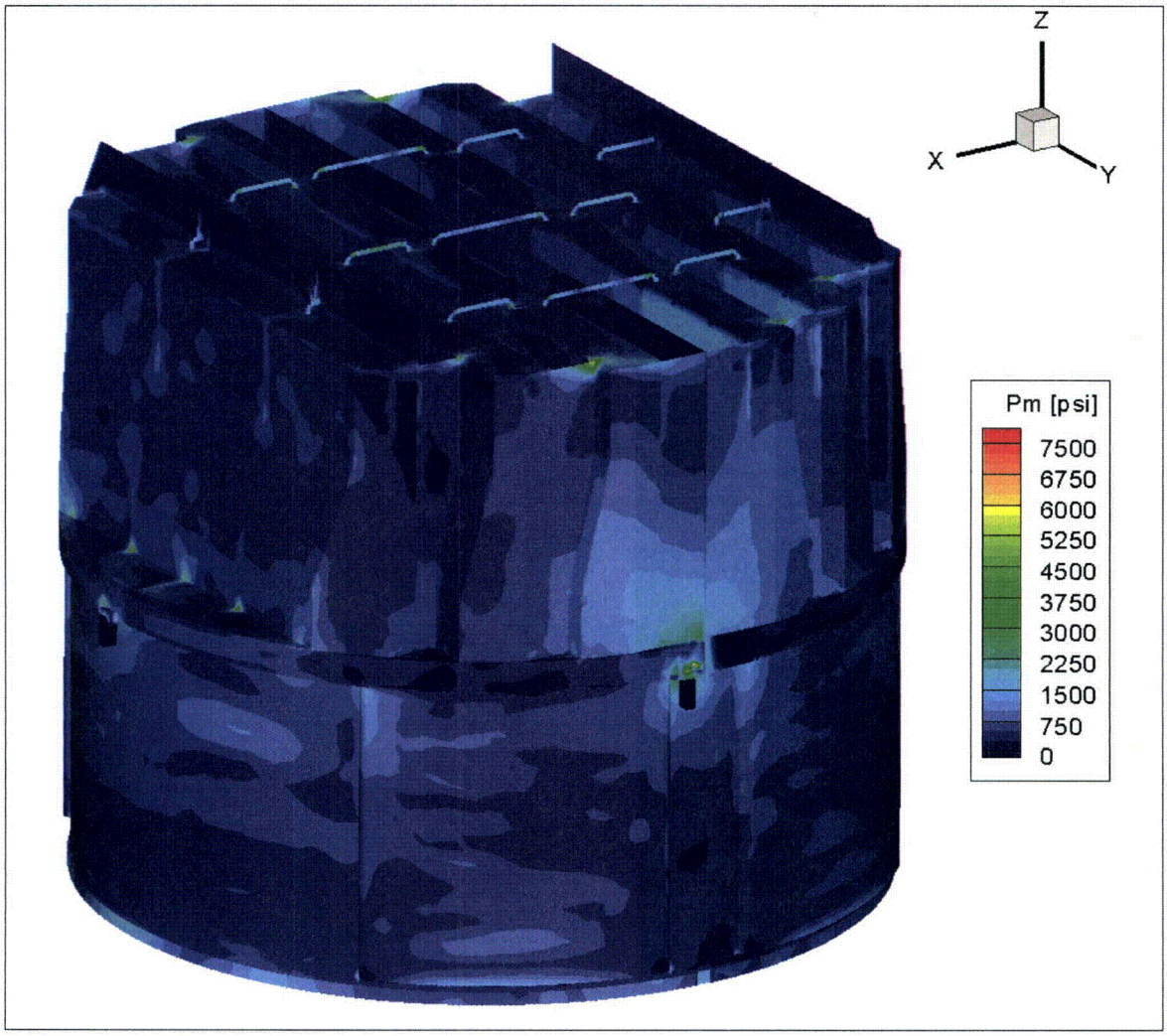

Figure 14a. Contour plot of maximum membrane stress intensity, Pm, for CLTP load with +10% frequency shift. The maximum stress intensity is 7,729 psi.

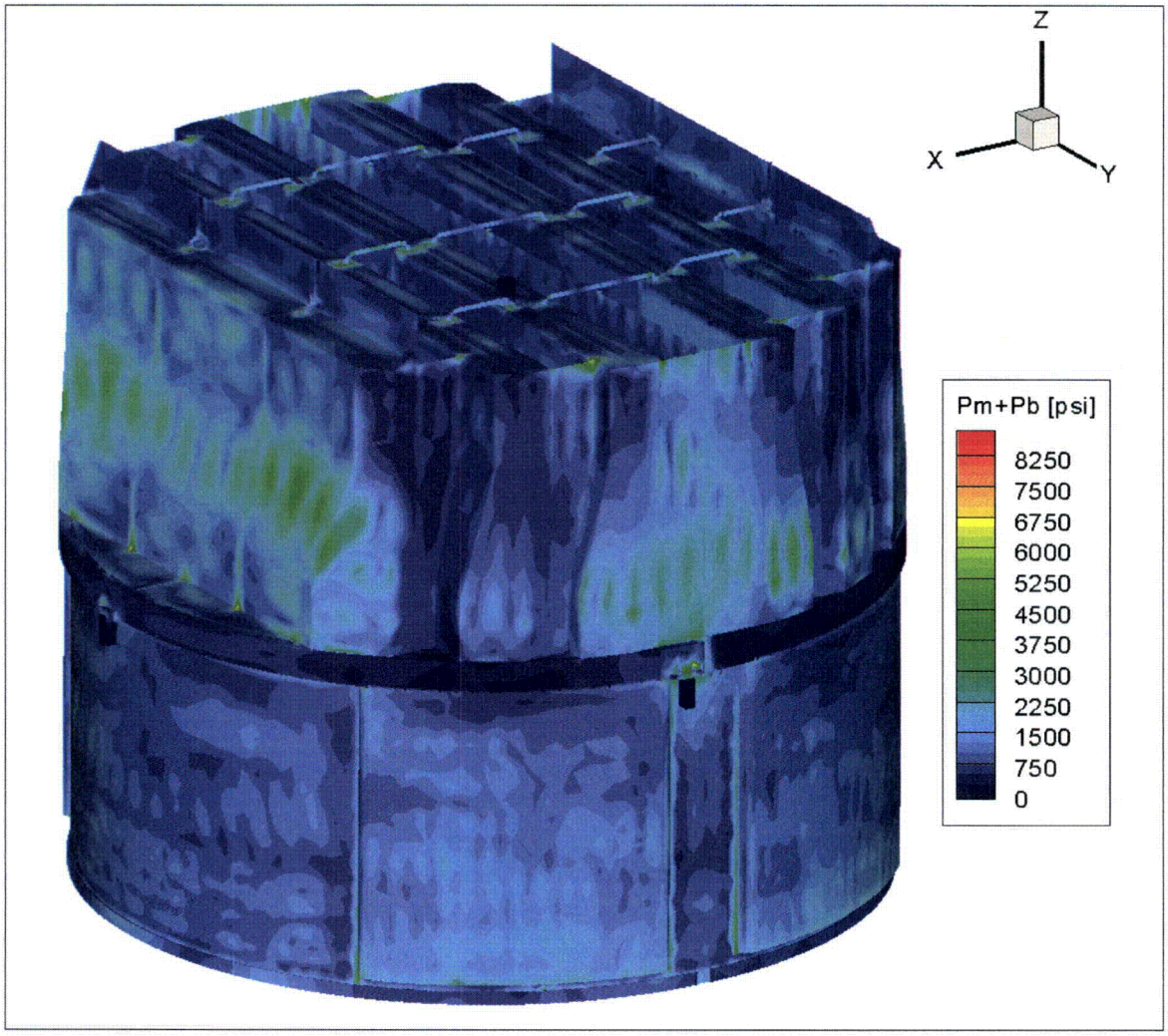

Figure 14b. Contour plot of maximum membrane+bending stress intensity, Pm+Pb, for CLTP load with +10% frequency shift. The maximum stress intensity is 8,580 psi.

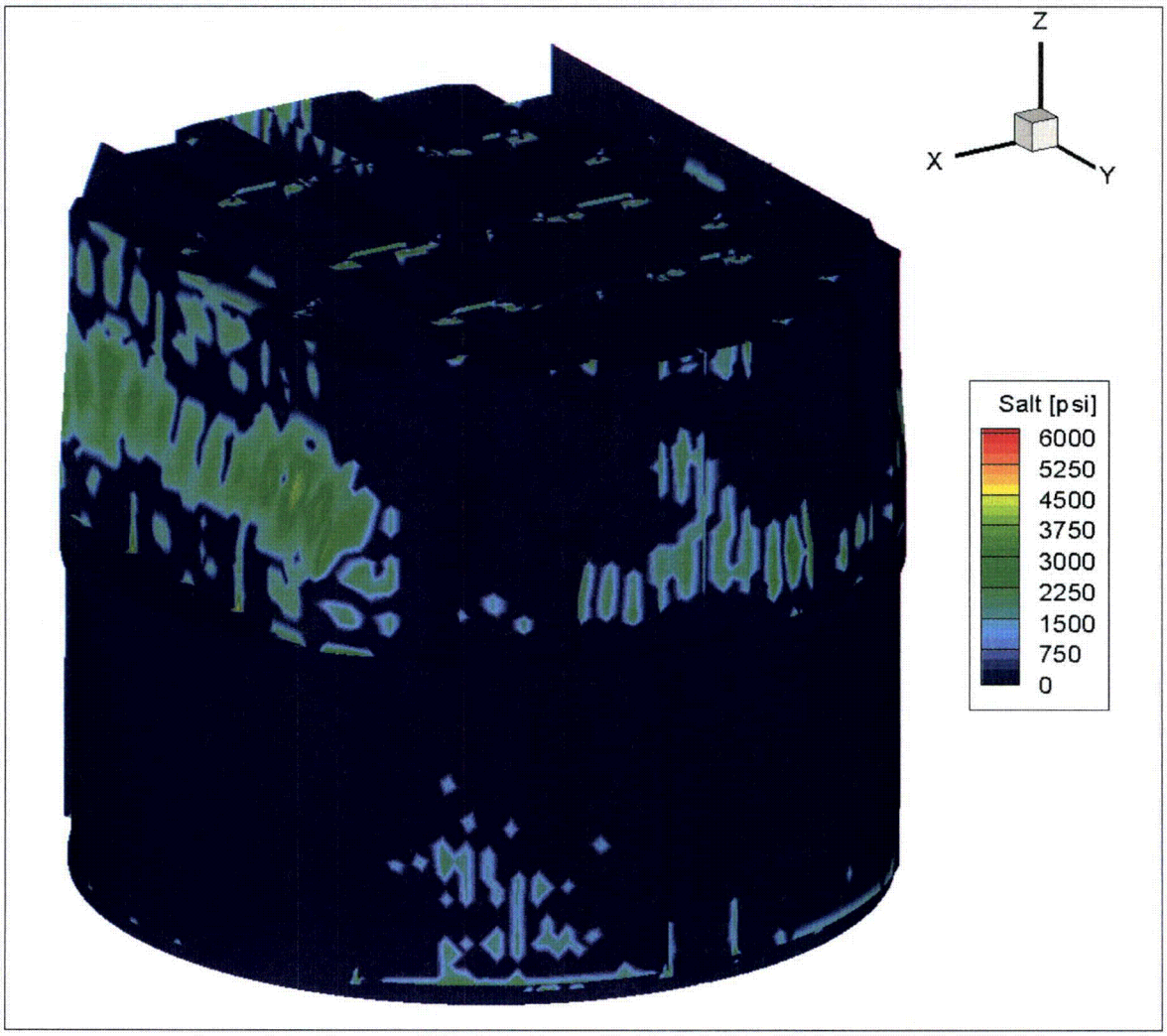

Figure 14c. Contour plot of alternating stress intensity, S_{alt}, for CLTP load with +10% frequency shift. The maximum alternating stress intensity is 5,957 psi.

5.2 Load Combinations and Allowable Stress Intensities

The stress ratios computed for CLTP at nominal frequency and with frequency shifting are listed in Table 8. The stress ratios are grouped according to type (SR-P for maximum membrane and membrane+bending stress, SR-a for alternating stress) and location (away from welds or on a weld).

For CLTP operation at nominal frequency the minimum stress ratio is identified as an alternating stress, SR-a=1.06, and occurs at the junction of the middle hood, the hood support and the adjacent base plate. The minimum stress ratio due to maximum stress intensity, SR-P=1.32, occurs at the dryer supports connecting to the upper support ring. The next two lowest stress ratios also involve hood support junctions. The lowest stress ratio location away from a hood support occurs where the drain channels join to the skirt. All of these locations lie on welds as summarized in Table 8a and the accompanying Figure 15.

The effects of frequency shifts can be conservatively accounted for by identifying the minimum stress ratio at every node, where the minimum is taken over all the frequency shifts considered (including the nominal or 0% shift case). The resulting stress ratios are then processed as before to identify the smallest stress ratios anywhere on the structure, categorized by stress type (maximum or alternating) and location (on or away from a weld). The results are summarized in Table 8b and show that the minimum stress ratio, SR-a=049, is identified with an alternating stress and occurs where outer hood, hood support and cover plate meet. This is the smallest stress ratio encountered anywhere on the structure for any frequency shift at the CLTP condition. The smallest stress ratio associated with a maximum stress is SR-P=0.93 and occurs at the same location.

Because the worst case stress ratios (i.e., the minimum stress ratio over all frequency shifts) are most important for conservative structural assessment, the locations of *all* nodes having maximum stress ratios, SR-P<1.5 are plotted in Figure 16e and all nodes having alternating stress ratios SR-a<1.5 are plotted in Figure 16h-i. These plots differ from the preceding ones where (see discussion in Section 5.3), the smallest stress ratio in a 10" region is identified and all other nodes in this region excluded from display and tabulation. In the current plots, this blanking is not performed so that a more complete picture of where stress ratios are low, is conveyed. These plots show that all maximum stress ratios, SR-P<1.5 occur at: (i) the hood/hood support/cover or base plate junctions and (ii) the steam dryer supports. All alternating stress ratios, SR-a<1.5 occur at: (i) the joints between the bottoms of the hood supports and adjacent components (vane banks, hoods and base or cover plates); (ii) the bottoms of the skirt/drain channel welds; (iii) the tops of the inner closure plates where they join to the vane banks and large middle plate; (iv) the connection between the large middle plate and the central top tie bar; and (v) the vane bank end plates.

In summary, the general picture that the outer and middle hood supports experience high stresses, particular at negative frequency shifts. As discussed in Section 5.1, the low stress ratio locations and their repositioning with frequency shift can be explained by the presence of a strong 218 Hz component in the loads. The fact that all stress ratios are above 1.0 at nominal operation (no frequency shift) is consistent with actual successful sustained dryer operation.

While frequency shifting is designed to promote conservatism in the FE analysis, in this case the results appear overly conservative given that structural integrity of the BFN2/3 dryer has been maintained during actual dryer operation despite the minimum stress ratio, SR-a=0.49 obtained at the -10% frequency shift. Nevertheless, this result does show that the structural response is sensitive to peaks in the load spectrum. In the present case the response is dominated by the 218 Hz signal (or its shifted counterpart). The option of reducing the stresses by eliminating this signal should therefore be considered. Therefore the stress intensities and ratios were recalculated with this 218 Hz component removed, and are reported in the next section.

Table 8a. Locations with minimum stress ratios for CLTP conditions with no frequency shift. Stress ratios are grouped according to stress type (maximum – SR-P; or alternating – SR-a) and location (away from a weld or at a weld). Bold text indicates minimum stress ratio of any type on the structure. Locations are depicted in Figure 15.

Stress Ratio	Location	Weld	Location (in.)				Stress Intensity (psi)			Stress Ratio	
			x	y	z	node	Pm	Pm+Pb	S_{alt}	SR-P	SR-a
SR-P	1. cover plate	No	-102.5	60.4	0.0	15602	864	7039	2090	3.90	5.92
SR-a	1. submerged drain channel	No	71.8	99.2	-100.5	20940	1947	4071	3826	6.74	3.23
	2. lock gusset		78.3	31.4	91.6	75086	2646	3622	3471	6.92	3.56
SR-P	1. upper support ring/support	Yes	5.8	122.4	-6.5	7532	7643	7643	<1500	1.32	>4
"	2. outer hood/hood support/cover plate	"	102.0	-28.7	0.0	90804	6665	8023	4601	1.51	1.49
"	3. outer hood/cover plate	"	102.0	-61.0	0.0	90780	4343	8340	3385	1.81	2.03
"	4. submerged drain channel/skirt	"	-91.0	76.7	-100.5	86525	1962	8284	5274	1.82	1.30
"	5. inner hood/middle closure plate/top cover plate	"	31.5	108.4	88.9	84319	5363	5779	1925	1.88	3.57
SR-a	**1. middle hood/hood support/outer base plate**	**Yes**	**70.8**	**54.6**	**0.0**	**85038**	**3745**	**7375**	**6451**	**2.05**	**1.06**
"	2. outer hood/hood support/cover plate	"	102.0	28.7	0.0	83543	4996	8119	5381	1.86	1.28
"	3. middle base plate/hood support/vane bank	"	55.0	54.6	0.0	83942	1126	5613	5295	2.69	1.30
"	4. submerged drain channel/skirt	"	-91.0	76.7	-100.5	86525	1962	8284	5274	1.82	1.30
"	5. submerged drain channel/skirt	"	11.5	118.4	-100.5	81700	1903	5556	4731	2.72	1.45
"	6. outer base plate/hood support/vane bank	"	86.0	28.7	0.0	85129	1490	4869	4376	3.10	1.57
"	7. outer hood/cover plate	"	-102.0	61.0	0.0	90427	4123	8111	3424	1.86	2.01

See Table 7a for coordinates description.

Table 8b. Locations with minimum stress ratios for CLTP conditions with frequency shifts. Stress ratios at every node are recorded as the lowest stress ratio identified during the frequency shifts. Stress ratios are grouped according to stress type (maximum – SR-P; or alternating – SR-a) and location (away from a weld or at a weld). Bold text indicates minimum stress ratio of any type on the structure. Locations are depicted in Figure 16.

Stress Ratio	Location	Weld	% Freq. Shift	Location (in.)				Stress Intensity (psi)			Stress Ratio	
				x	y	z	node	Pm	Pm+Pb	S_{alt}	SR-P	SR-a
SR-P	1. bottom of outer hood support	No	-10	-94.0	-28.7	0.0	18882	1147	9477	9022	2.90	1.37
SR-a	1. bottom of outer hood support	No	-10	-94.0	-28.7	0.0	18882	1147	9477	9022	2.90	1.37
"	2. outer hood support	"	-10	-93.6	-28.7	12.3	18856	698	6617	6600	4.15	1.87
"	3. bottom of middle hood support	"	-10	62.9	54.6	0.0	19298	694	6239	5997	4.40	2.06
SR-P	1. outer hood/hood support/cover plate	Yes	-10	-102.0	-28.7	0.0	81525	5441	16262	13902	0.93	0.49
"	2. outer base plate/hood support/vane bank	"	-10	-86.0	-28.7	0.0	82135	1898	13406	12751	1.13	0.54
"	3. upper support ring/support	"	+7.5	-5.8	-122.4	-6.5	7705	7932	7932	<1500	1.27	>4
"	4. middle hood/hood support/outer base plate	"	-10	70.8	54.6	0.0	85038	3745	10796	9853	1.40	0.70
"	5. outer hood/cover plate	"	-10	102.0	-61.0	0.0	90780	4888	9838	5004	1.53	1.37
"	6. submerged drain channel/skirt	"	-5	-91.0	-76.7	-100.5	79884	2904	9542	6649	1.58	1.03
SR-a	**1. outer hood/hood support/cover plate**	**Yes**	**-10**	**-102.0**	**-28.7**	**0.0**	**81525**	**5441**	**16262**	**13902**	**0.93**	**0.49**
"	2. outer base plate/hood support/vane bank	"	-10	-86.0	-28.7	0.0	82135	1898	13406	12751	1.13	0.54
"	3. middle hood/hood support/outer base plate	"	-10	70.8	54.6	0.0	85038	3745	10796	9853	1.40	0.70
"	4. middle base plate/hood support/vane bank	"	-10	55.0	54.6	0.0	83942	1126	9455	9232	1.60	0.74
"	5. outer hood/hood support	"	-10	-102.0	-28.7	11.5	81517	794	8701	8678	1.74	0.79

See Table 7a for coordinates description.

Table 8b (continued). Locations with minimum stress ratios for CLTP conditions with frequency shifts. Stress ratios at every node are recorded as the lowest stress ratio identified during the frequency shifts. Stress ratios are grouped according to stress type (maximum – SR-P; or alternating – SR-a) and location (away from a weld or at a weld).

Stress Ratio	Location	Weld	% Freq. Shift	Location (in.)				Stress Intensity (psi)			Stress Ratio	
				x	y	z	node	Pm	Pm+Pb	S_{alt}	SR-P	SR-a
SR-a	6. hood support/vane bank	Yes	-10	-86.0	-28.7	12.1	82187	611	8458	8421	1.79	0.82
"	7. inner hood/hood support/base plate	"	+7.5	39.8	59.8	0.0	90643	4453	8086	7055	1.87	0.97
"	8. submerged drain channel/skirt	"	-5	-91.0	-76.7	-100.5	79884	2904	9542	6649	1.58	1.03
"	9. hood support/vane bank	"	-10	55.0	54.6	12.1	86621	533	6392	6351	2.36	1.08
"	10. top perforated plate/inner closure plate	"	+7.5	15.0	118.9	88.9	88303	1884	8280	6338	1.82	1.08
"	11. submerged drain channel/skirt	"	-7.5	11.5	118.4	-100.5	81700	2750	7196	6261	2.10	1.10
"	12. inner base plate/hood support/vane bank	"	+7.5	24.0	59.8	0.0	83750	1144	5995	5691	2.52	1.21
"	13. middle hood/hood support	"	-10	70.8	54.6	11.5	84804	626	5700	5638	2.65	1.22
"	14. outer hood/cover plate	"	-10	102.0	-61.0	0.0	90780	4887	9837	5004	1.53	1.37

See Table 7a for coordinates description.

Table 8c. Locations with minimum stress ratios at CLTP conditions with -10% frequency shift. Stress ratios are grouped according to stress type (maximum – SR-P; or alternating – SR-a) and location (away from a weld or at a weld). Bold text indicates minimum stress ratio of any type on the structure. Locations are depicted in Figure 17. Stress ratios at non-weld locations are greater than 4.0.

Stress Ratio	Location	Weld	Location (in.)				Stress Intensity (psi)			Stress Ratio	
			x	y	z	node	Pm	Pm+Pb	S_{alt}	SR-P	SR-a
SR-P	1. hood support	No	-94.0	-28.7	0.0	18882	1028	9477	9022	2.90	1.37
SR-a	1. hood support	No	-94.0	-28.7	0.0	18882	1028	9477	9022	2.90	1.37
"	2. hood support	"	-93.6	-28.7	12.3	18856	489	6617	6600	4.15	1.87
"	3. hood support	"	62.9	54.6	0.0	19298	601	6239	5997	4.40	2.06
SR-P	1. outer hood/hood support/cover plate	Yes	-102.0	-28.7	0.0	81525	5036	16262	13902	0.93	0.49
"	2. outer base plate/hood support/vane bank	"	-86.0	-28.7	0.0	82135	1107	13406	12751	1.13	0.54
"	3. upper support ring/support	"	-5.8	-122.4	-6.5	7705	7710	7710	0	1.31	755.56
"	4. middle hood/hood support/outer base plate	"	70.8	54.6	0.0	85038	2490	10796	9853	1.40	0.70
"	5. outer hood/cover plate	"	102.0	-61.0	0.0	90780	4888	9838	5004	1.53	1.37
SR-a	**1. outer hood/hood support/cover plate**	**Yes**	**-102.0**	**-28.7**	**0.0**	**81525**	**5036**	**16262**	**13902**	**0.93**	**0.49**
"	2. outer base plate/hood support/vane bank	"	-86.0	-28.7	0.0	82135	1107	13406	12751	1.13	0.54
"	3. middle hood/hood support/outer base plate	"	70.8	54.6	0.0	85038	2490	10796	9853	1.40	0.70
"	4. middle base plate/hood support/vane bank	"	55.0	54.6	0.0	83942	795	9455	9232	1.60	0.74
"	5. outer hood/hood support	"	-102.0	-28.7	11.5	81517	486	8701	8678	1.74	0.79
"	6. hood support/vane bank	"	-86.0	-28.7	12.1	82187	450	8458	8421	1.79	0.82
"	7. hood support/vane bank	"	55.0	54.6	12.1	86621	280	6392	6351	2.36	1.08
"	8. middle hood/hood support	"	70.8	54.6	11.5	84804	574	5701	5639	2.65	1.22
"	9. outer hood/cover plate	"	102.0	-61.0	0.0	90780	4888	9838	5004	1.53	1.37

See Table 7a for coordinates description.

Table 8d. Locations with minimum stress ratios for at CLTP conditions with +10% frequency shift. Stress ratios are grouped according to stress type (maximum – SR-P; or alternating – SR-a) and location (away from a weld or at a weld). Bold text indicates minimum stress ratio of any type on the structure. Locations are depicted in Figure 18.

Stress Ratio	Location	Weld	Location (in.)				Stress Intensity (psi)			Stress Ratio	
			x	y	z	node	Pm	Pm+Pb	S_{alt}	SR-P	SR-a
SR-P	1. middle closure plate	No	34.4	108.4	88.9	17571	4907	4995	1642	3.73	7.53
SR-a	1. outer hood	No	96.5	51.1	45.2	47491	407	4130	4116	6.65	3.00
"	2. lock gusset	"	78.3	-31.4	91.6	75109	2971	5399	4047	5.08	3.05
SR-P	1. upper support ring/support	Yes	-5.8	-122.4	-6.5	7705	7729	7729	<1500	1.30	>4
"	2. outer hood/hood support/cover plate	"	102.0	-28.7	0.0	90804	5954	8457	4727	1.69	1.45
"	3. inner hood/middle closure plate/top cover plate	"	31.5	108.4	88.9	84319	5708	6506	2704	1.76	2.54
SR-a	**1. outer hood/hood support/cover plate**	**Yes**	**102.0**	**28.7**	**0.0**	**83543**	**5250**	**8580**	**5957**	**1.76**	**1.15**
"	2. outer base plate/hood support/vane bank	"	86.0	28.7	0.0	85129	1310	5574	5093	2.71	1.35
"	3. inner side panel/top cover plate/inner closure plate	"	-15.0	-118.9	88.9	83324	1881	6605	4467	2.29	1.54
"	4. outer hood/outer end wall	"	99.3	-70.8	31.9	81237	519	4404	4221	3.43	1.63
"	5. tie bar/top cover plate		48.0	3.0	88.9	82037	915	3900	3884	3.87	1.77

See Table 7a for coordinates description.

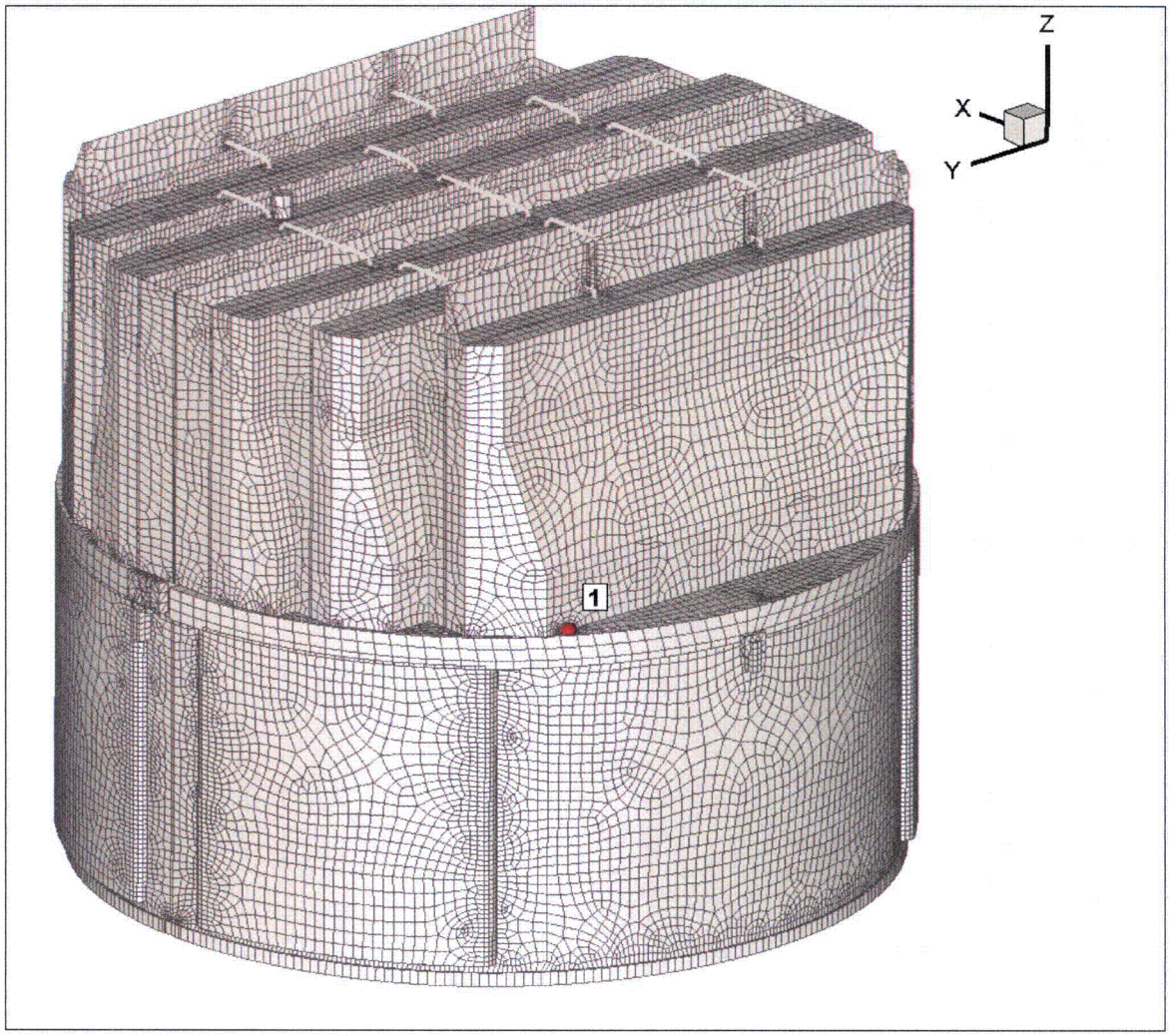

Figure 15a. Location of smalles stress ratio, SR-P, associated with a maximum stress at non-welds for nominal CLTP operation. Number refers to the enumerated locations for SR-P values at non-welds in Table 8a.

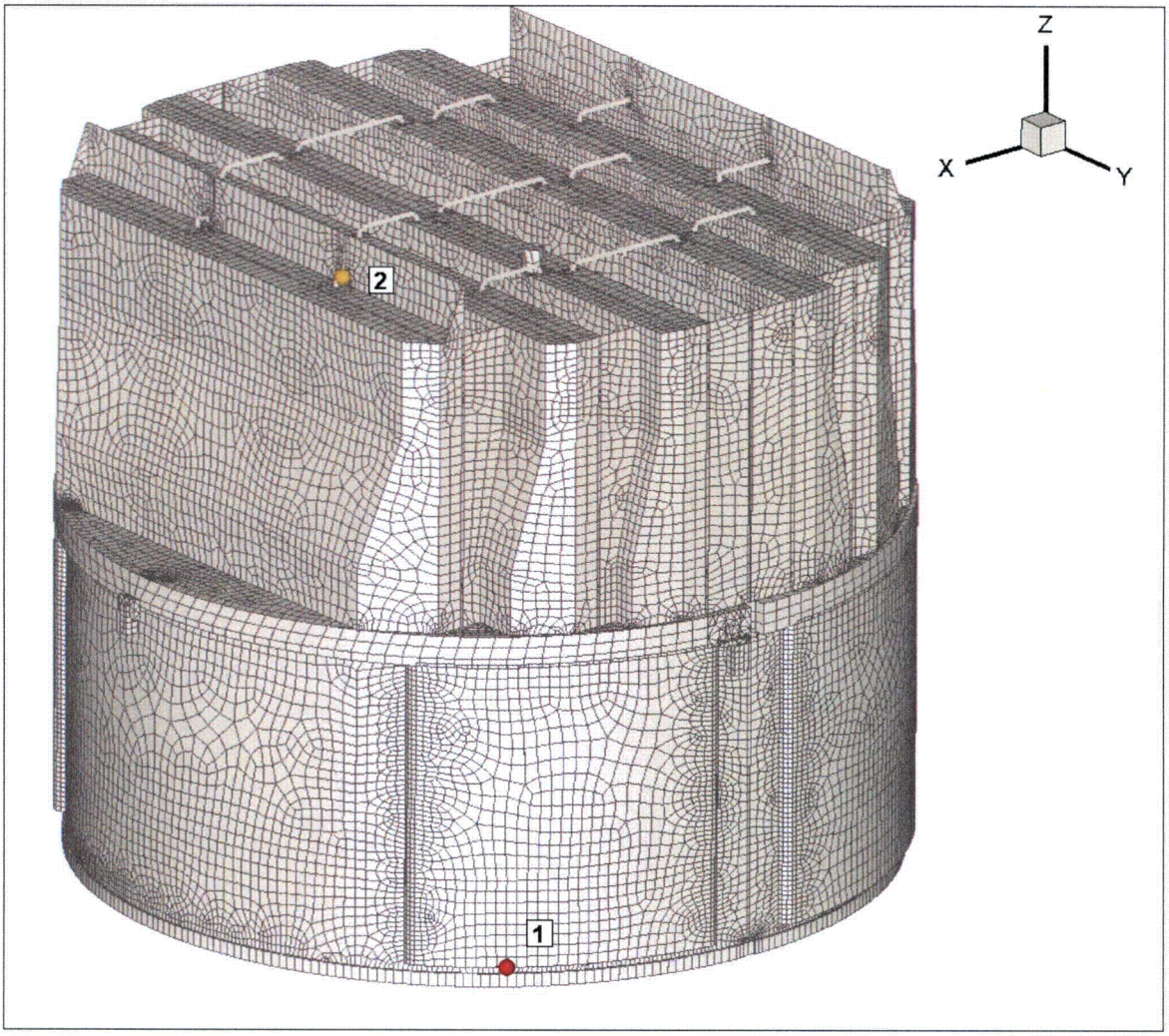

Figure 15b. Location of minimum alternating stress ratio, SR-a, at non-welds for nominal CLTP operation. Number refers to the enumerated locations for SR-a values at non-welds in Table 8a.

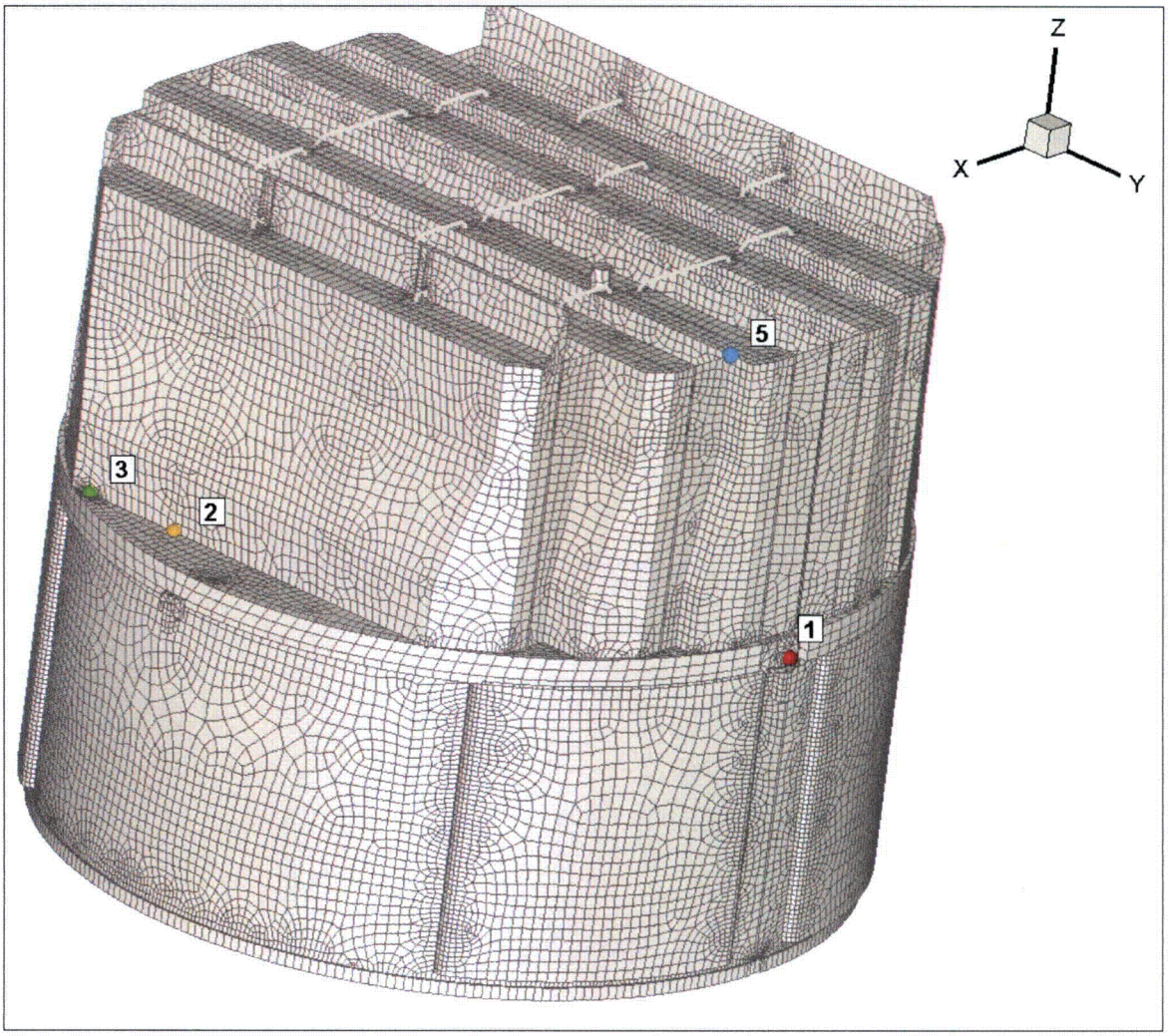

Figure 15c. Locations of smallest stress ratios, SR-P, associated with maximum stresses at welds for nominal CLTP operation. Numbers refer to the enumerated locations for SR-P values at welds in Table 8a. This view shows locations 1-3 and 5.

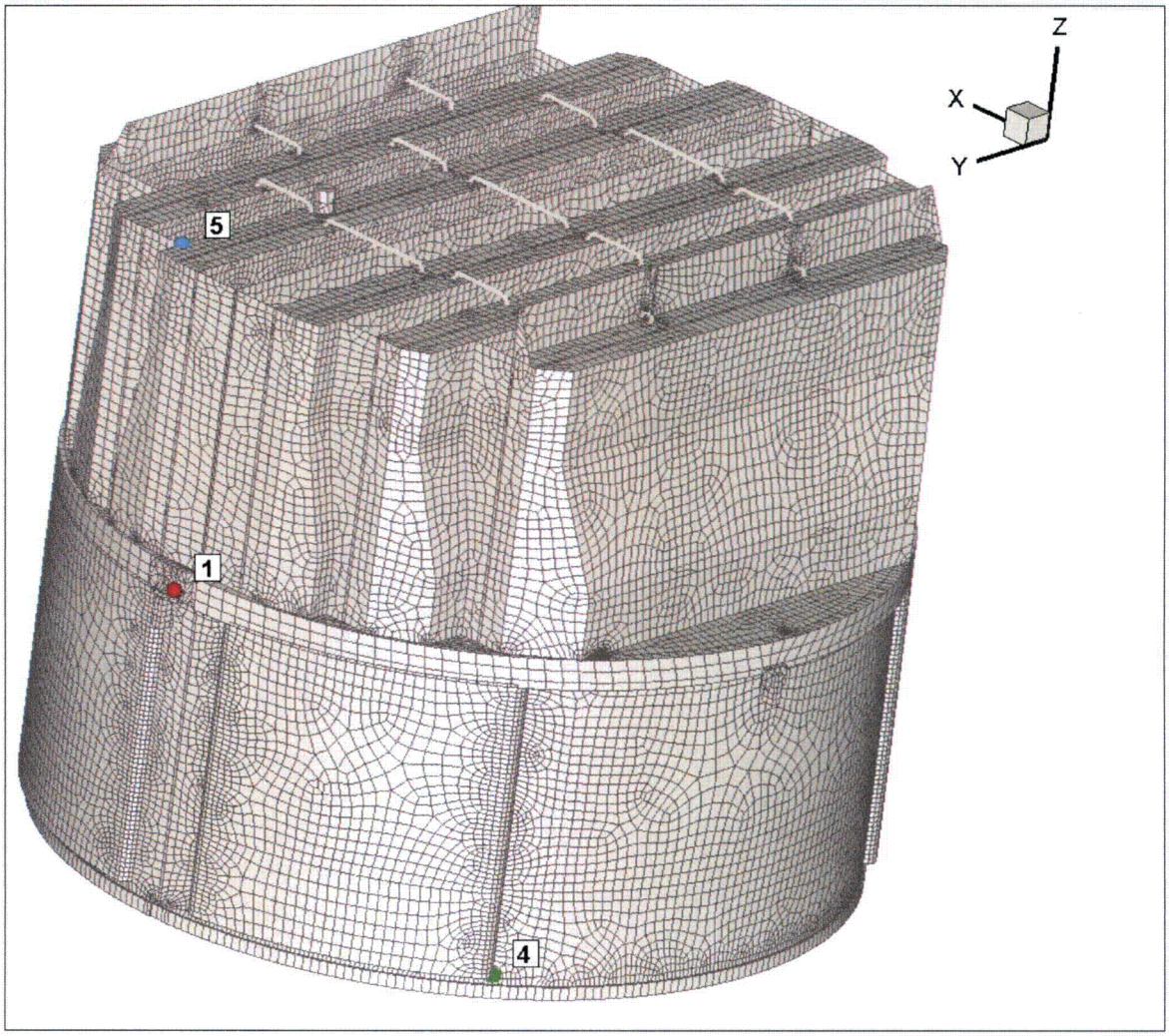

Figure 15d. Locations of minimum stress ratios, SR-P, associated with maximum stresses at welds for nominal CLTP operation. Numbers refer to the enumerated locations for SR-P values at welds in Table 8a. This view shows locations 1, 4 and 5.

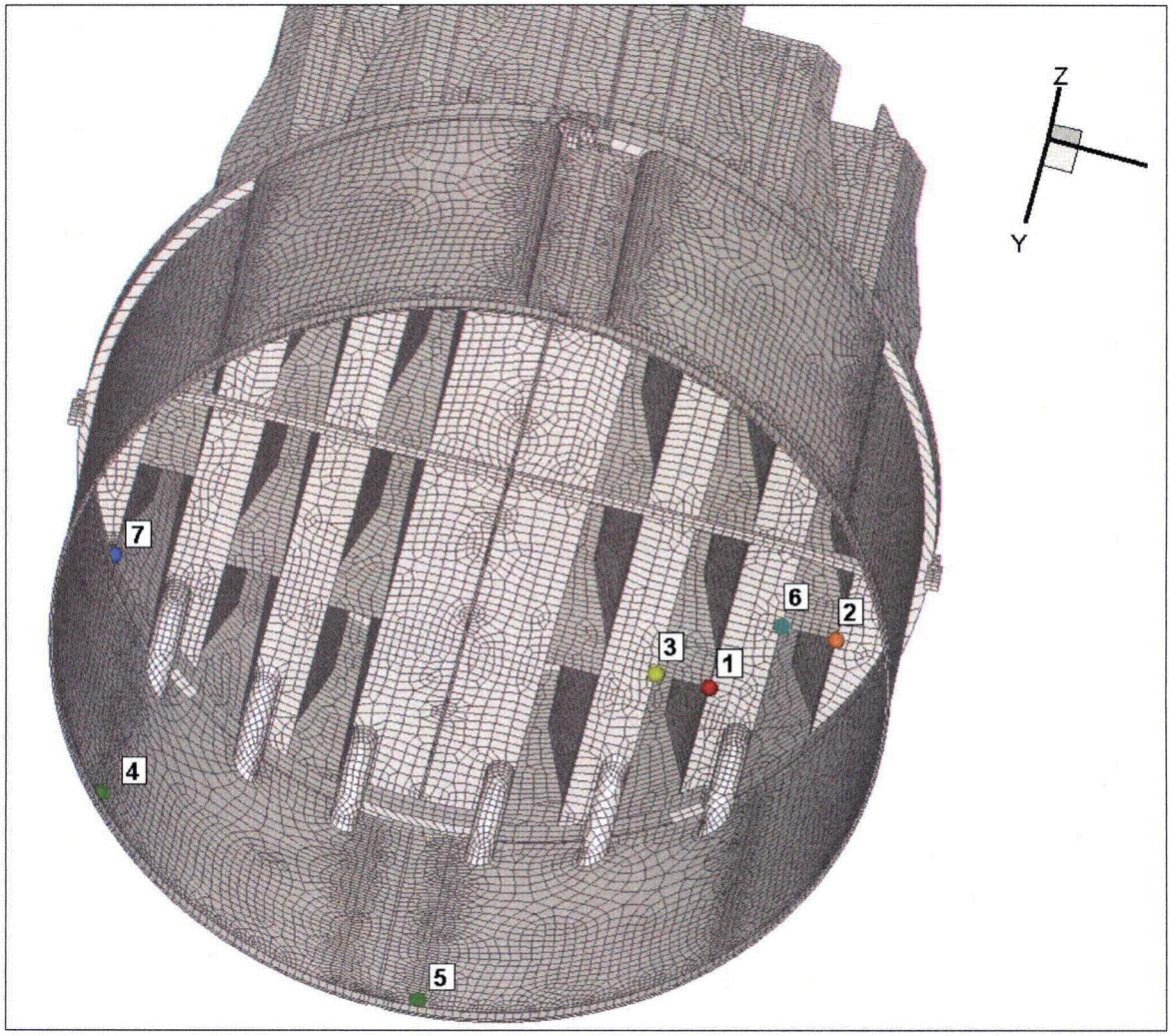

Figure 15e. Locations of minimum alternating stress ratios, SR-a, at welds for nominal CLTP operation. Numbers refer to the enumerated locations for SR-a values at welds in Table 8a. Locations 1-7 are shown.

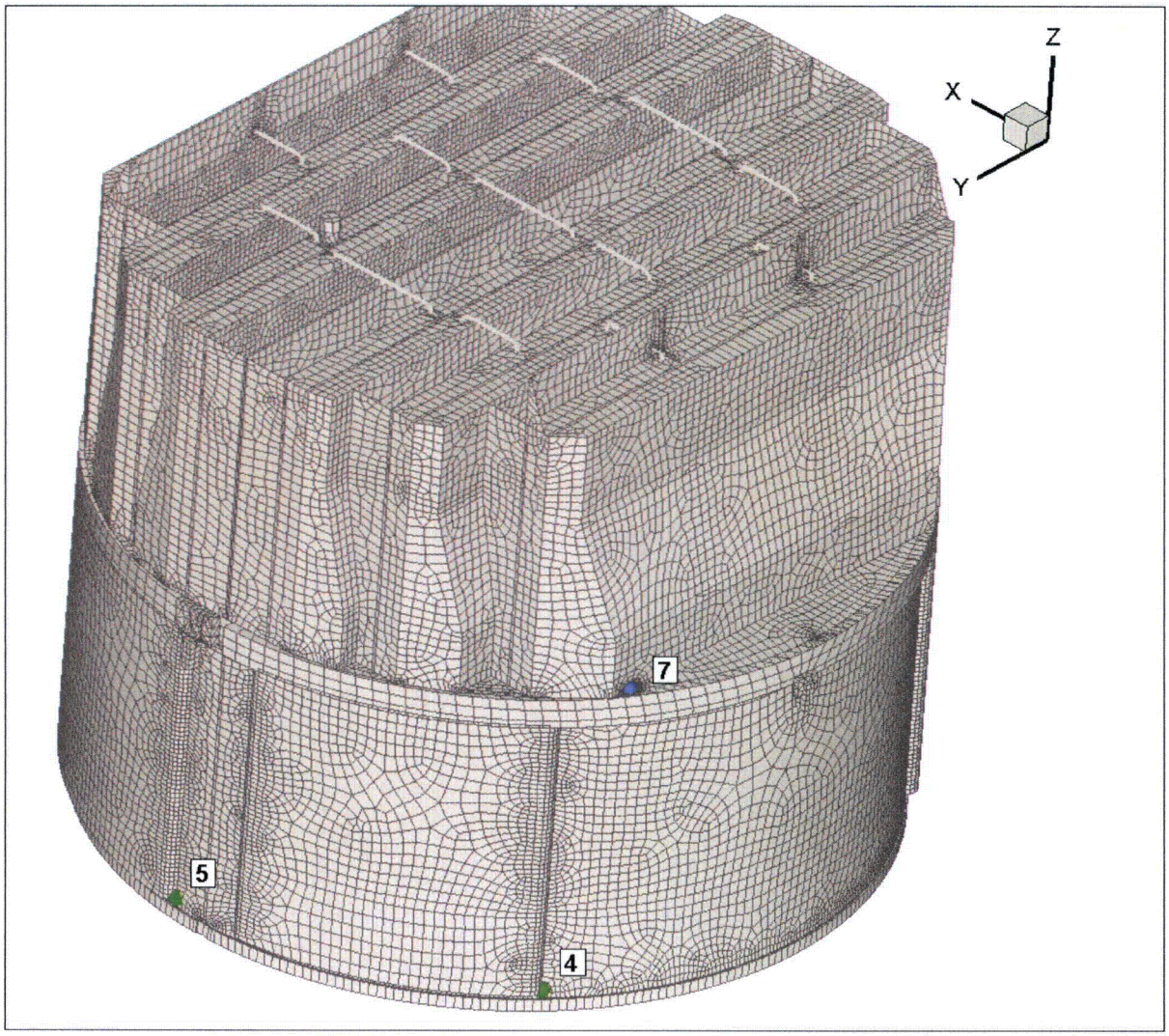

Figure 15f. Locations of minimum alternating stress ratios, SR-a, at welds for nominal CLTP operation. Numbers refer to the enumerated locations for SR-a values at welds in Table 8a. Locations 4, 5 and 7 are shown.

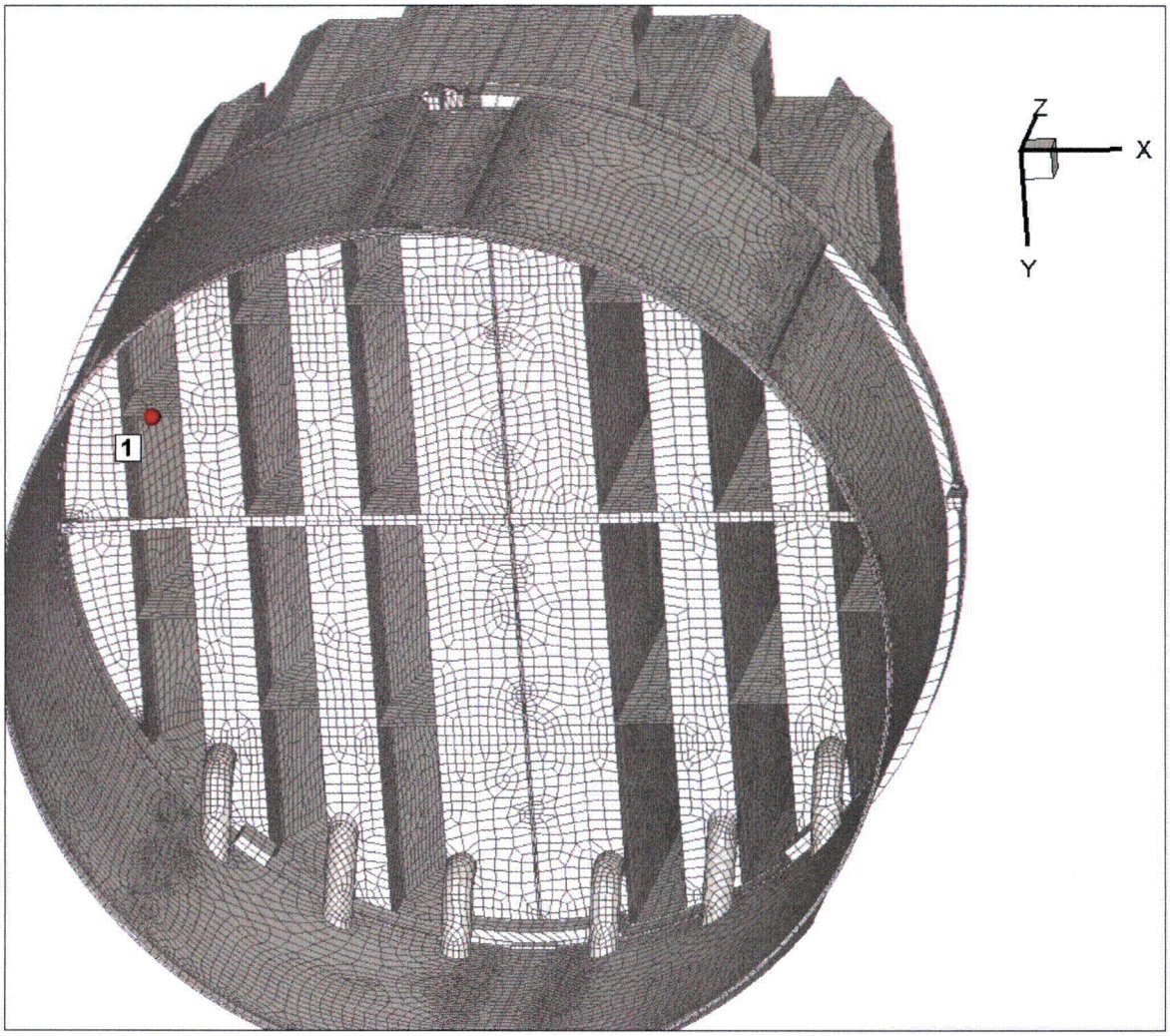

Figure 16a. Location of minimum stress ratio, SR-P, associated with maximum stresses at non-welds for CLTP operation with frequency shifts. The recorded stress ratio is the minimum value taken over all frequency shifts. The number refers to the enumerated location for SR-P values at non-welds in Table 8b.

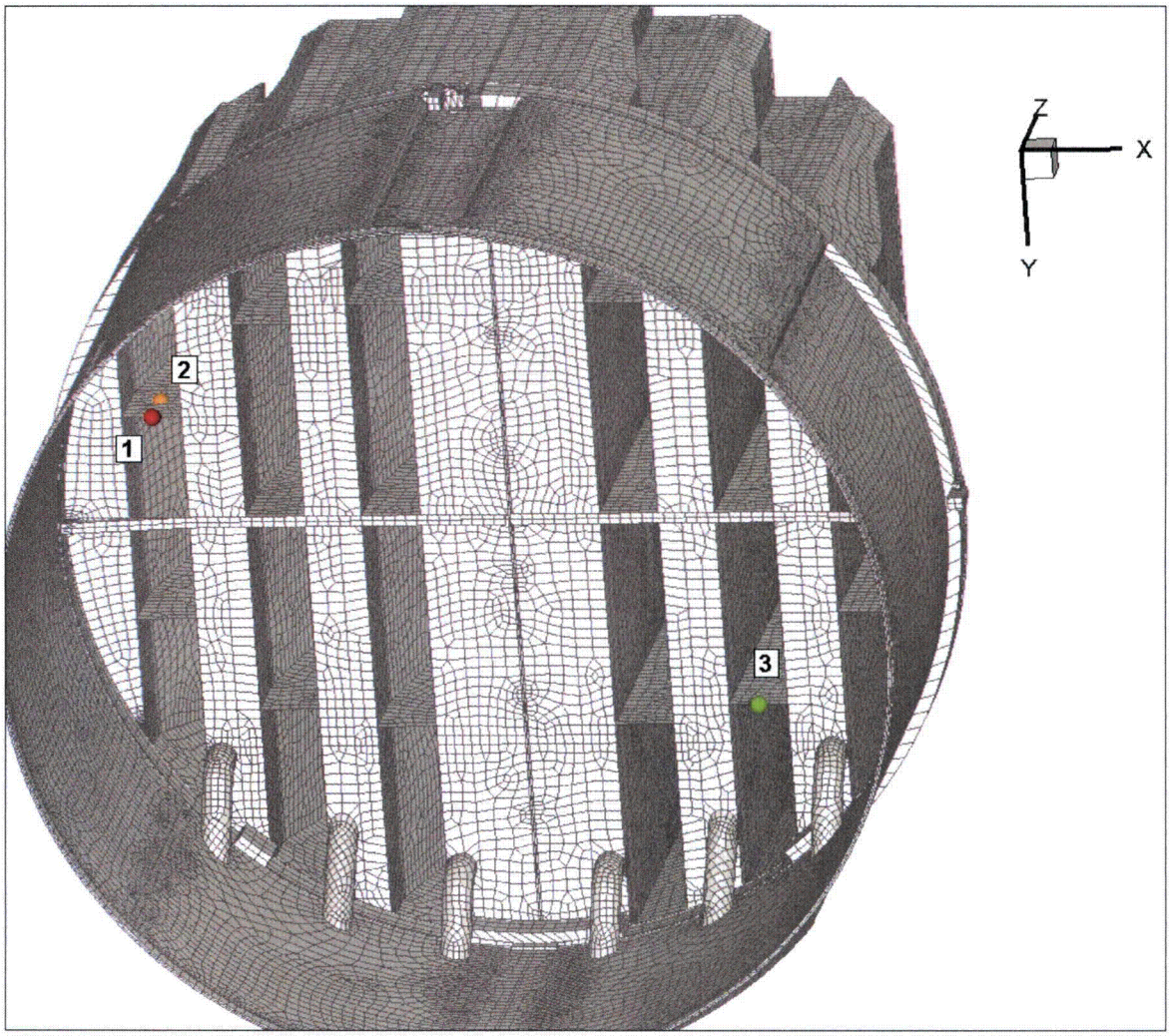

Figure 16b. Locations of minimum alternating stress ratios, SR-a, at non-welds for CLTP operation with frequency shifts. The recorded stress ratio at a node is the minimum value taken over all frequency shifts. Numbers refer to the enumerated locations for SR-a values at non-welds in Table 8b.

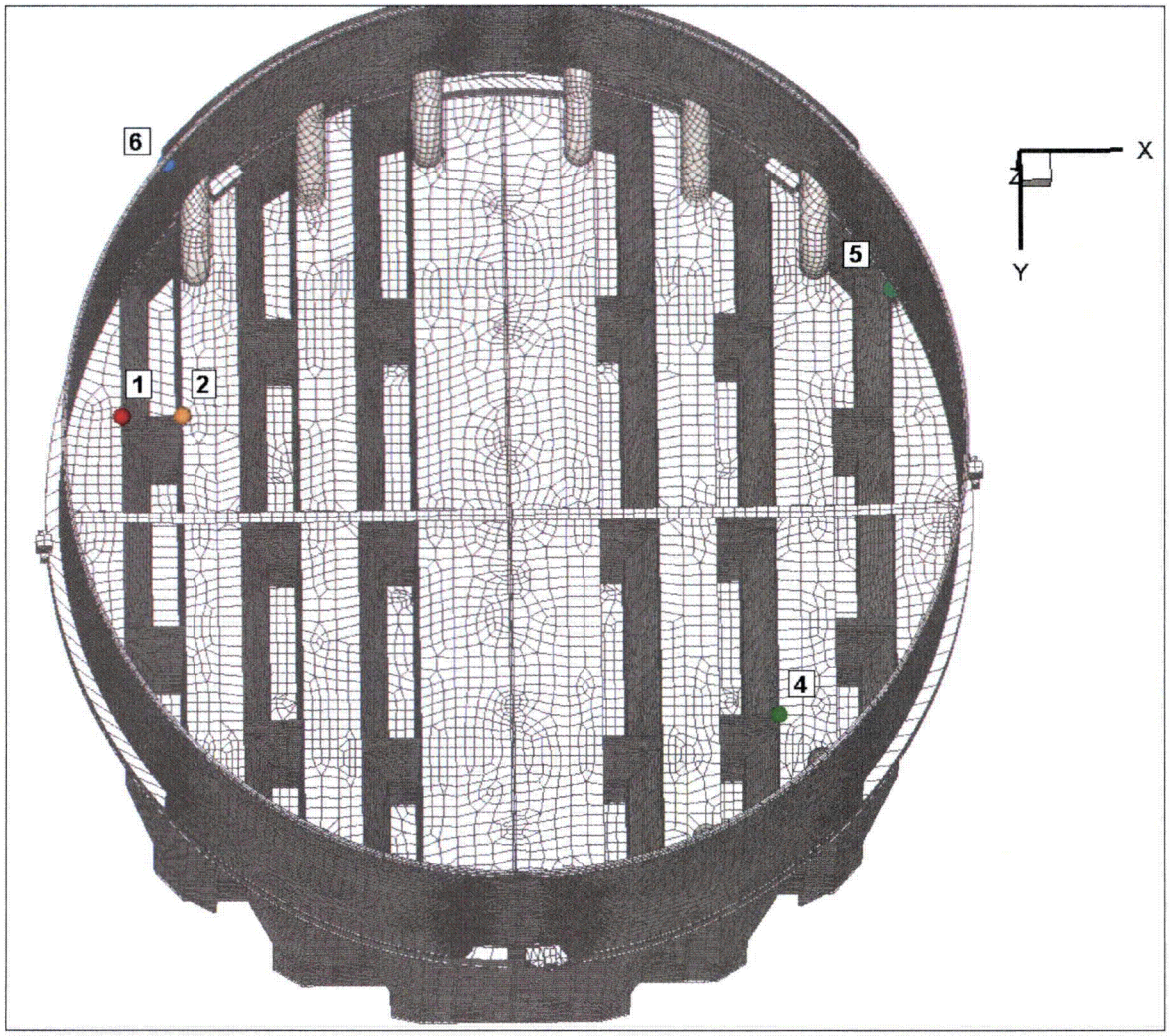

Figure 16c. Locations of minimum stress ratios, SR-P, associated with maximum stresses at welds for CLTP operation with frequency shifts. The recorded stress ratio at a node is the minimum value taken over all frequency shifts. Numbers refer to the enumerated locations for SR-P values at welds in Table 8b. This view shows locations 1, 2 and 4-6.

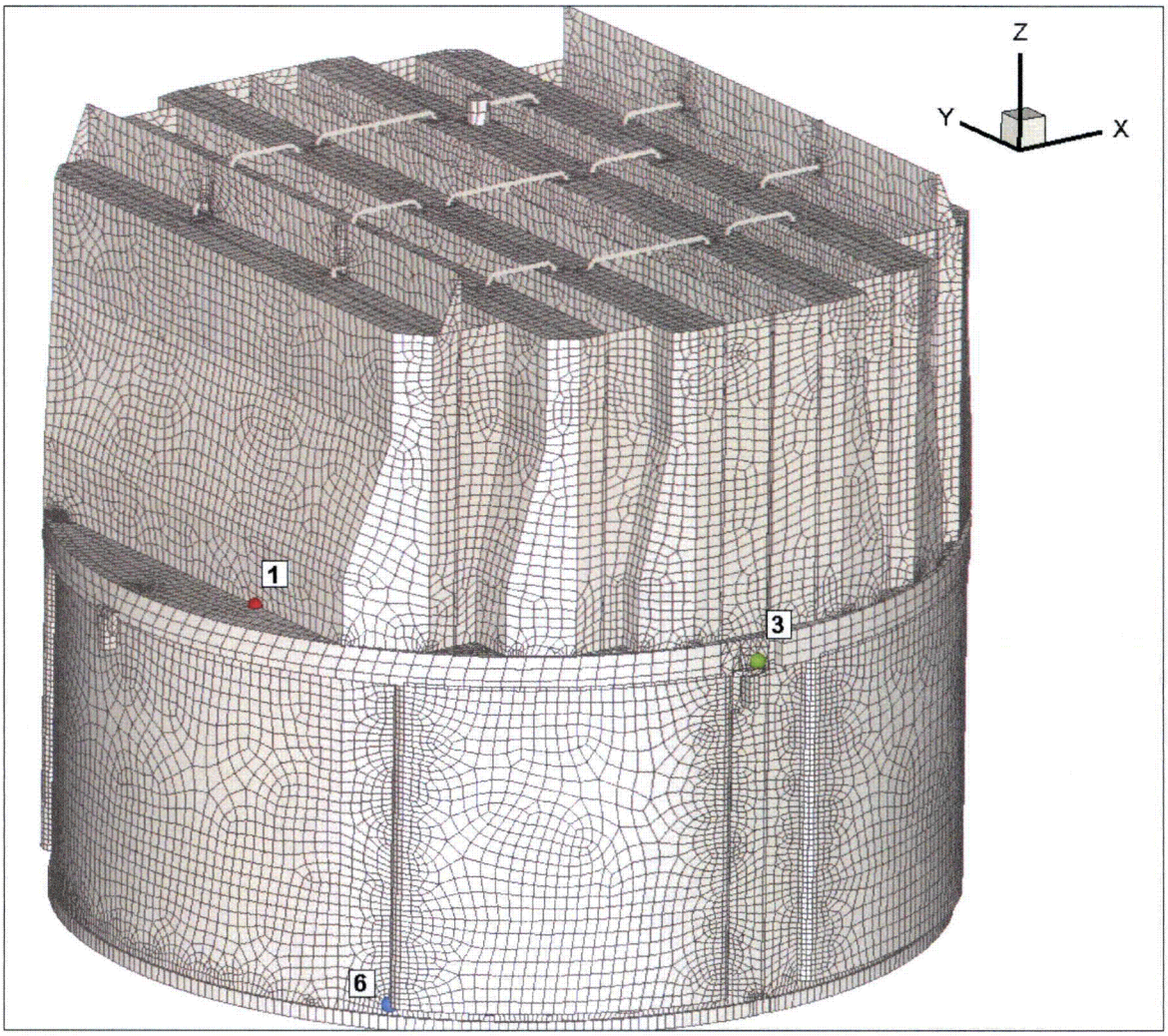

Figure 16d. Locations of minimum stress ratios, SR-P, associated with maximum stresses at welds for CLTP operation with frequency shifts. The recorded stress ratio at a node is the minimum value taken over all frequency shifts. Numbers refer to the enumerated locations for SR-P values at welds in Table 8b. This view shows locations 1, 3 and 6.

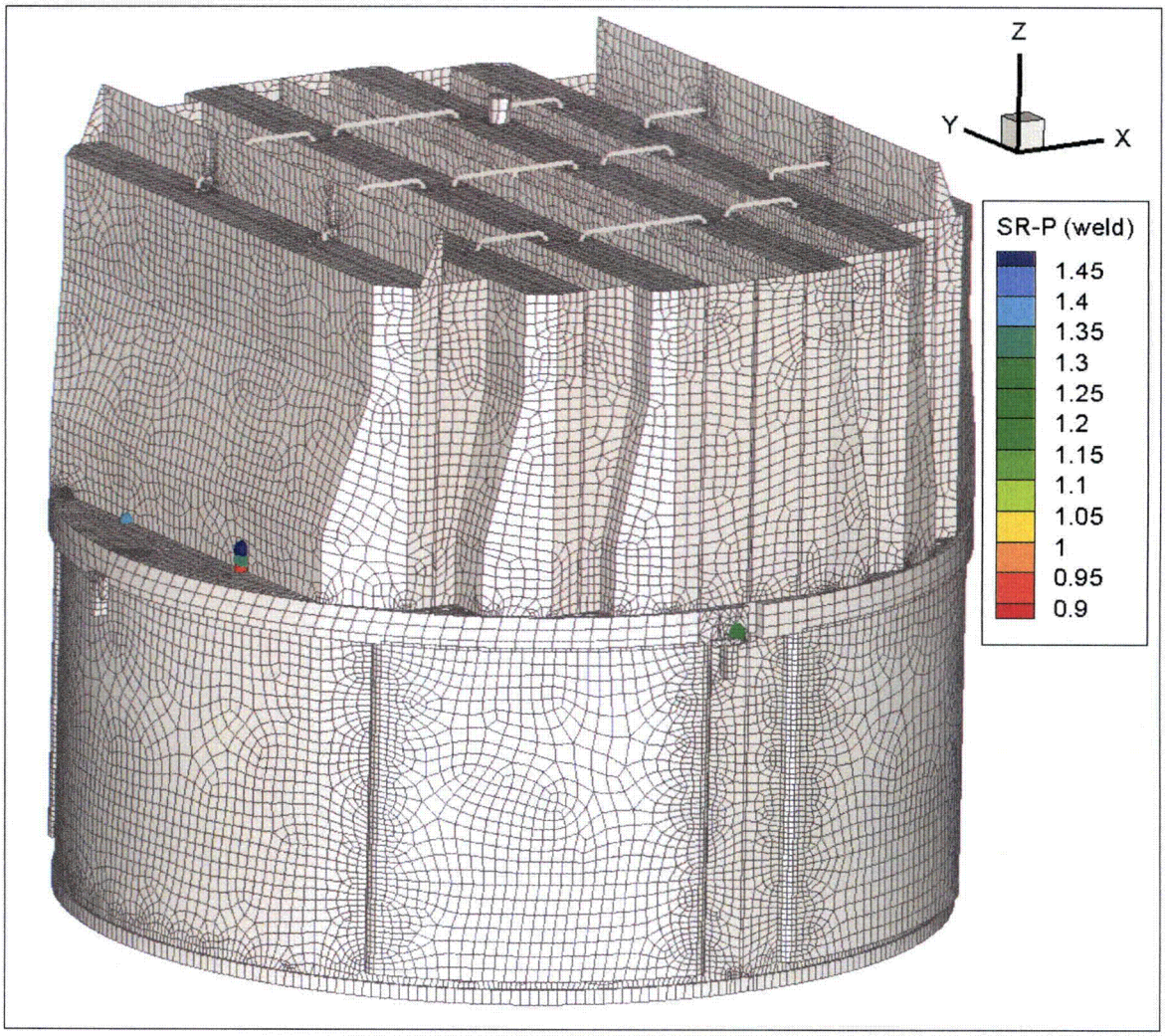

Figure 16e. Locations of minimum stress ratios, SR-P, associated with maximum stresses at welds for CLTP operation with frequency shifts. The recorded stress ratio at a node is the minimum value taken over all frequency shifts. This view displays *all* nodes with SR-a<1.5.

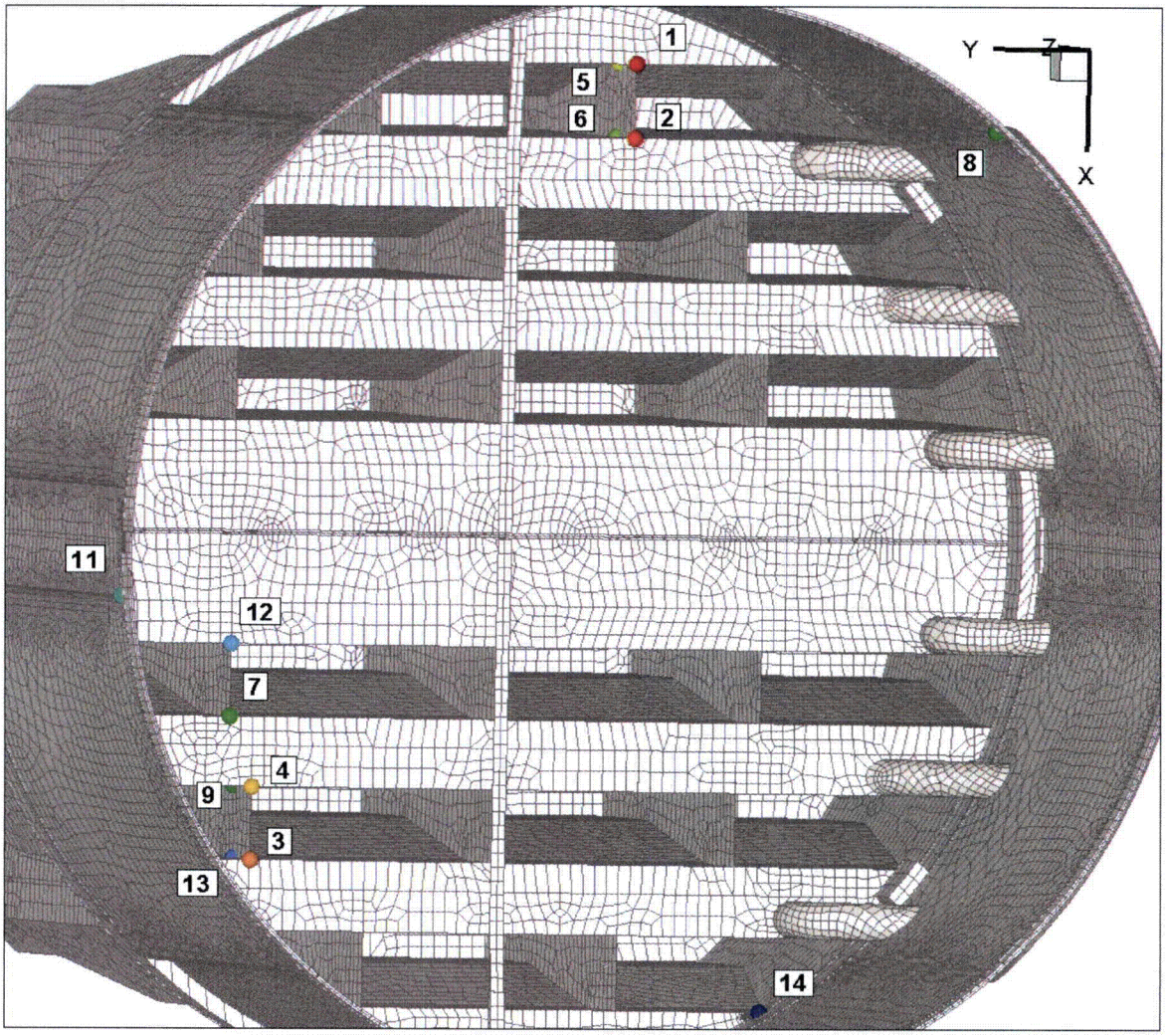

Figure 16f. Locations of minimum alternating stress ratios, SR-a, at welds for CLTP operation with frequency shifts. The recorded stress ratio at a node is the minimum value taken over all frequency shifts. Numbers refer to the enumerated locations for SR-a values at welds in Table 8b. First view showing enumerated locations 1-9 and 11-14.

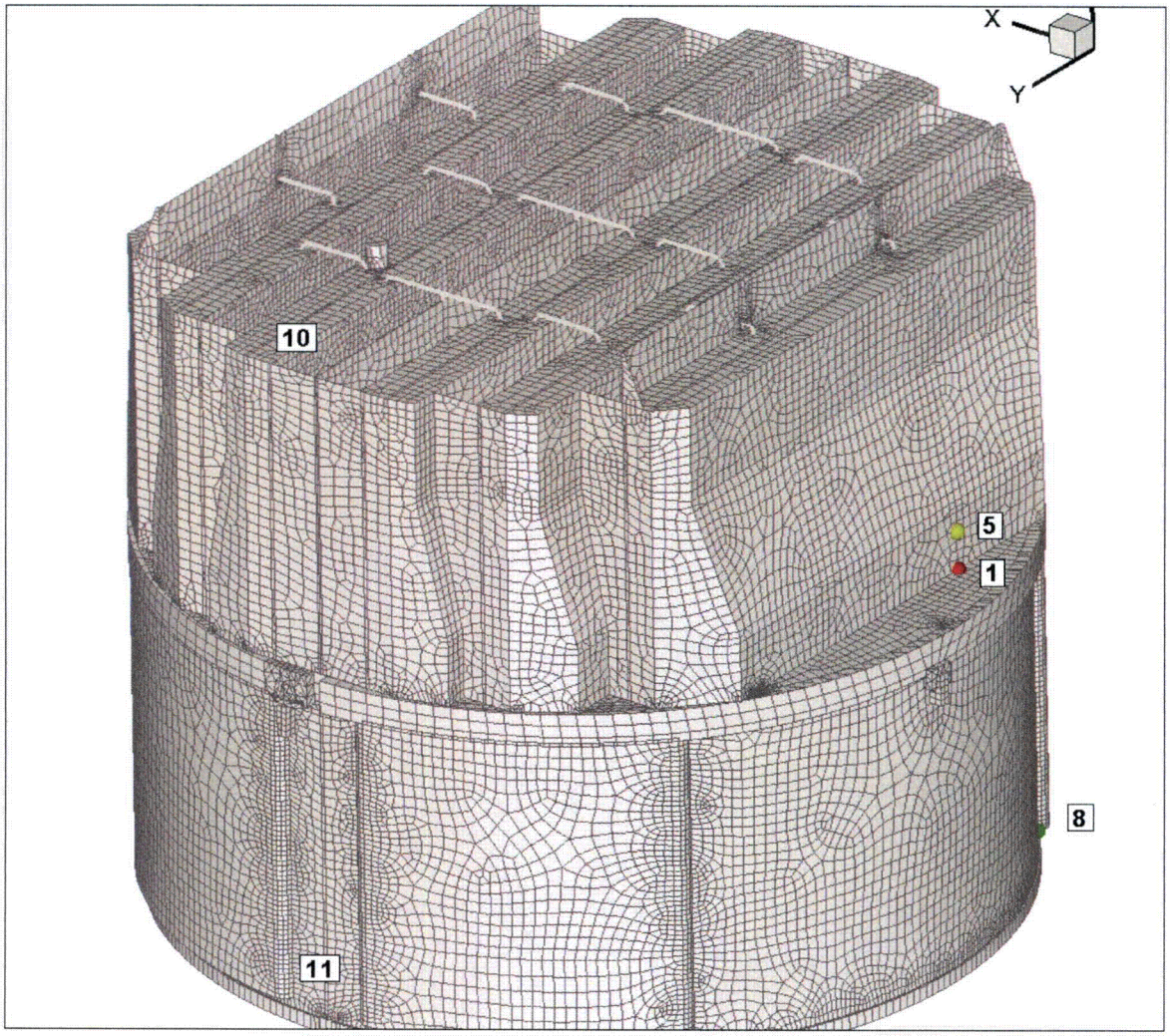

Figure 16g. Locations of minimum alternating stress ratios, SR-a, at welds for CLTP operation with frequency shifts. The recorded stress ratio at a node is the minimum value taken over all frequency shifts. Numbers refer to the enumerated locations for SR-a values at welds in Table 8b. Second view showing locations 1, 5, 8, 10 and 11.

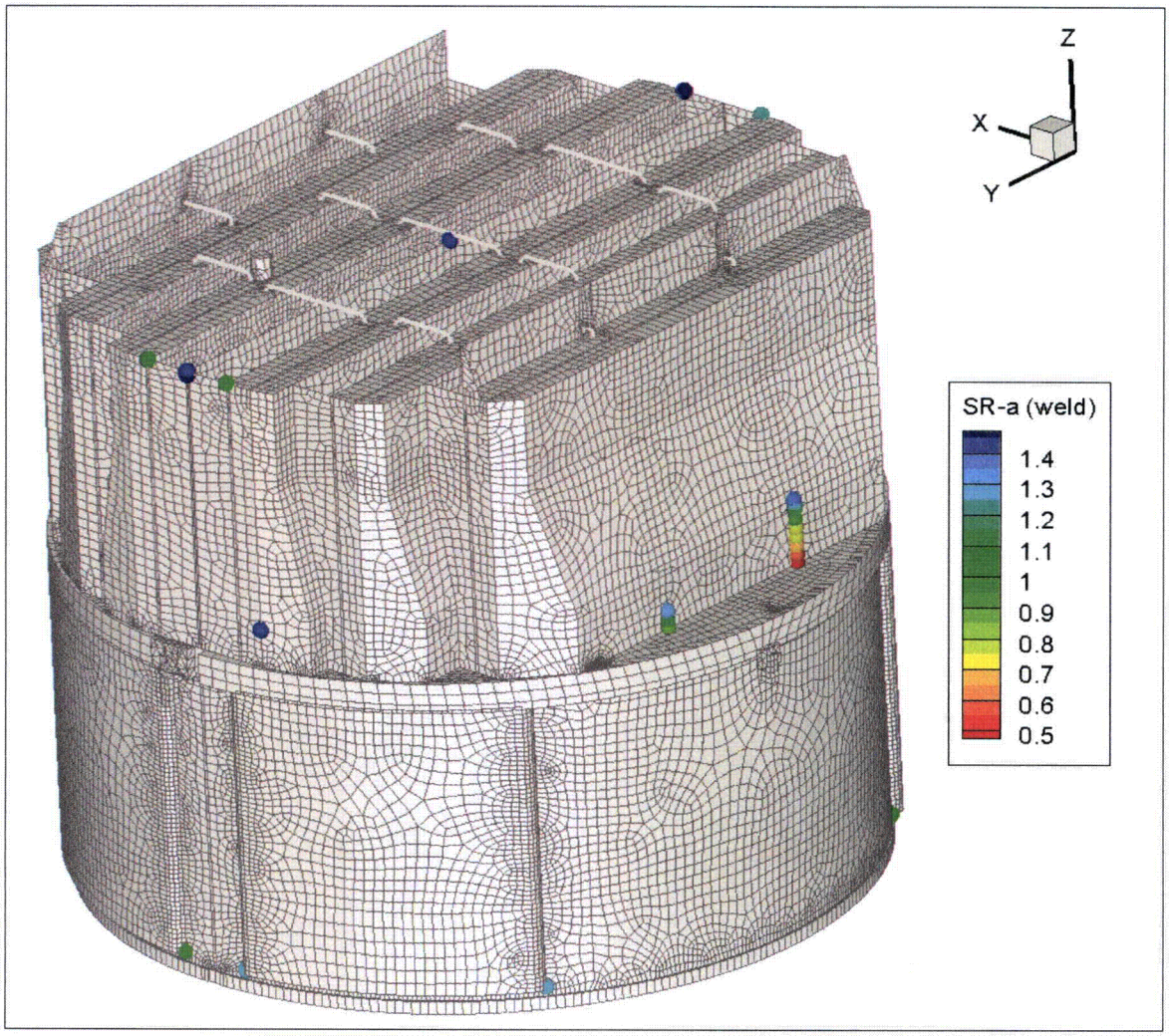

Figure 16h. Locations of minimum alternating stress ratios, SR-a, at welds for CLTP operation with frequency shifts. The recorded stress ratio at a node is the minimum value taken over all frequency shifts. This figure shows *all* nodes with SR-a<1.5. View 1 (from bottom).

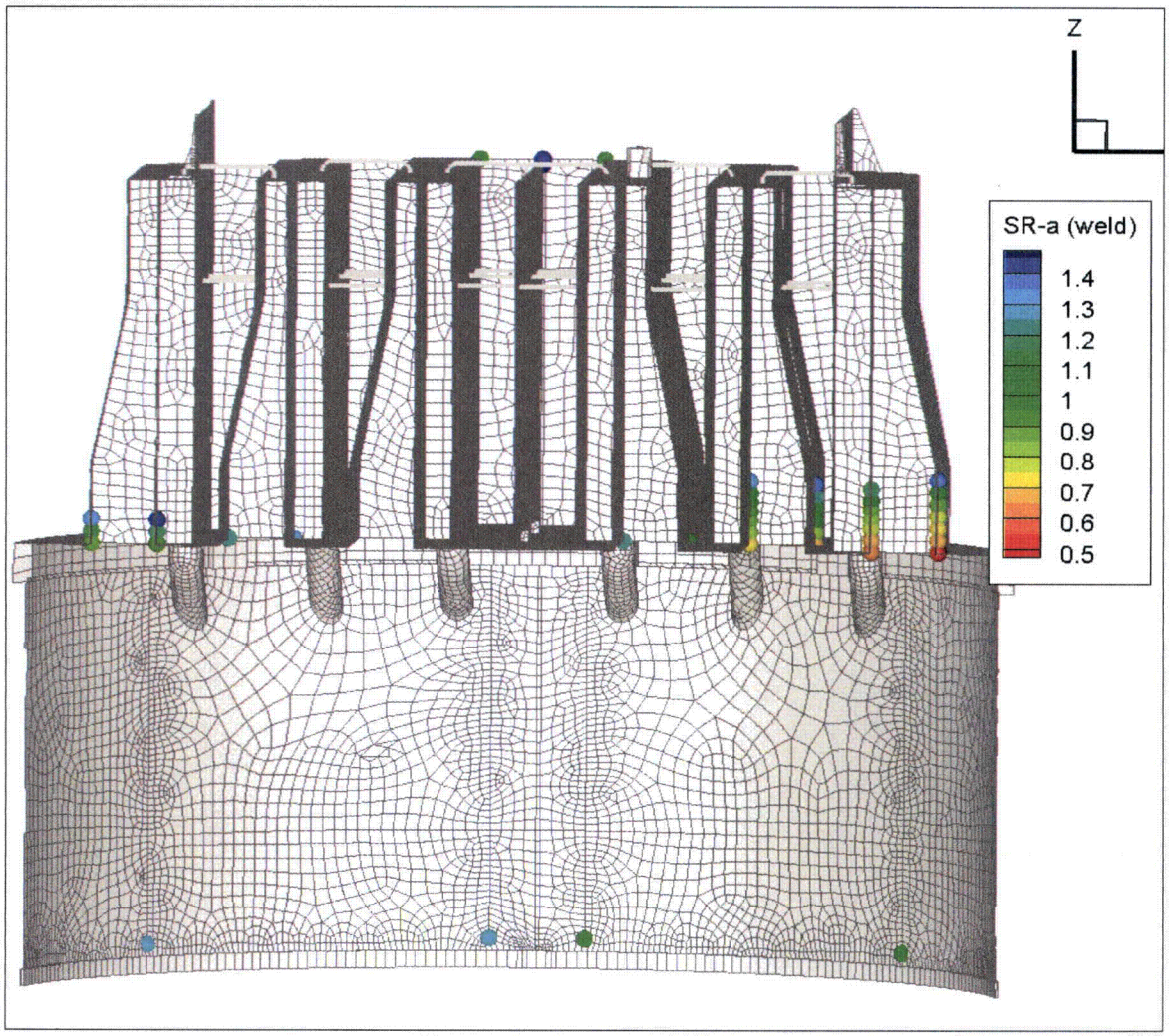

Figure 16i. Locations of minimum alternating stress ratios, SR-a, at welds for CLTP operation with frequency shifts. The recorded stress ratio at a node is the minimum value taken over all frequency shifts. This figure shows *all* nodes with SR-a<1.5. This second cut-away view shows the high stress spots on the outer and middle hood supports.

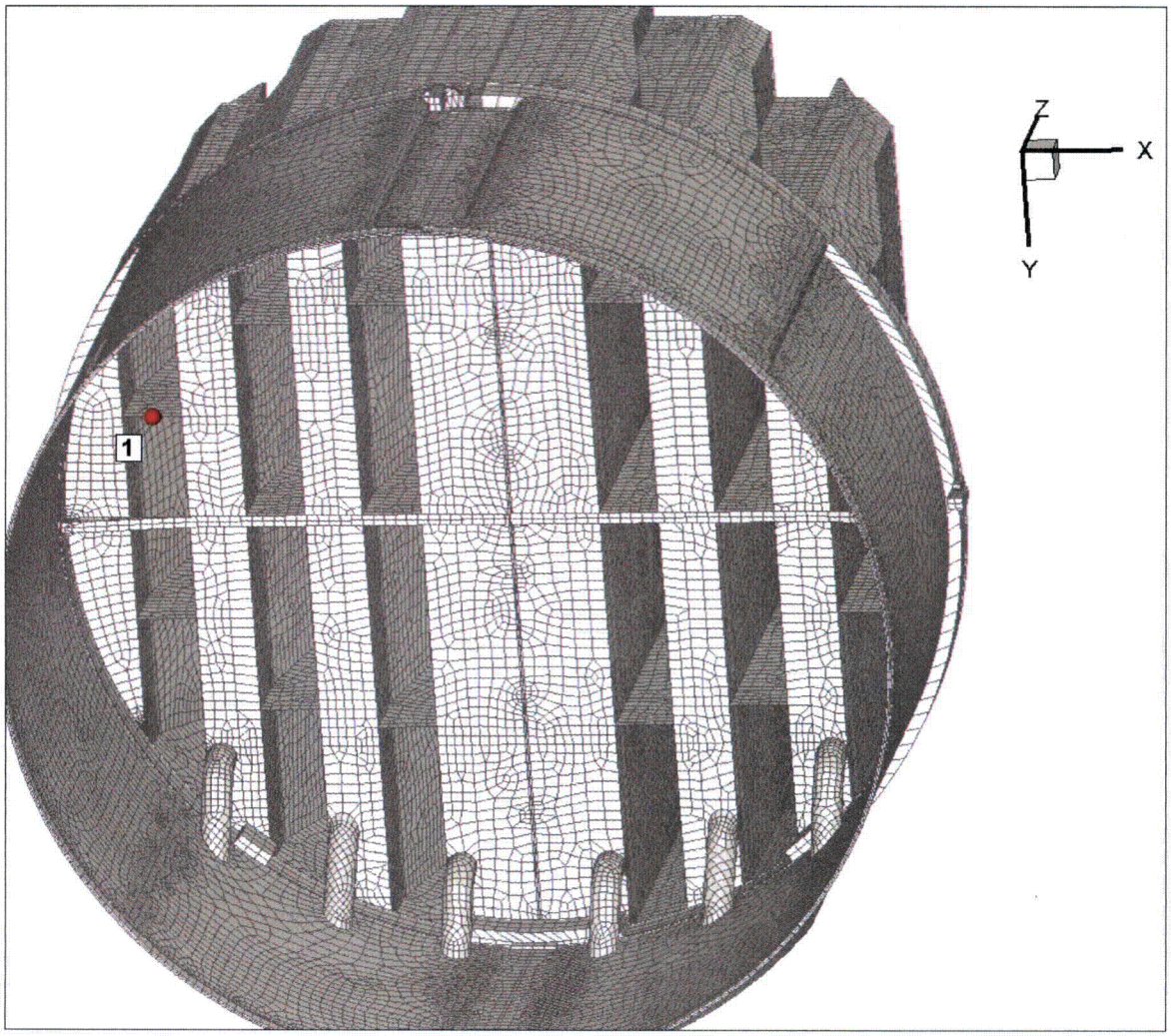

Figure 17a. Locations of minimum stress ratios, SR-P, associated with maximum stresses at non-welds for CLTP operation with -10% frequency shift. Numbers refer to the enumerated locations for SR-P values at non-welds in Table 8c. The figure is identical to the one in Figure 16a since this the -10% shift yielded the lowest stress ratio.

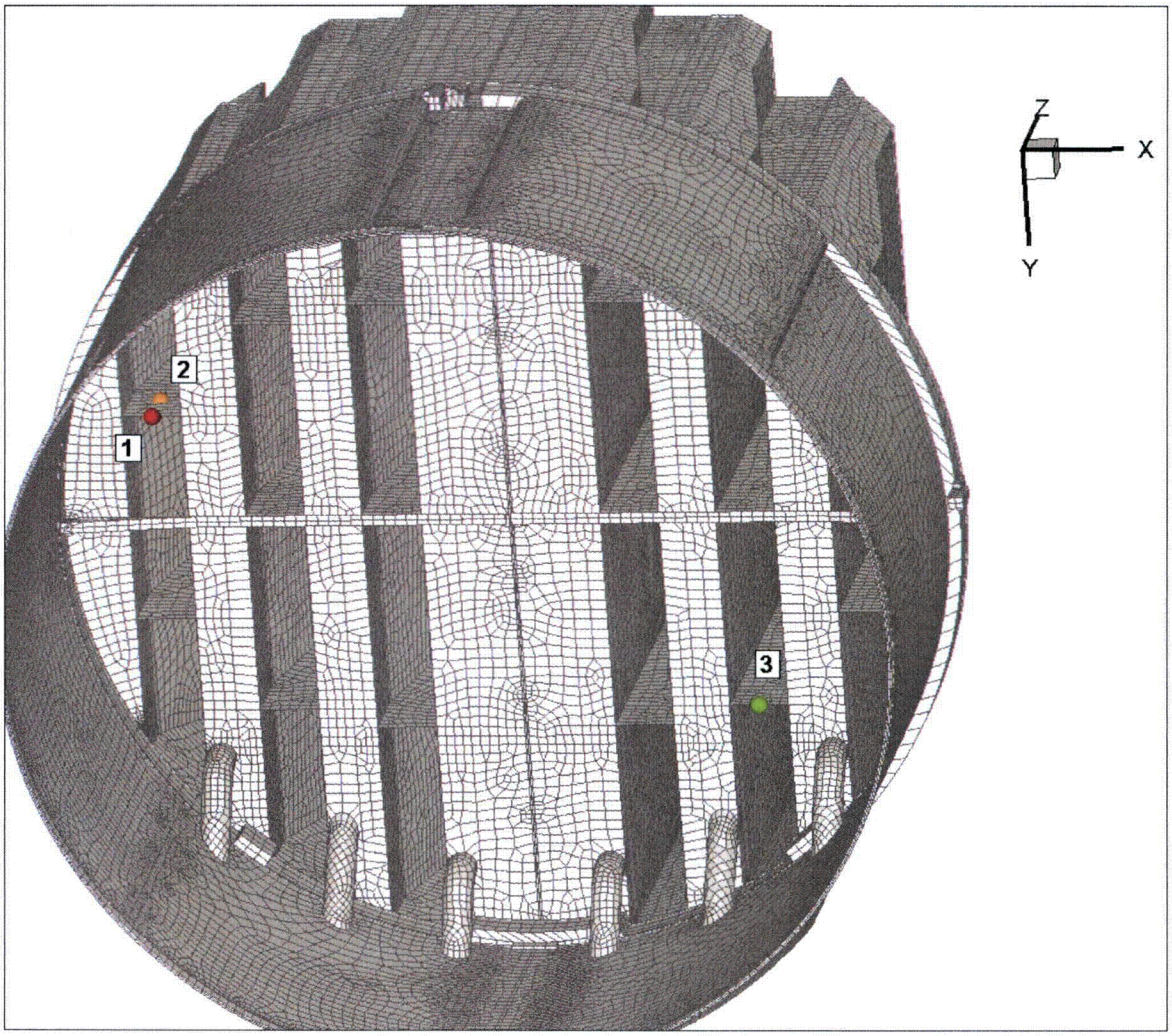

Figure 17b. Locations of minimum alternating stress ratios, SR-a, at non-welds for CLTP operation with -10% frequency shift. Numbers refer to the enumerated locations for SR-a values at non-welds in Table 8c. The figure is identical to the one in Figure 16b since this the -10% shift yielded the lowest stress ratio.

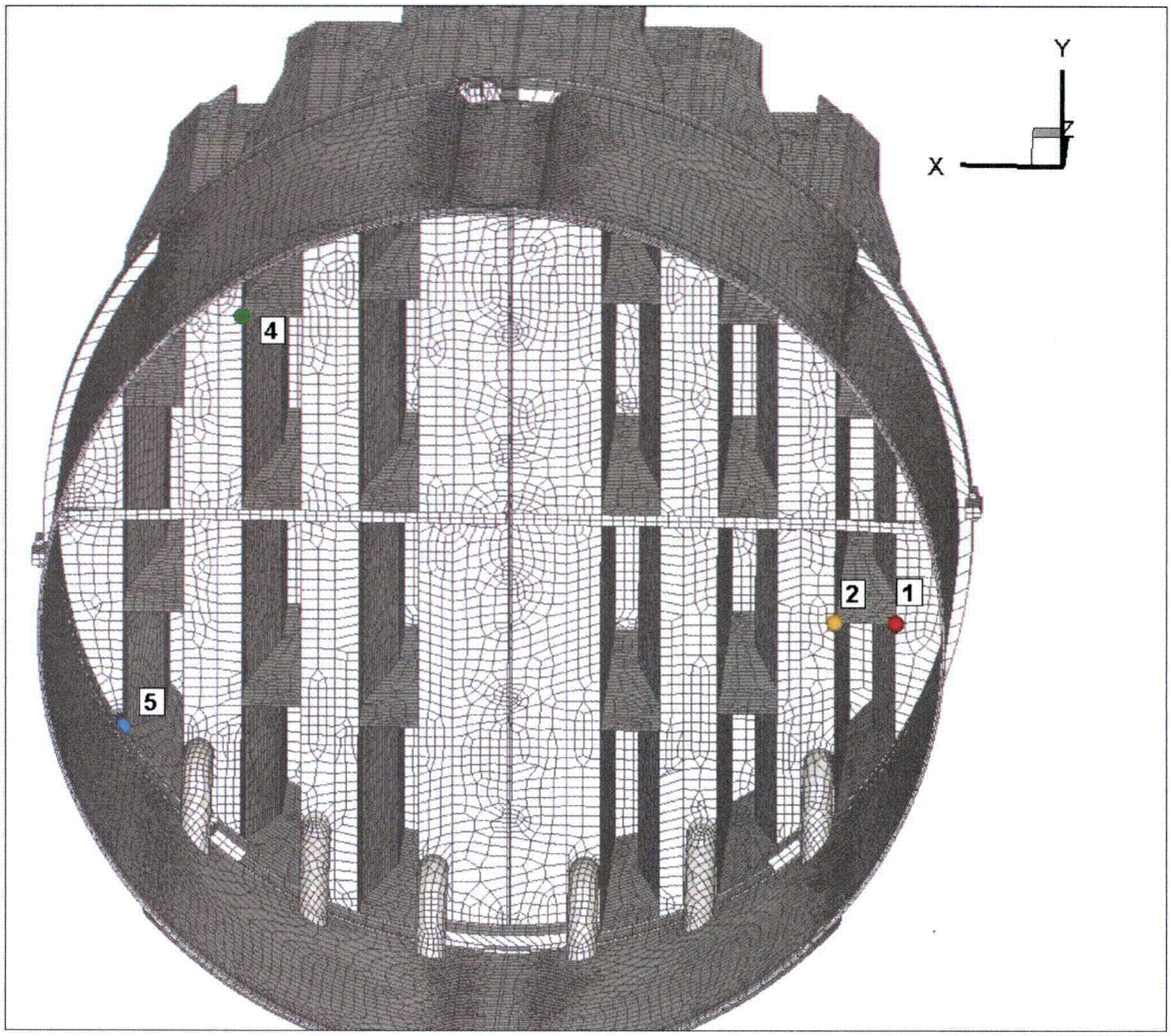

Figure 17c. Locations of minimum stress ratios, SR-P, associated with maximum stresses at welds for CLTP operation with -10% frequency shift. Numbers refer to the enumerated locations for SR-P values at welds in Table 8c. View 1 showing locations 1,2, 4 and 5.

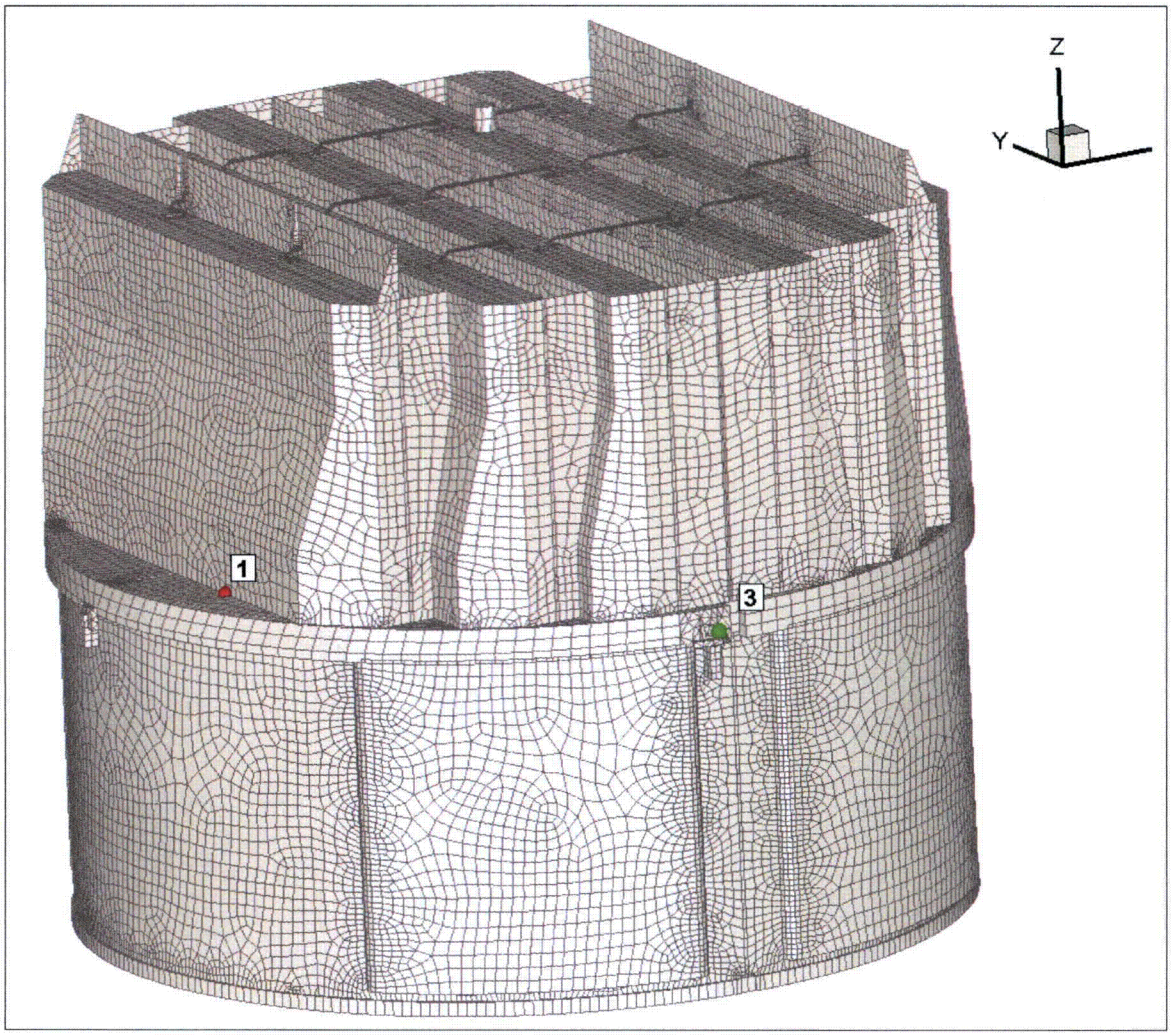

Figure 17d. Locations of minimum stress ratios, SR-P, associated with maximum stresses at welds for CLTP operation with -10% frequency shift. Numbers refer to the enumerated locations for SR-P values at welds in Table 8c. View 2 showing locations 1 and 3.

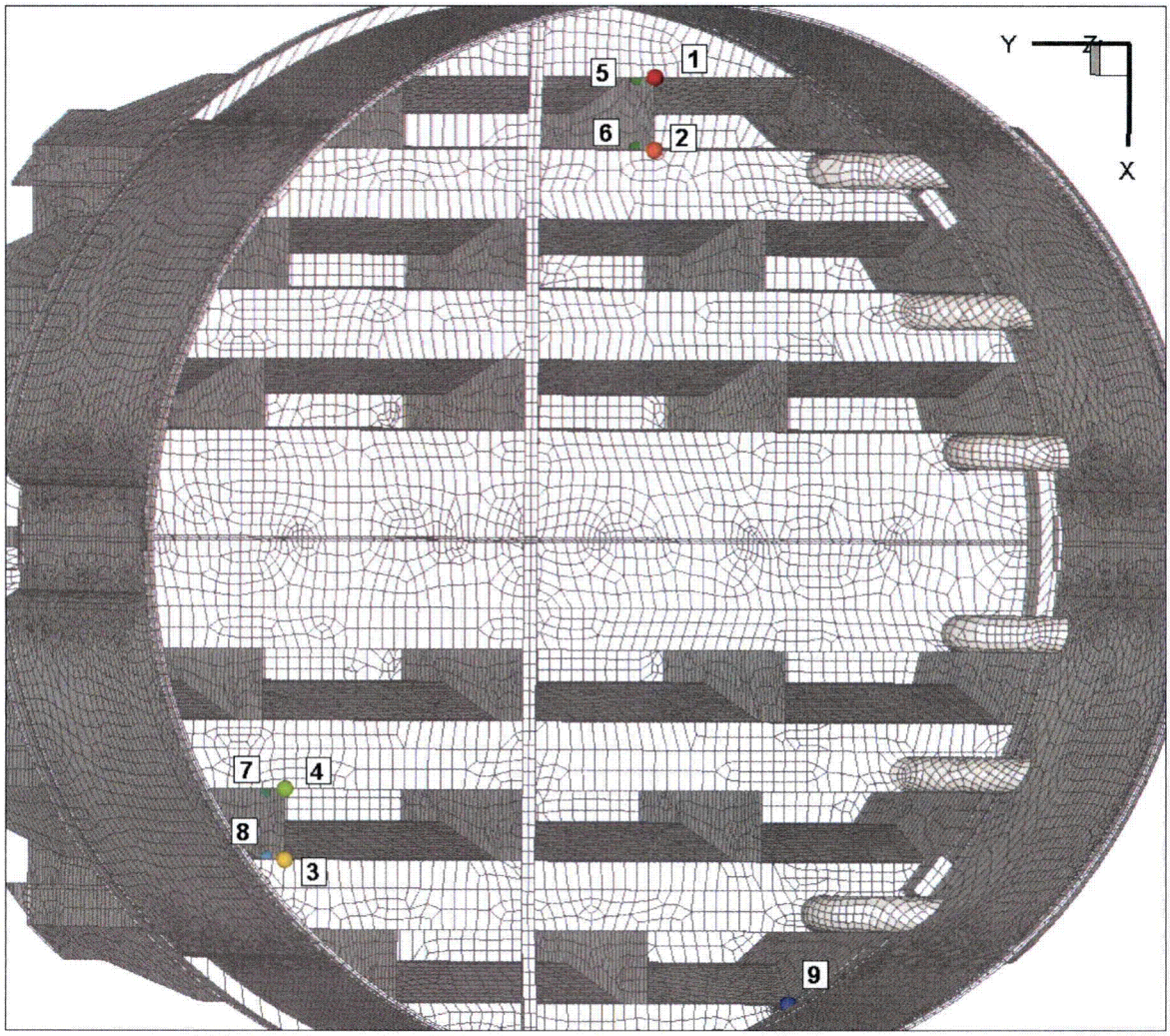

Figure 17e. Locations of minimum alternating stress ratios, SR-a, at welds for CLTP operation with -10% frequency shift. Numbers refer to the enumerated locations for SR-a values at welds in Table 8c.

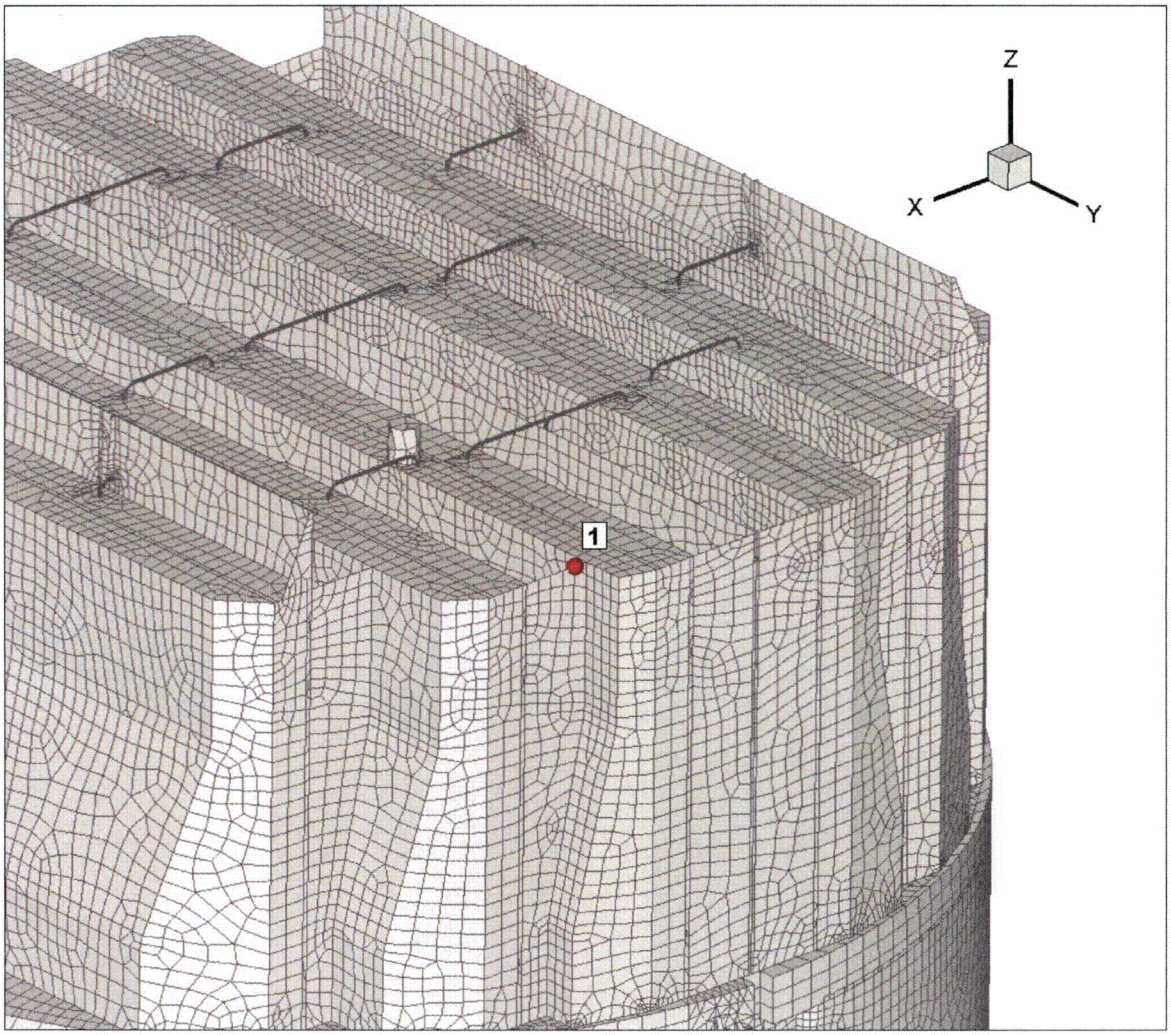

Figure 18a. Locations of minimum stress ratios, SR-P, associated with maximum stresses at non-welds for CLTP operation with +10% frequency shift. Numbers refer to the enumerated locations for SR-P values at non-welds in Table 8d.

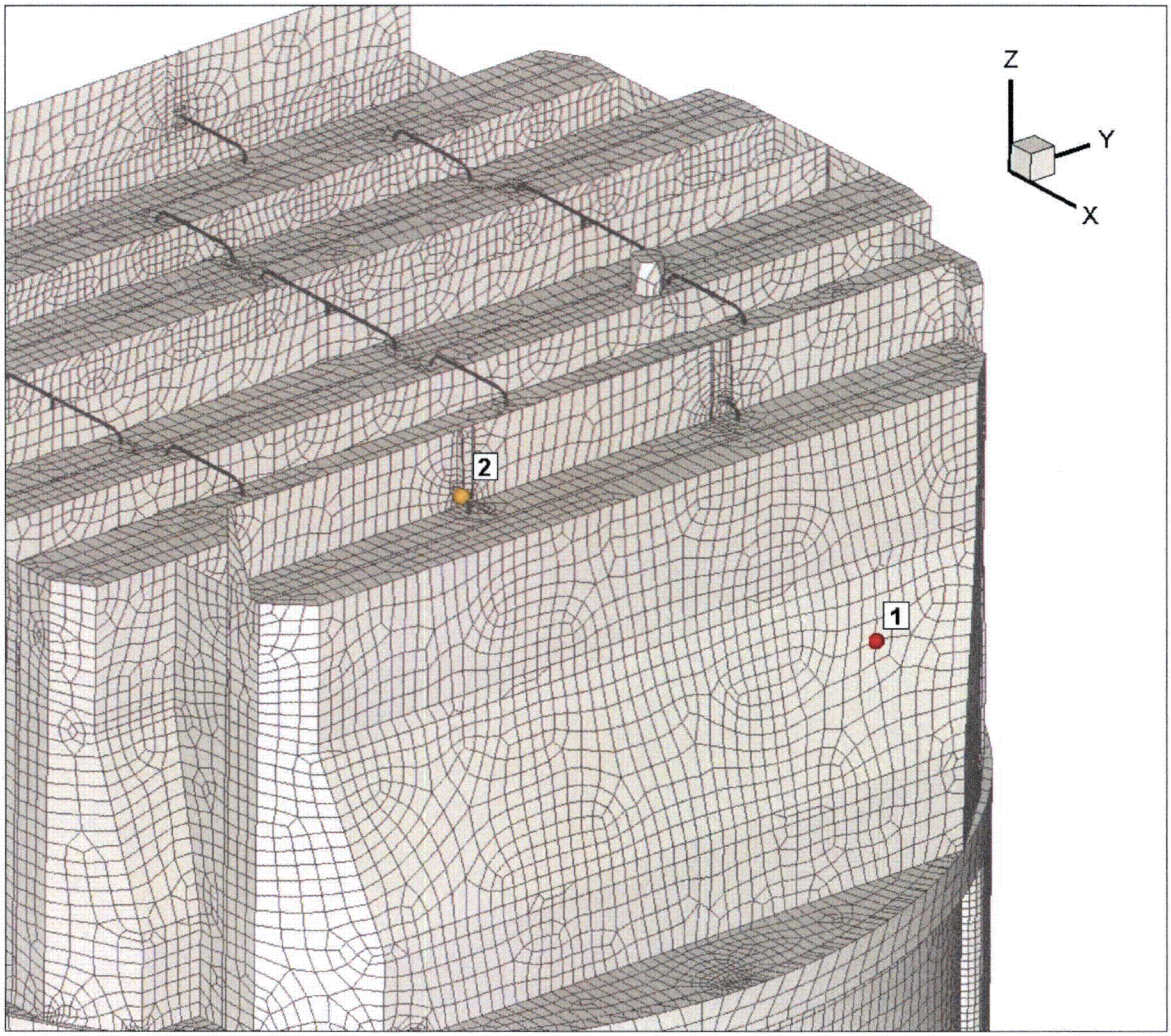

Figure 18b. Locations of minimum alternating stress ratios, SR-a, at non-welds for CLTP operation with +10% frequency shift. Numbers refer to the enumerated locations for SR-a values at non-welds in Table 8d.

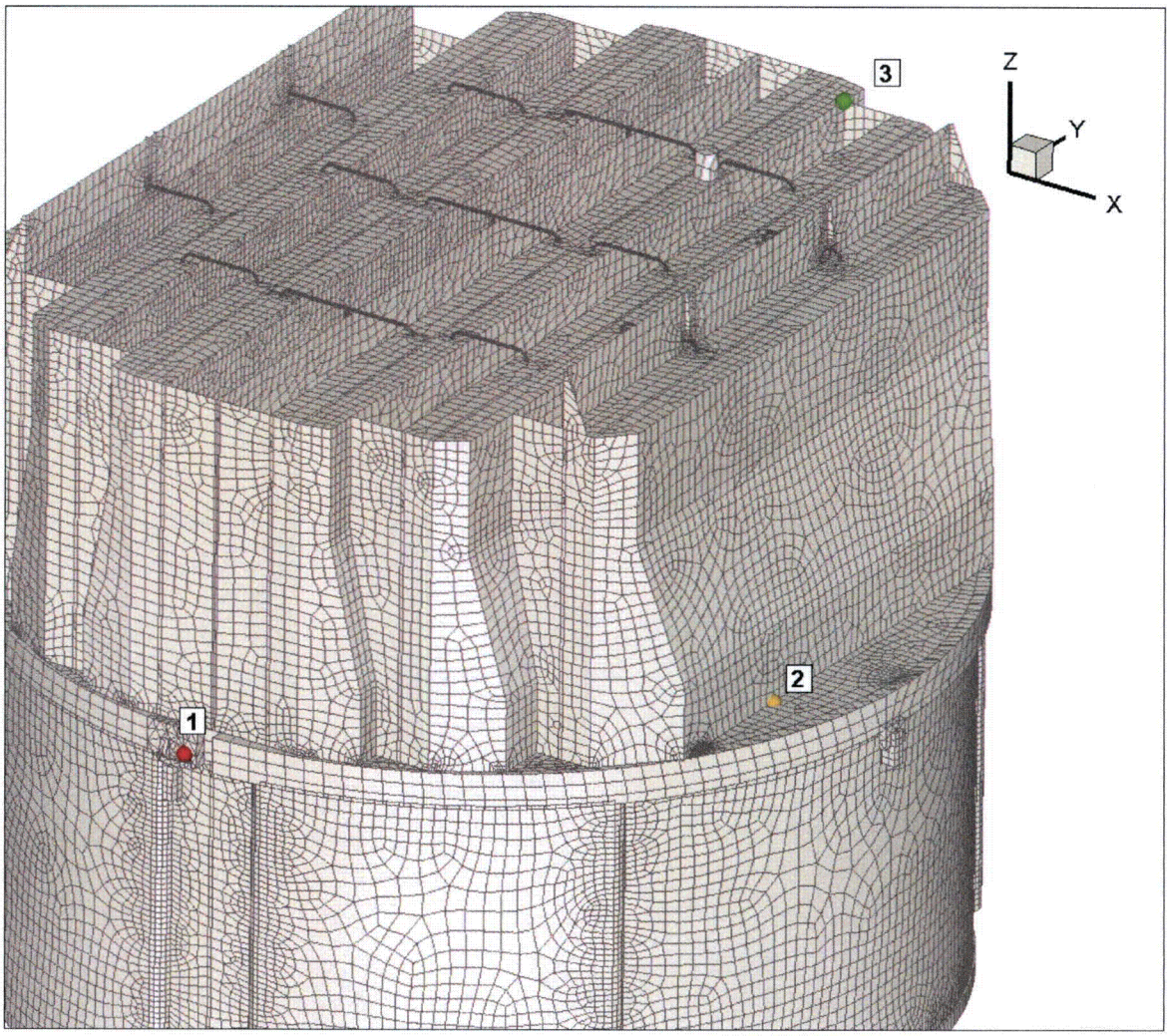

Figure 18c. Locations of minimum stress ratios, SR-P, associated with maximum stresses at welds for CLTP operation with +10% frequency shift. Numbers refer to the enumerated locations for SR-P values at welds in Table 8d.

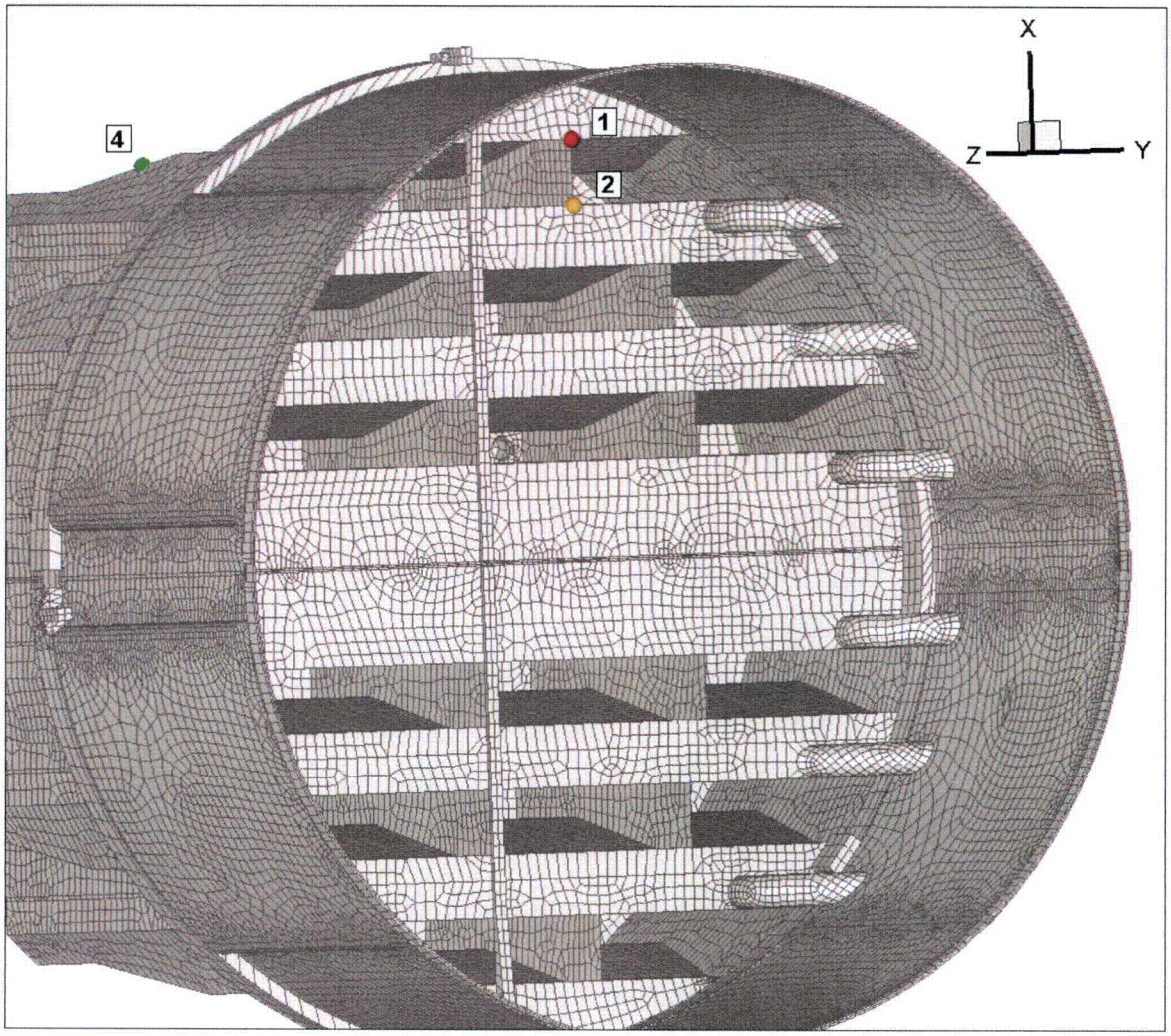

Figure 18d. Locations of minimum alternating stress ratios, SR-a, at welds for CLTP operation with +10% frequency shift. Numbers refer to the enumerated locations for SR-a values at welds in Table 8d. First view showing locations 1, 2 and 4.

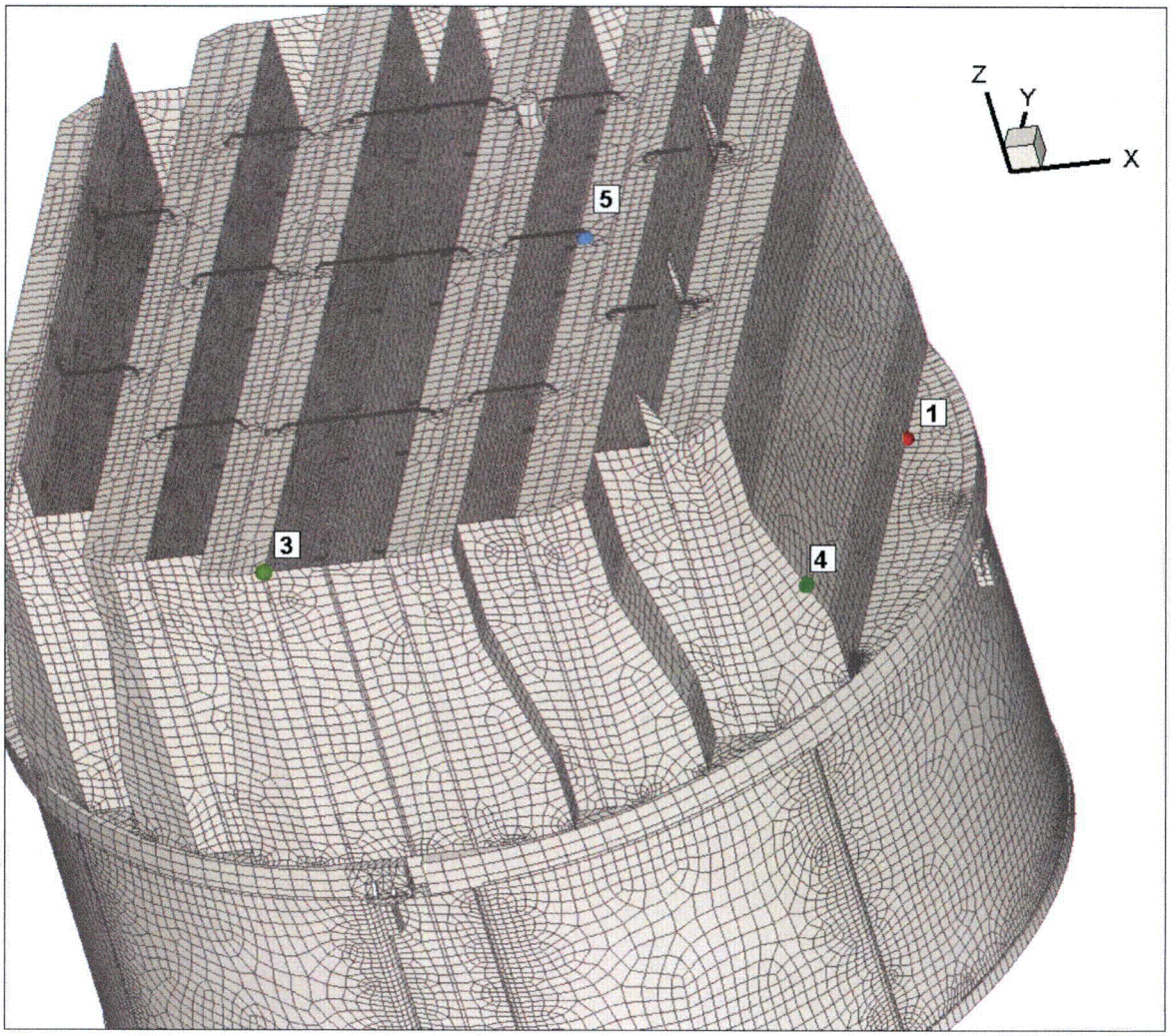

Figure 18e. Locations of minimum alternating stress ratios, SR-a, at welds for CLTP operation with +10% frequency shift. Numbers refer to the enumerated locations for SR-a values at welds in Table 8d. Second view showing locations 1 and 3-5.

5.3 Frequency Content and Filtering of the Stress Signals

As indicated previously, both the loads and stress signals contain a strong 218 Hz component that can be identified with the blanked off standpipes in the system. This can be seen by examining the accumulative PSDs for the two nodes that gave the lowest alternating stress ratios at nominal (zero frequency shift) CLTP operation according to Table 8a. The accumulative PSDs are computed directly from the Fourier coefficients as

$$\Sigma(\omega_n) = \sqrt{\sum_{k=1}^{n} |\tilde{\sigma}(\omega_k)|^2}$$

where $\tilde{\sigma}(\omega_k)$ is the complex stress harmonic at frequency, ω_k. Accumulative PSD plots are useful for determining the frequency components and frequency ranges that make the largest contributions to the fluctuating stress. Unlike PSD plots, no 'binning' or smoothing of frequency components is needed to obtain smooth curves. Steep step-like rises in $\Sigma(\omega)$ indicate the presence of a strong component at a discrete frequency whereas gradual increases in the curve imply significant content over a broader frequency range. From Parsivals theorem equality between $\Sigma(\omega_N)$ (where N is the total number of frequency components) and the RMS of the stress signal in the time domain is established.

The selected nodes are:

Node 85038 - located on the junction of the middle hood/hood support/outer base plate junction. The associated PSDs are shown in Figure 19.

Node 86525 - located on the welded drain channel/skirt junction. The associated PSDs are shown in Figure 20.

Both plots show a pronounced rise at 218 Hz. For node 85038 this is clearly the dominant component and, given the sharp rise in $\Sigma(\omega)$ at this frequency, the component is narrow band. Closer examination of the signal shows a major rise at 218.84 Hz and a lesser one at 219.84 Hz. The corresponding time response shows a 1 Hz beating phenomenon due to the close proximity of the two components. For node 86525 there is also a gradual rise in $\Sigma(\omega)$ with frequency prior to the 218 Hz jump.

In order to examine how the stresses change when the 218 Hz signal is removed (e.g., via insertion of plugs at the terminations of the eight unused standpipes in main steam lines A and D; the four unused standpipes in main steam lines B and C are located on the dead-headed branches and do not contribute to the 218 Hz signal [17]), the pressure signals in each MSL were filtered by a simple Gaussian notch filter centered at 218 Hz according to:

[[[3]]]

where f is the frequency, and the stress intensities and stress ratios re-evaluated.

These are reported in Table 9 for: (i) nominal CLTP operation and (ii) as the minimum (worst case) stress ratios taken over all frequency shifts. It is clear that the elimination of this signal results in a significant reduction in alternating stresses and corresponding increase in alternating stress ratios. Comparing the minimum stress ratio over all frequency shifts before (SR-a=0.49 in Table 8b) and after filtering (SR-a=1.77 in Table 9b) of the 218Hz signal shows that worst case stresses are reduced by a factor of 3.61. The worst case stress ratios associated with maximum stress intensities also increase from SR-P=0.93 to SR-P=1.32. This smaller relative increase reflects the dominance of the static component to the maximum stress at the support locations.

Since acoustic loads scale roughly with the square of the steam flow, it is reasonable to anticipate that under EPU conditions (where steam flow increases by 16%) the stresses would increase by approximately $(116\%)^2=1.35$. Under this assumption the minimum alternating stress ratio would reduce from 1.77 to 1.77/1.35=1.31, which given that the applied loads already account for all end-to-end biases and uncertainties, still contains sufficient margin for sustained EPU operation.

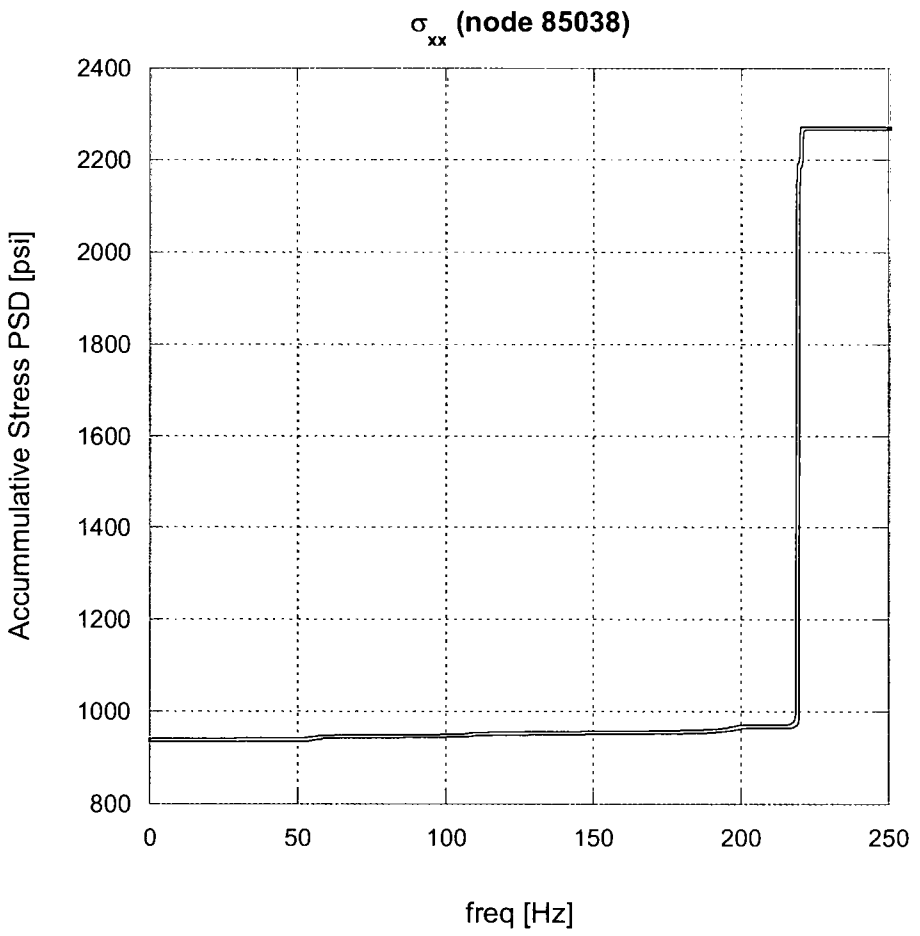

Figure 19. Accumulative PSD of the σ_{xx} stress response at node 85038 for nominal CLTP operation.

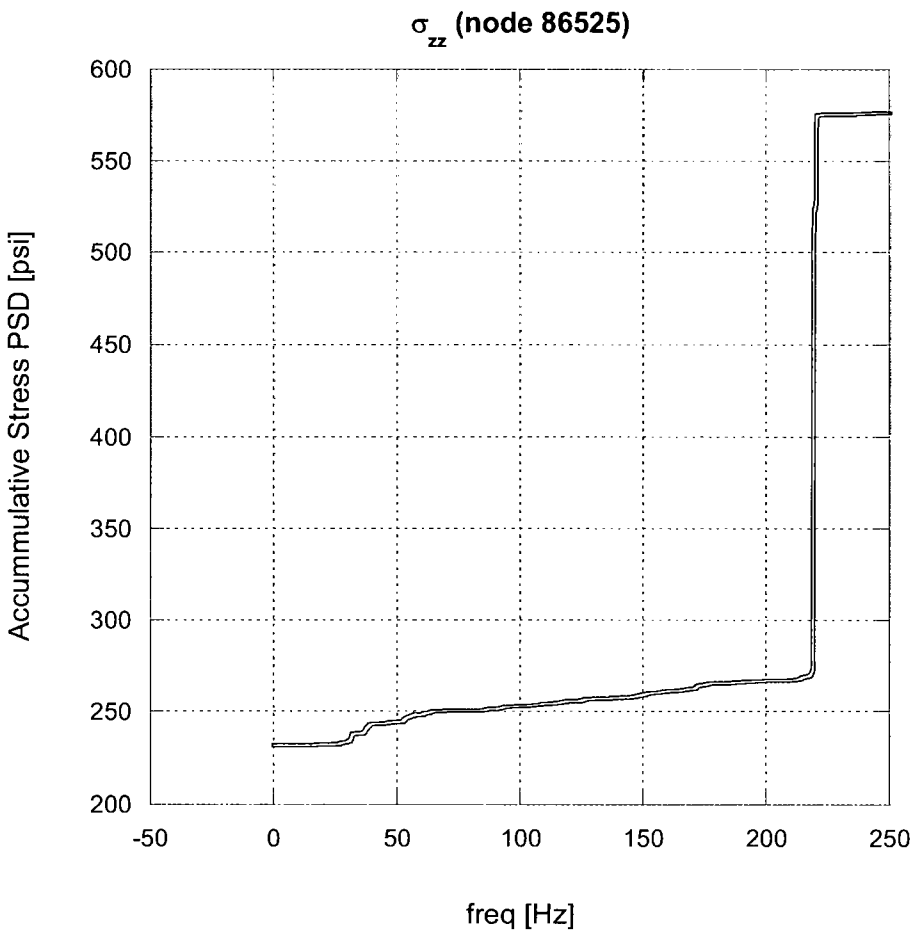

Figure 20. Accumulative PSD of the σ_{ZZ} stress response at node 86525 for nominal CLTP operation.

Table 9a. Locations with minimum stress ratios for CLTP conditions with no frequency shift using loads with 218Hz component filtered. Stress ratios are grouped according to stress type (maximum – SR-P; or alternating – SR-a) and location (away from a weld or at a weld). Bold text indicates minimum stress ratio of any type on the structure.

Stress Ratio	Location	Weld	Location (in.)				Stress Intensity (psi)			Stress Ratio	
			x	y	z	node	Pm	Pm+Pb	S_{alt}	SR-P	SR-a
SR-P	N/A	No	All nodes at non welds have SR-P > 4								
SR-a	N/A	No	All nodes at non welds have SR-P > 4								
SR-P	**1. upper support ring/support**	**Yes**	**5.8**	**122.4**	**-6.5**	**7532**	**7446**	**7446**	**<1500**	**1.35**	**>4**
"	2. outer hood/hood support/cover plate	"	-102.0	28.7	0.0	90383	5498	6343	2845	1.83	2.41
"	3. outer hood/cover plate	"	102.0	-61.0	0.0	90780	3759	6997	2057	2.16	3.34
"	4. inner hood/middle closure plate/top cover plate	"	-31.5	-108.4	88.9	86029	4664	4842	<1500	2.16	>4
	5. inner hood/hood support/base plate	"	39.8	-59.8	0.0	90626	3730	3905	1539	2.70	4.46
SR-a	1. tie bar/inner vane bank top cover plate	Yes	-29.5	3.0	88.9	83984	590	2904	2845	5.20	2.41
"	2. outer hood/hood support/cover plate	"	-102.0	28.7	0.0	90383	5498	6343	2845	1.83	2.41
"	3. tie bar/top cover plate	"	48.0	3.0	88.9	82037	426	2759	2746	5.47	2.50
"	4. tie bar/top cover plate	"	-81.5	-30.2	88.9	84995	534	3973	2721	3.80	2.52

See Table 7a for coordinates description.

Table 9b. Locations with minimum stress ratios for CLTP conditions with frequency shifts using loads with 218Hz component filtered. Stress ratios at every node are recorded as the lowest stress ratio identified during the frequency shifts. Stress ratios are grouped according to stress type (maximum – SR-P; or alternating – SR-a) and location (away from a weld or at a weld). Bold text indicates minimum stress ratio of any type on the structure.

Stress Ratio	Location	Weld	% Freq. Shift	Location (in.)				Stress Intensity (psi)			Stress Ratio	
				x	y	z	node	Pm	Pm+Pb	S_{alt}	SR-P	SR-a
SR-P	N/A	No		All nodes at non welds have SR-P > 4								
SR-a	1. lock gusset	No		-78.3	-31.4	91.6	75063	2722	3827	3443	6.72	3.59
SR-P	**1. upper support ring/support**	**Yes**		**-5.8**	**-122.4**	**-6.5**	**7705**	**7639**	**7639**	**<1500**	**1.32**	**>4**
"	2. outer hood/hood support/cover plate	"		102.0	-28.7	0.0	90804	5826	6865	3308	1.73	2.08
"	3. outer hood/cover plate	"		102.0	-61.0	0.0	90780	3958	7393	2283	2.04	3.01
"	4. inner hood/middle closure plate/top cover plate	"		31.5	108.4	88.9	84319	4754	4961	<1500	2.12	>4
SR-a	1. tie bar/top cover plate	Yes		48.0	3.0	88.9	82037	477	4047	3881	3.73	1.77
"	2. outer hood/hood support/cover plate	"		102.0	28.7	0.0	83543	4650	6324	3636	2.16	1.89
"	3. tie bar/inner vane bank top cover plate	"		29.5	3.0	88.9	82159	552	3760	3522	4.02	1.95
"	4. top pipe/inner vane bank top cover plate	"		27.3	57.2	88.9	83194	712	4019	3378	3.76	2.03
	5. tie bar/top cover plate			-81.5	-30.2	88.9	84995	565	3973	2983	3.80	2.30

See Table 7a for coordinates description.

6. Conclusions

A frequency-based steam dryer stress analysis has been used to calculate high stress locations and calculated / allowable stress ratios for the Browns Ferry Unit 2 and 3 steam dryer at CLTP load conditions using plant measurement data. A detailed description of the frequency-based methodology and the finite element model for the BFN2/3 steam dryer is presented. The CLTP loads obtained in a separate acoustic circuit model [2] including end-to-end bias and uncertainty [3], were applied to a finite element model of the steam dryer consisting mainly of the ANSYS Shell 63 elements, brick continuum elements, and beam elements. The resulting stress histories were analyzed to obtain maximum and alternating stresses at all nodes for comparison against allowable levels. These results are tabulated in Table 8 of this report. The minimum stress ratio at nominal operation is 1.06 and the minimum stress ratio taken over all frequency shifts is 0.49. In both cases the minimum stress ratio corresponds to an alternating stress.

Examination of the stress response reveals a strong 218 Hz component which is attributable to acoustics in the dead head safety valve standpipes. The structural response is largely explained by the excitation of structural modes in the vicinity of this frequency. Elimination of this signal by plugging these unused standpipes results in a significant stress reduction. The minimum alternating stress ratio is increased to SR-a=1.77 which qualifies the steam dryer with substantial margin for EPU conditions. The minimum stress ratio associated with maximum stress intensities also increases from SR-P=0.93 (with 218Hz signal) to SR-P=1.32 (218 Hz signal removed).

On the basis of these CLTP plant loads, the dynamic analysis of the steam dryer shows that the combined acoustic, hydrodynamic, and gravity loads produce the following minimum stress ratios:

Frequency Shift	Minimum Stress Ratio (no filtering)		Minimum Stress Ratio (218 Hz signal removed)	
	Max. Stress, SR-P	Alternating Stress, SR-a	Max. Stress, SR-P	Alternating Stress, SR-a
0% (nominal)	1.32	1.06	1.35	2.41
-10%	0.93	0.49	1.34	2.42
-7.5%	1.04	0.61	1.32	2.70
-5%	1.28	0.80	1.35	2.94
-2.5%	1.32	1.19	1.37	2.45
+2.5%	1.32	0.96	1.32	1.89
+5%	1.31	1.13	1.32	2.00
+7.5%	1.27	0.97	1.32	1.77
+10%	1.30	1.15	1.32	1.92
All shifts	0.93 – 1.32	0.49 – 1.19	1.32 - 1.37	1.77 – 2.94

7. References

1 Continuum Dynamics, Inc. (2005). "Methodology to Determine Unsteady Pressure Loading on Components in Reactor Steam Domes (Rev. 6)." C.D.I. Report No. 04-09 (Proprietary).

2. Continuum Dynamics, Inc. (2007). "Acoustic and Low Frequency Hydrodynamic Loads at CLTP Power Level on Browns Ferry Nuclear Unit 2 Steam Dryer to 250 Hz (Rev. 0)." C.D.I. Report No. 07-10P (Proprietary)

3. Continuum Dynamics, Inc. (2007). "Methodology to Predict Full Scale Steam Dryer Loads from In-Plant Measurements, with the Inclusion of a Low Frequency Hydrodynamic Contribution," C.D.I. Report No. 07-09P (Proprietary).

4. Structural Integrity Associates, Inc. (2006). "Main Steam Line 100% CLTP Strain Data Transmission." SIA Letter Report No. GSZ-06-017.2.

5. ANSYS Release 10.0. URL http://www.ansys.com. Documentation: ANSYS 10.0 Complete User's Manual Set

6. Press, W. H., S. A. Teukolsky, et al. (1992). *Numerical Recipes*, Cambridge University Press.

7. O'Donnell W.J. (1973). "Effective Elastic Constants For the Bending of Thin Perforated Plates With Triangular and Square Penetration Patterns," ASME Journal of Engineering for Industry, Vol. 95, pp. 121-128.

8. Idel'chik, I E. and Fried, E. (1989). *Flow Resistance, a Design Guide for Engineers*, Taylor & Francis, Washington D.C., p 260.

9. DeSanto, D.F. (1981). "Added Mass and Hydrodynamic Damping of Perforated Plates Vibrating in Water," Journal of Pressure Vessel Technology, Vol. 103, p. 176-182.

10. Continuum Dynamics, Inc. (2007). "Dynamics of BWR Steam Dryer Components," C.D.I. Report No. 07-11P

11. U.S. Nuclear Regulatory Commission, (2007). Regulatory Guide 1.20 "Comprehensive Vibration Assessment Program for Reactor Internals During Preoperational and Initial Startup Testing," March 2007.

12. WRC Bulletin 432 (1998). "Fatigue Strength Reduction and Stress Concentration Factors For Welds In Pressure Vessels and Piping," WRC, NY, p.32

13. Pilkey W.D. (1997). *Peterson's Stress Concentration Factors*, 2nd ed., John Wiley, NY, p.139.

14. Lawrence F.V., Ho N.-J., Mazumdar P.K. (1981). "Predicting the Fatigue Resistance of Welds," Ann. Rev. Mater. Sci., vol. 11, pp. 401-425.

15. General Electric (GE) Nuclear Energy (2003). Supplement 1 to Service Information Letter (SIL) 644, "BWR/3 Steam Dryer Failure," September 5, 2003.

16. Tecplot 10 (2004). URL: http://www.tecplot.com. Documentation: *Tecplot* User's Manual Version 10 Tecplot, Inc. Bellevue, Washington October.

17. Nelson G. (2006). "BFN Frequencies by GCN.xls" file received by email 31 October 2006.

18. Flugge, W. (ed.) (1962). *Handbook of Engineering Mechanics*, McGraw-Hill, p.61-62.

19. Blevins R. (1979). "Formulas for Natural Frequency and Mode Shape," van Nostrand-Reinhold Co., p. 261

20. ASME (2004). ASME Boiler and Pressure Vessel Code, Section III, Article A-8000, Stresses in Perforated Flat Plates.

Appendix A. Comparison of ANSYS Frequency Predictions Against Analytical Formulas for Flat Plates

The computed modal masses affect the response amplitude, and while these masses can be computed using the ANSYS finite element (FE) software, there are no modal mass measurements or analytical solutions they can be compared against. One recourse for assessing bias errors and uncertainties is to consider a geometrically simple structure (e.g., a flat plate) for which analytical solutions for the modal amplitudes, masses, and responses are available. Predictions of these properties using an ANSYS FE model having the same elements and connections present in the steam dryer model can then be compared against these analytical results thus allowing one to estimate the errors in frequency as a function of response frequency.

Modal analysis was performed for: (i) a simply supported plate of dimensions comparable to the vane bank side panel; and (ii) a clamped rectangular plate with dimensions comparable to the section of the middle hood that experienced the lowest alternating stress ratios at SMT EPU conditions with +10% frequency shift. In all cases, the mesh has spatial resolution similar to that used in the steam dryer model and the same element type SHELL63 is employed. For the simply supported plate, simple analytical solutions are available for any aspect ratio. For the clamped plate case, tabulated frequency predictions are available only at selected aspect ratios. Thus, for this case dimensions were chosen to correlate most closely with the steam dryer dimensions while adhering to one of the tabulated aspect ratios.

The material properties used in the finite element model were: Young's modulus, E=25.55 10^6 psi; density, ρ=0.284 lbm/in^3 and Poisson's ratio, ν=0.3. Modal frequencies are readily obtained in ANSYS. Modal masses are more difficult to extract due to underlying assumptions regarding the normalization of modes and the absence of analytical modal mass information. However, since any error in the modal mass will be reflected in the computed frequencies (the modal frequencies depend on the generalized stiffness for the mode and the associated modal mass), the errors in modal frequencies are a good estimate of the errors in modal masses. The comparisons between ANSYS and analytical modal frequency predictions follow below.

Simply Supported Plate

Analytical eigenfrequencies for simply supported plates are given by [18]:

$$f_{mn} = \frac{\pi}{2}\sqrt{\frac{D}{\rho h}}\left(\frac{m^2}{a^2}+\frac{n^2}{b^2}\right)$$

where $D = \frac{Eh^3}{12(1-\nu^2)}$, E is the Young's modulus, ρ is the density, h is the plate thickness, a and b denote the plate dimensions, and m and n are modal numbers. For the model of the vane bank side panel, h = 0.375", a = 8.5" and b = 88.4375". Then: D = 13940.6 Nm, and the lowest frequencies and relative errors are (note: m and n are mode numbers):

Table A1. Comparison of analytical and ANSYS predictions of natural frequencies for simply-supported plate.

m	n	Analytical frequency, Hz	ANSYS frequency, Hz	Rel. Error (%)
1	1	464.1	462.4	-0.37
1	2	476.8	474.8	-0.42
1	3	498.1	495.5	-0.52
1	4	527.8	524.4	-0.64

Thus the errors in computed frequencies are less than 1% and are due to mesh resolution.

Clamped Plate

The middle hood is modeled with plate of thickness h=0.125" and side lengths, a=17.92" and b = 44.8". This corresponds to the section of plate immediately adjacent to the location of high stress in the SMT calculation at EPU with +10% frequency shift. At this aspect ratio, b/a=2.5, the analytical eigenfrequencies are given by [19]:

$$f_{ij} = \frac{\lambda_{ij}^2}{2\pi b^2}\sqrt{\frac{D}{\rho h}}$$

where D = 516.32 Nm and the coefficients λ_{ij}^2, the lowest frequencies and relative errors are shown in the table below.

Table A2. Comparison of analytical and ANSYS predictions of natural frequencies for clamped plate.

i	j	λ_{ij}^2	Analytical frequency, Hz	ANSYS frequency, Hz	Rel. Error (%)
1	1	147.8	82.69	82.98	0.35
1	2	173.9	97.29	96.01	-1.32
1	3	221.5	123.92	121.14	-2.03
1	4	291.9	163.3	158.73	-2.8

The mesh used to calculate plate eigenfrequencies and the mesh on the steam dryer model are shown below.

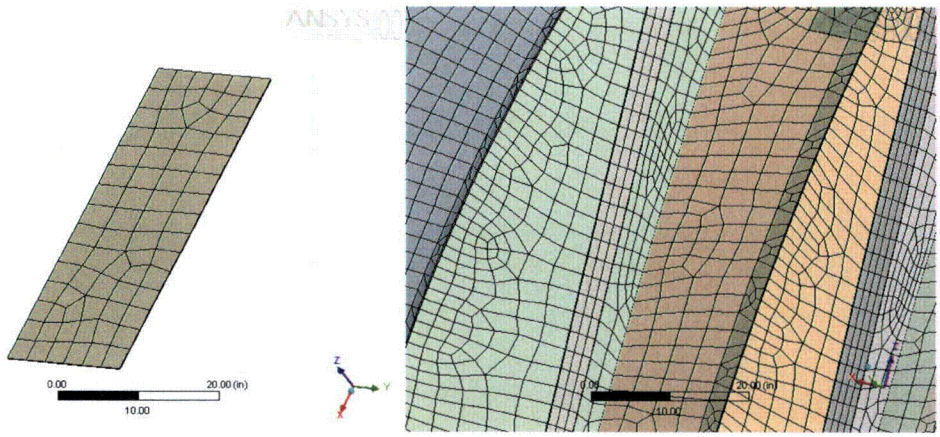

Left – mesh on the flat plate model for eigenvalue comparison calculations; right – mesh on the actual steam dryer FE model. The size of elements in both models is kept similar.

Appendix B. Comparison of Transient and Frequency-Based Simulations for the Browns Ferry Unit 1 Dryer

[[

[3]]]

[[

[3]]]

[[

[3]]]

[[

[3]]]

Figure 21a. [[

[3]]]

[[

[3]]]

Figure 21b. [[

[3]]]

[[

[3]]]

Figure 22a. [[
[3]]]

[[

[3]]]

Figure 22b. [[[3]]]

[[

[3]]]

Figure 22c. [[
[3]]]

[[

[3]]]

Figure 22d. [[
[3]]]

Appendix C. Structural Modeling of Perforated Plates

Modeling the perforated plates in the steam dryer assembly explicitly is computationally prohibitive and an alternative approach is adopted where the plates are characterized by modified material properties adjusted to match the key static and dynamic behavior. This Appendix summarizes the modeling method employed and its verification against measurements.

The perforated plates used in the steam dryer assembly are very thin, i.e. the ratio of thickness and pitch of perforation is less than unity so that the effective properties provided in ASME B&PVC, [20], for thick perforated plates cannot be used. Therefore, to model the steam dryer we have adopted the effective material properties reported by O'Donnell in [7] which directly apply to the bending of thin plates. In his work the effective properties are calculated by equating an average stress field over the periodicity cell in a perforated plate. Thus, for a given static loading the solid plate with the effective or modified material properties will yield a similar stress field as the perforated plate with original material properties. Comparisons are made against the values provided in ASME Code [20], as well as to experimental data where good agreement is obtained.

In order to apply these results to the steam dryer analysis the staggered 45° perforation was approximated with an equilateral staggered 60° perforation. The difference was judged insignificant for modeling purposes. The effective properties were therefore inferred from Fig. 8 (Young's modulus) and Fig. 9 (Poisson ratio) of [7].

Verification

[[

[3]]]

[[

[3]]]

Figure 23. [[

[3]]]

[[

[3]]]

Figure 24. [[[3]]]